RCQ 8/30/05

~~DSBSC~~

Design Calculation or Analysis Cover Sheet

Complete only applicable items.

1. QA: QA
2. Page i

3. System	4. Document Identifier
Waste Isolation System	CAL-WIS-AC-000004 REV 0A

5. Title

Creep Deformation of the Drip Shield

6. Group

Post Closure Activities-Seismic Studies

7. Document Status Designation

☐ Preliminary ☒ Committed ☐ Final ☐ Cancelled

8. Notes/Comments

The preparer and checker for each Section in this report are identified as follows:

Section	Preparer	Checker
1 to 6, Attachments I-V	Branko Damjanac	Tim Schmitt
Output DTN	Branko Damjanac	Yiming Sun

Attachments	Total Number of Pages
Attachment I - Derivation of Creep Equations for Ti-7 and Ti-24	20
Attachment II - One-Dimensional Creep Test Simulation	6
Attachment III - Effect of Element Discretization on Drip Shield Creep Results from the flac3d Code	8
Attachment IV - Comparison of Flac3d to Analytic Solution for Creep-Induced Stress Relaxation in a One-Dimensional Bar	4
Attachment V - Derivation of Scalar Strain Measure	4

RECORD OF REVISIONS

9. No.	10. Reason For Revision	11. Total # of Pgs.	12. Last Pg. #	13. Originator (Print/Sign/Date)	14. Checker (Print/Sign/Date)	15. Approved/Accepted (Print/Sign/Date)
0A	Initial Issue	122	V-2	Branko Damjanac R.C. Lewis for BD	Tim Schmitt 8/30/05 Yiming Sun 8/30/05	Paul Dixon 8-30-05

CONTENTS

Page

CONTENTS (Continued)

Page

FIGURES

Page

FIGURES (Continued)

Page

FIGURES (Continued)

Page

FIGURES (Continued)

Page

TABLES

Page

INTENTIONALLY LEFT BLANK

ACRONYMS

ASME	American Society of Mechanical Engineers
BSC	Bechtel SAIC Company
DIRS	document input reference system
DOE	Department of Energy
DTN	data tracking number
EBS	engineered barrier system
ELI	extra low interstitial
FD	finite difference
g	acceleration of gravity
MT	metric ton
PC	personal computer
PGV	peak ground velocity
PSHA	probabilistic seismic hazard analysis
RT	room temperature
STN	software tracking number
TBD	to be determined
Ti-2	Titanium Grade 2
Ti-5	Titanium Grade 5
Ti-7	Titanium Grade 7
Ti-24	Titanium Grade 24
Ti-29	Titanium Grade 29
TSPA-LA	Total System Performance Assessment-License Application
UNS	unified numbering system

INTENTIONALLY LEFT BLANK

1. PURPOSE

The purpose of the drip shield is to divert water that may seep into emplacement drifts from contacting the waste packages and to protect the waste packages from impact or static loading from rockfall. The results of a series of engineering calculations developed to study the effect of static and dynamic loads on the mechanical performance of the drip shield were summarized and reported in *Mechanical Assessment of the Drip Shield Subject to Vibratory Motion and Dynamic and Static Rock Loading* (BSC 2004 [DIRS 169753]). The potential drip shield mechanical loads are a result of:

- Potential earthquake vibratory ground motion and resulting mechanical interaction of the drip shield, waste package and emplacement pallet, and drift invert;
- Dynamic impacts of rockfall resulting from emplacement drift damage due to earthquake vibratory motion; and
- Static load of the caved rock rubble (rubble) that may come to rest on the drip shield as a result of earthquake vibratory motion or from time-dependent yielding of the rock mass surrounding the emplacement drift.

The drip shield is designed from Titanium Grade 7 (SB-265 Ti-7 [UNS R52400]) and Titanium Grade 24 (SB-265 Ti-24 [UNS R56405]). Stability of the drip shield under static load of the rubble was analyzed previously in *Structural Stability of a Drip Shield Under Quasi-Static Pressure* (BSC 2004 [DIRS 170791]) for short-term elasto-plastic deformation of titanium. Creep of titanium and its consequences on stability of the drip shield were not analyzed in that document. Because titanium creeps even at RT (Dutton 1996 [DIRS 174750], Section 2, Kissel and Sinnott 1953 [DIRS 174853]), stability of the drip shield can potentially be affected by creep. This document presents an analysis of creep of the drip shield structure for 10,000 years under static load of the rubble, and provides an assessment of the stability of the drip shield structure after 10,000 years as a result of creep.

The dynamic impact of rockfall resulting from emplacement drift damage may result in denting of the drip shield plates (BSC 2005 [DIRS 174052]). One of the consequences of potential denting is development of residual tensile stresses in the plates in the localized region of the dent. If these residual tensile stresses exceed a certain threshold, stress corrosion cracking through the plates will be facilitated, increasing the potential for creation of a pathway for water seepage. As a result of the time-dependent (creep) deformation of titanium, the residual tensile stresses in the plates will decrease gradually, reducing the potential for stress corrosion cracking. (The block bounces off the drip shield after the impact. Therefore, relaxation of residual stresses is analyzed for practically unloaded structure.) Time-dependent relaxation of the residual stresses in the drip shield plates after impact by the rock blocks was analyzed and the results are reported in this document. Potential for stress corrosion cracking was assessed based on the distribution of residual stresses in the drip shield plate. If a continuous path with stresses that exceed the stress corrosion cracking threshold exists between the outer and inner surface of the drip shield plate, than there is a potential for stress corrosion cracks to propagate through the drip shield plate. However, the effect of stress corrosion cracking on stresses in the plate was not

considered. Fracture mechanics analysis of crack initiation and propagation was not conducted in this report.

The drip shield is classified as a Safety Category item by the *Q-List* (BSC 2005 [DIRS 174269], p. A-6 under Engineered Barrier System). Therefore, this calculation is subject to the requirements of *Quality Assurance Requirements and Description* (DOE 2004 [DIRS 171539]). This document is prepared in accordance with LP-3.12Q-BSC, *Design Calculations and Analyses*.

2. METHOD

The drip shield calculations presented in this document are conducted using commercial finite difference (FD) software, FLAC3D V2.1 (STN: 10502-2.1-00 [DIRS 161947]). The FD method is a numerical technique commonly used for analysis of engineering problems. The method requires discretization of the structure into a number of elements (the FD mesh or grid) that are interconnected by nodal (or grid) points. The governing equations of motion, subject to imposed boundary and initial conditions, are solved to provide the solution of the transient mechanical response of the drip shield. The boundary and initial conditions are a result of the constraints supplied by the emplacement pallet and invert, and from the applied static load by the rubble. The explicit FD method with the central difference method of time integration (Itasca 2002 [DIRS 160331], Section 1.1 of FLAC3D Theory and Background Volume) was employed in all calculations. Results of the FD analysis are given in terms of transient stresses, strains and displacements of the FD mesh. Three-dimensional graphical representation of the stress and strain states are used to aid in interpretation of the analysis results. FLAC3D has integral mesh development and postprocessing graphical display capability. However, the FD mesh geometry is created by using TrueGrid V2.2.0b and was imported into FLAC3D.

After the simulations were completed, results of the analysis were presented in terms of contours of a scalar measure of creep strain or contours of the major (most tensile) principal stress (as a measure of the relaxation of the residual stresses). Stability of the drip shield structure was assessed by comparison of the calculated creep strains with the critical creep strain corresponding to the onset of tertiary creep. The effect of residual stress relaxation on stress corrosion cracking was assessed by determining the time required for the major principal stress to decay below the stress-corrosion cracking threshold.

INTENTIONALLY LEFT BLANK

3. ASSUMPTIONS

Assumptions used in the analyses documented here are described below.

3.1 ASSUMPTIONS REQUIRING VERIFICATION

Assumptions that require verification are not used in this document.

3.2 ASSUMPTIONS NOT REQUIRING VERIFICATION

3.2.1 The density and Poisson's ratio are not available for SB-265 Ti-7 [UNS R52400] and SB-265 Ti-24 [UNS R56405] except at room temperature (RT) (20°C). The RT density and RT Poisson's ratio are assumed for these materials.

Rationale–The impact of using RT density and RT Poisson's ratio is anticipated to be negligible. The rationale for this assumption is that the material properties in question do not have a dominant impact on the calculation results.

Where used: Sections 5.2.2, 5.4 and 5.5.

3.2.2 The friction coefficient for contacts occurring between the invert and Ti-7 is not available in the literature. Therefore, it is assumed that the dynamic (sliding) friction coefficient for this contact is 0.4.

Rationale–This friction coefficient represents a reasonable estimate based on available information for metal-on-stone contacts, which is between 0.3 and 0.7 (Beer and Johnston 1977 [DIRS 145138], Table 8.1, p. 306). This parameter does not have a significant effect on the results, as the relative surface-to-surface movement of these components is not a significant determining factor in the amount of deformation during static loading of a rubble. The calculation results are not expected to be affected significantly by the friction coefficient. For the sake of conservatism of the drip shield stability assessment, the friction coefficient used in this calculation is below the range average.

Where used: Sections 5.2.2, 5.2.3, 5.4 and 5.5.

3.2.3 The variation of functional friction coefficient between the static and dynamic values as a function of relative velocity of the surfaces in contact is not available in the literature for the materials used in the calculations (Section 5.2.2). Therefore, the effect of relative velocity of the surfaces in contact is not considered in these calculations by assuming that the functional friction coefficient and static friction coefficient are both equal to the dynamic friction coefficient. The impact of this assumption on results presented in this document is anticipated to be negligible.

Rationale–This assumption maximizes the relative motion of the drip shield by minimizing the friction coefficient within the given analysis framework. However, the results indicate that there is practically no sliding of the drip shield on the invert.

Consequently, a greater friction angle (corresponding to static value) between the drip shield and the invert would not effect the results.

Where used: Sections 5.2.3, 5.4 and 5.5.

3.2.4 The temperature of the drip shield is assumed to be 150°C for temperature-dependent material properties.

Rationale–This temperature overestimates drip shield temperature for most of the 10,000 years period for high-temperature operating modes and strictly for low-temperature operating modes. The waste package temperature in an open drift remains below 150°C for approximately 97.0 percent of 10,000 years (BSC 2005 [DIRS 173944], Figure 6.3-67), and the drip shield temperature is less than the waste package temperature. In addition, the drip shield temperature of 150°C is considered appropriate for the case of potential drift collapse, which could accompany a low-probability seismic event or result from time-dependent strength loss of the surrounding rock mass. In either case, the drip shield could be partially or completely surrounded by rubble. The *Multiscale Thermohydrologic Model* (BSC 2005 [DIRS 173944], Section 6.3.7 and Table 6.3-42) was used to conduct a parameter study of the impact of thermohydrologic parameters on the in-drift environment. The results show that the peak waste package temperature in a collapsed drift for the base-case thermal conductivity of the rubble is greater than 200°C for a very brief period of time—less than 100 years—and the waste package temperature drops below 150°C within approximately 350 years after collapse, even for the "hottest" waste package considered in the parameter study. These results are for the case of a collapse occurring coincident with the closure of the repository. It follows that 150°C overestimates the drip shield temperature and is a reasonable value for evaluation of material properties in a collapsed drift over 96.5 percent of the 10,000 years period.

Where used: Sections 5.2, 5.3, 5.4 and 5.5, and Attachment I.

3.2.5 The thickness of the Ti-7 and Ti-24 plates are reduced by 2 mm to account for general corrosion effects over the 10,000 year period.

Rationale–For Ti-7, this thickness reduction results from using the 95th percentile general corrosion rate values used in TSPA-LA for both sides of the titanium plate (BSC 2004 [DIRS 169845], Section 6.5.5, Tables 16 and 17; DTN: MO0408MWDGLCDS.002 [DIRS 171486]). For the outside and inside plates, the 95th percentile general corrosion-rate values are 1.12E-4 mm/yr and 8.59E-5 mm/yr, respectively. Thus, in 10,000 years, about 1.12 mm is removed from the outer surface by general corrosion, and about 0.86 mm are removed from the inner surface (i.e., a total loss of about 2 mm of thickness). Alternatively, the highest measured general corrosion rate from the 5-year exposed Ti samples used for validation of the TSPA-LA general corrosion distributions is 77 nm/yr (BSC 2004 [DIRS 169845], Table 23; DTN: MO0408MWDGLCDS.002 [DIRS 171486]). Using this value for both sides of the drip shield, a total loss of about 1.54 mm of thickness can be calculated over an exposure period of 10,000 years. Thus, a thickness reduction of 2 mm is a reasonable

estimate of the total thickness loss for Ti-7 due to general corrosion in 10,000 years. For Ti-24, the thickness reduction over a 10,000-year period was determined to be about 0.75 mm per exposed surface in the *Aqueous Corrosion Rates for Waste Package Materials* report (BSC 2004 [DIRS 169982], Section 6.5.2). Therefore, a thickness reduction of 2 mm is a reasonable estimate of the total thickness loss for Ti-24 due to general corrosion in 10,000 years.

Where used: Sections 5.4 and 5.5.

3.2.6 The drip shield sidewalls are assumed to be unconstrained in the lateral direction during the 10,000-year period in the calculation of static loading by the rockfall (with the exception of the lateral constraint provided by the emplacement pallet).

Rationale–The gantry rail is made of carbon steel sets as described in *Repository Subsurface Emplacement Drifts Steel Invert Structure Sect. & Committed Materials* (BSC 2004 [DIRS 169776]), which are not anticipated to remain intact (will eventually corrode away) during the 10,000-year period.

Where used: Sections 5.4 and 5.5.

3.2.7 The lifting feature and drip shield connector assembly are excluded from the FD representations for simplicity.

Rationale–The effect of these drip shield components on the calculation results is negligibly small.

Where used: Sections 5.4 and 5.5.

3.2.8 In the calculation of effective stiffness of the rubble that fills the space between the drip shield and the intact drift wall, the distance between the drip shield and the intact drift wall is assumed to be 2.5 m.

Rationale–Analysis of drift collapse shows (e.g., Figure 6-171 of the *Drift Degradation Analysis* AMR, BSC 2004 [DIRS 166107]) that most of the rockfall comes from the drift crown. (Collapse of the emplacement drift located in lithophysal rock units is expected when the drift is subjected to strong seismic ground motions that have peak ground velocity (PGV) greater than approximately 2 m/s.) The rubble fills the space between the drip shield and the drift wall, reducing—or even preventing—deterioration of the walls. The maximum initial horizontal distance from the drip shield to the drift wall is approximately 1.5 m. Accounting for some rockfall from the walls, the distance between the drip shield and the intact drift wall is taken to be 2.5 m.

Where used: Section 5.4.1.3.

3.2.9 The onset of tertiary creep, considered to coincide with a drip shield collapse, is assumed to occur when 10 percent creep strain is reached at any point in the structure.

Rationale–The creep equations (Section 5.3.1) used for analysis of the time-dependent deformation of the drip shield are transient, with monotonically-decreasing creep rate. Such a trend is consistent with observations until a time when the critical creep strain corresponding to onset of tertiary creep is reached (if it is ever reached). Tertiary creep is characterized by accelerated creep strains and precedes failure (creep rupture) of the material. Because tertiary creep was not included in the creep equations, the accumulated creep strain in the structure was compared to the assumed threshold of tertiary creep to assess stability of the structure after a certain period of creep. Laboratory evidence indicates that the onset of tertiary creep takes place at a creep strain greater than 10 percent (e.g., ~15 percent according to Drefahl et al. 1985, page 2389 and Figure 3, [DIRS 174820] and Dutton 1996, Section 5.1 [DIRS 174750]). It was assumed in the calculation that 10 percent creep strain is the threshold for onset of tertiary creep. Additional level of conservatism is due to the fact that collapse of the drip shield is assumed to occur when 10 percent creep strain is reached at any point of the structure. Similarly as yielding at a point of a structure does not mean collapse of a structure, onset of tertiary creep at a point does not mean collapse of a structure. When the tertiary creep is triggered at a point the stresses will redistribute and collapse of a structure will not take place until the entire cross-Section is in the state of tertiary creep.

Where used: Sections 5.3.1 and 5.4.

3.2.10 Time is used as the evolution parameter in the creep equations.

Rationale–Expressing creep rate, $\dot{\varepsilon}$, as a function of time (Equation 5.3-2) is appropriate if the loading stress is constant, because the creep rates are derived by the differentiation of the creep equation (Equation 5.3-1) determined from the results of constant-stress laboratory tests. In general, the stress state at a point of a structure will change as a function of time as a result of creep. In that case, strain at a point will be accumulated as a function of time according to different relations. For example, if stress is initially σ_1 and subsequently changes to σ_2, the strain rate changes from

$$\dot{\varepsilon}_1 = B\sigma_1^n t^p \qquad \text{(Eq. 3.2-1)}$$

to

$$\dot{\varepsilon}_2 = B\sigma_2^n t^p \qquad \text{(Eq. 3.2-2)}$$

and accumulated strain and time are not equivalent measures of evolution of deformation of the problem. The strain cannot be expressed as

$$\varepsilon = A\sigma^n t^m \qquad \text{(Eq. 3.2-3)}$$

Instead, it should be expressed as

$$\varepsilon = B\int_0^t \sigma(t)^n t^p dt \qquad \text{(Eq. 3.2-4)}$$

Thus, the accumulated creep strain is a more appropriate evolution parameter when stresses change during simulation of the creep deformation. Time is assumed to be the evolution parameter in the creep and stress relaxation calculations reported in this document. This assumption results in overprediction of creep deformation of the drip shield. As a result of creep, the stresses are redistributed from initially highly stressed regions to less stressed regions. By assuming time to be a creep-evolution parameter, the creep rate reduction that occurred at early times due to strain accumulation at higher stresses is not considered, overpredicting creep rates at later times. This approach could overpredict the rate of stress relaxation. Therefore, different creep equations were considered in the stress relaxation analysis (Section 5.3.2) to provide bounding responses.

Where used: Section 5.3.1, 5.3.2, 5.4, 5.5 and Attachment I.

3.2.11 Yield strength of Ti-24 at 150ºC is assumed to be 683 MPa.

Rationale–The temperature-dependent tensile and yield strengths of Ti-24 are not available from the American Society of Mechanical Engineers (ASME) Boiler and Pressure Vessel Code (ASME 2001 [DIRS 158115]). However, vendor data for these material properties are available (Timet 1993 [DIRS 157726]). Therefore, the tensile and yield strengths of Ti-24 at 400°F from Timet 1993 [DIRS 157726], will be normalized and used with the room temperature values from ASME to calculate the tensile and yield strengths of Ti-24 at 150°C. The rationale for this assumption is that the ASME Boiler and Pressure Code states the minimum material properties. Therefore, calculating the minimum properties at elevated temperatures with this method provides bounding values of tensile and yield strengths of Ti-24 for this calculation.

Where used: Sections 5.2, 5.4, 5.5 and Attachment I.

3.2.12 The stress-corrosion cracking threshold is assumed to be 50 percent of the yield strength at a given temperature.

Rationale– The stress corrosion cracking (SCC) initiation stress threshold for Ti-7 and Ti-24 is taken as 50 percent of the materials yield strength as described in (BSC 2004 [DIRS 172203], Section 6.2.1). This threshold value was selected based on a series of constant load and U-bend type SCC tests performed on Ti-16 and Ti-7 specimens exposed to a range of high temperature brines. For results obtained on Ti-7 constant load specimens, a stress reduction factor of 2.2 was applied to the lowest apparent stress at which 'SCC' failure was observed, i.e., at 110 percent of the at temperature yield strength. This reduction factor resulted in an initiation stress threshold value of 50 percent of the at-temperature yield strength. In BSC 2004 [DIRS 172203], Section 6.2.1, a further added conservatism was applied by selecting the yield strength value at the highest expected drip shield temperature of 140°C This value was specified as 221 MPa and resulted in a threshold initiation stress of 110.5 MPa. However, subsequently, constant load tests were performed in air at 105°C on archive specimens from the same heat of material tested in the 105°C brine. Air failure times at a given stress were very similar to those failure times observed in the 105°C test brine indicating that the brine exposed 'SCC' failures were very likely a result of creep rupture rather than

SCC (Andresen 2005 [DIRS 173867]). Consequently, based on these constant load air tests, the threshold stress defined in (BSC 2004 [DIRS 172203], Section 6.2.1) for initiation of SCC in Ti-7 (110.5 MPa) underpredicts the true SCC threshold. Thus, a threshold stress value of 50 percent of the actual at-temperature yield strength for both Ti-7 and Ti-24 is assumed for these calculations.

Where used: Section 5.5 and Attachment IV.

3.2.13 Ti-2 and commercially-pure titanium are assumed to be analogous to Ti-7.

Rationale– Per ASTM B265-99 (1999 [DIRS 132376], Table 1) and equivalently, ASME (2001 [DIRS 158115], Section II, Part B, SB-265, Table 1), the tensile properties of Ti-7 and commercial purity Ti-2 are equivalent. Also, per ASTM B265-99 (1999 [DIRS 132376], Table 1), the allowable room temperature yield strength for Ti-2 and Ti-7 varies from a minimum of 275 MPa to a maximum of 450 MPa. For annealed material, this yield strength range depends primarily on orientation and on interstitial element content, which is limited by specification to a maximum of 0.25 percent oxygen, 0.03 percent nitrogen and 0.08 percent carbon. The significant effect of oxygen on yield strength at temperatures below about 300°C is readily evident (Dutton 1996 [DIRS 174750], Figure 2). Similarly, low-temperature creep strength is controlled by these same interstitials through a process involving thermally activated overcoming of interstitial impurity atoms by dislocations (Dutton 1996 [DIRS 174750], p. 7). Since both yield strength and creep strength in higher purity and commercial purity titanium are controlled to a significant extent by interstitial element content, a subset of low temperature creep literature data were selected for further analysis from available results for commercial or higher purity titanium with reported yield strengths approximately within the allowable range for Ti-2 and Ti-7.

Where used: Section 5.3 and Attachment I.

3.2.14 Titanium Grade 5 (Ti-6Al-4V) is assumed to be analogous to Ti-24.

Rationale–Per ASTM B265-99 (1999 [DIRS 132376], Table 1) and equivalently, ASME (2001 [DIRS 158115], Section II, Part B, SB-265, Table 1), the tensile properties of Ti-5 and Ti Grade 24 are equivalent. Also, per ASTM B265-99 (1999 [DIRS 132376], Table 1), the allowable room temperature yield strength for Ti-5 and 24 must exceed a minimum of 828 MPa. However, unlike commercial purity titanium, the yield strength of Ti-5 and 24 are dependent primarily on the addition of the alloying elements aluminum (4-6 percent) and vanadium (3.5-4.5 percent) although interstitial impurities such as oxygen also contribute to a lesser extent. In addition to the major alloying elements, aluminum and vanadium, Ti-24 also has a small amount of palladium (0.04-0.08 percent) added for improved localized corrosion resistance. This higher strength class of alloys is commonly referred to as Ti-6-4 or Ti-6Al-4V. In addition to Ti-24 which has a maximum allowable interstitial content of 0.20 percent oxygen, 0.05 percent nitrogen and 0.08 percent carbon, Ti-29 (which contains 0.08-0.14 ruthenium in place of palladium) is being considered as a lower cost, more readily available alternate for Ti-24. Because Ti-29 has a lower maximum allowable interstitial element content, (0.13 percent oxygen,

0.03 percent nitrogen and 0.08 percent carbon), it has a slightly lower allowable room temperature yield strength of 759 MPa and it is referred to as an extra low interstitial (ELI) grade. However, the measured creep responses of the normal interstitial level grades and the ELI grades of Ti-6Al-4V are similar (Odegard and Thompson 1974 [DIRS 174750], p. 1,211) and thus it is assumed in this calculation that the creep responses of Ti-5, Ti-24 and Ti-29 are equivalent.

Where used: Section 5.3 and Attachment I.

3.2.15 The creep activation energy for Ti-7 and Ti-24 is assumed to be 30 kJ/mol.

Rationale–Change in creep rate (or creep strain) due to increase in temperature predicted assuming creep activation energy of 30 kJ/mol is compared with experimental results by Kiessel and Sinnott (1953), Figure 12 [DIRS 174853]. Comparison (shown in Figure I-3) indicates that assumed value of 30 kJ/mol provides a good approximation of temperature effect.

Where used: Attachment I.

3.2.16 The Tresca yield criterion with perfectly plastic post-yield behavior is used for titanium.

Rationale–Tresca criterion is very similar to the von Mises criterion, commonly used for metals. The von Mises criterion predicts that the pure-shear yield stress is approximately 15 percent greater than that predicted by the Tresca criterion. Although titanium exhibits hardening when strained beyond yield, the hardening rate is relatively small (BSC 2004 [DIRS 169753]); thus, in the calculations reported here, for time independent behavior, titanium was represented as a perfectly plastic material.

Where used: Sections 5.2.1, 5.4 and 5.5.

3.2.17 The invert of the emplacement drift is assumed to be rigid in the analysis of drip shield creep deformation.

Rationale–Deformability of the invert under conditions when the drip shield is covered with the rubble will have a second order effect on creep deformation of the drip shield. If the drip shield is confined from all sides by the rubble, deformability of approximately 0.8 m thick crushed tuff in the invert will not significantly affect the loads on the drip shield or its deformation.

Where used: Sections 5.2.3 and 5.4.

INTENTIONALLY LEFT BLANK

4. USE OF COMPUTER SOFTWARE

4.1 QUALIFIED COMPUTER SOFTWARE

The controlled and baselined software, FLAC3D, used in analysis of time-dependent deformation and stress relaxation of the drip shield in the calculation reported in this document is identified in Table 4-1, including the software tracking number, version, operating environment and range of use. Table 4-1 also includes a discussion of why the software was selected and describes any limitations on outputs from the software. FLAC3D is appropriate for the applications used in this analysis and is consistent with its intended use. It was obtained from Software Configuration Management in accordance with LP-SI.11Q-BSC. FLAC3D was used only within the range of its validation, as specified in the software qualification documentation, and in accordance with LP-SI.11Q-BSC. The input and output files for this calculation have been submitted to the Technical Data Management System as noted in Section 5.6.

Table 4-1. List of Qualified Software Supporting the Calculations

Software Title/Version	Software Tracking Number	Operating Environment (Platform/Operating System)	Brief Description of Software (Range of Use/Selection/Limitations)
FLAC3D V2.1 (BSC 2002 [DIRS 161947])	10502-2.1-00	PC/Windows 2000	FLAC3D was used for creep and stress relaxation analysis of the drip shield. FLAC3D was selected because of its capabilities to accurately model visco-elasto-plastic deformation of solids, as well as the mechanical interaction of solid bodies when they contact each other. There are no known limitations on outputs. FLAC3D was used only within the range of its validation as specified in the Software Implementation Report (BSC 2002 [DIRS 168821])

4.2 OTHER SOFTWARE

TrueGrid V2.2.0b (XYZ Scientific Applications, Inc.) is used in this calculation solely to mesh geometric graphic representations of the domain. Thus, the use of TrueGrid V2.2.0b is exempt from the requirements defined in LP-SI.11Q-BSC (Section 2.1.2). The mesh is created on the HP 9000 series UNIX workstation (Operating System HP-UX 11.00) identified with YMP tag number 150689, and located in Las Vegas, Nevada.

In addition to the above item, the standard functions of commercial off-the-shelf software, including both Microsoft Excel 97 SR-2 and Mathcad V11.2a, were used. These software items were used to perform support calculation activities in Section 5, and associated Attachments. Microsoft Excel 97 SR-2 and Mathcad V11.2a were run on personal computers with a Pentium microprocessor and Microsoft Windows 2000 operating system. Microsoft Excel 97 SR-2 and Mathcad V11.2a are exempted software applications in accordance with LP-SI.11Q-BSC, Section 2.1.6.

INTENTIONALLY LEFT BLANK

5. CALCULATION

5.1 INTRODUCTION

Figure 5.1-1 illustrates the major components of the engineered barrier system (EBS) in a typical emplacement drift. The major EBS components are the waste package, the drip shield, and the fuel rod cladding, (The cladding is not shown in Figure 5.1-1.) These components provide barriers to the release of radionuclides from the EBS into the unsaturated zone. The effectiveness of these barriers is potentially compromised by the direct effects from an earthquake, including vibratory ground motion, fault displacement, rockfall induced by ground motion or other effects. Other, non-seismic mechanical effects could include rockfall resulting from time-dependent degradation of the emplacement drift. The effectiveness of these barriers also is potentially compromised by indirect effects after an earthquake, including changes in seepage, temperature and relative humidity, if an emplacement drift collapses during a low-probability earthquake. Stability of the drip shield for the different loading conditions expected during the regulatory period was analyzed; the results are summarized in *Mechanical Assessment of the Drip Shield Subject to Vibratory Motion and Dynamic and Static Rock Loading* (BSC 2004 [DIRS 169753]). Only the short-term mechanical behavior of the titanium structure of the drip shield was considered in those calculations. Time-dependent deformation and relaxation of impact dent-induced residual stresses of the titanium structure or plates were not assessed. Because of the long duration of the regulatory period and the tendency of titanium to creep at low temperatures (Dutton 1996, Section 2 [DIRS 174750]), creep of the drip shield subject to static load by the rubble formed by the caved rock blocks can affect the stability and structural integrity of the drip shield. In addition, residual tensile stresses in the drip shield after impact and denting by large rock blocks, which can contribute to stress corrosion cracking of the drip shield plates, will decay (relax) as a function of time. This potential residual stress reduction will reduce the potential for stress corrosion cracking. The time-dependent effects of deformation and stress relaxation of the drip shield titanium components are analyzed and reported in this document. Creep deformation of the drip shield structure for a period of 10,000 years, and its associated stability, were analyzed for six rubble load realizations, and results reported in Section 5.4. The relaxation of impact dent-induced residual stresses in the drip shield plates as a function of time is analyzed for different estimated creep equations of Ti-7 plates and is discussed in Section 5.5.

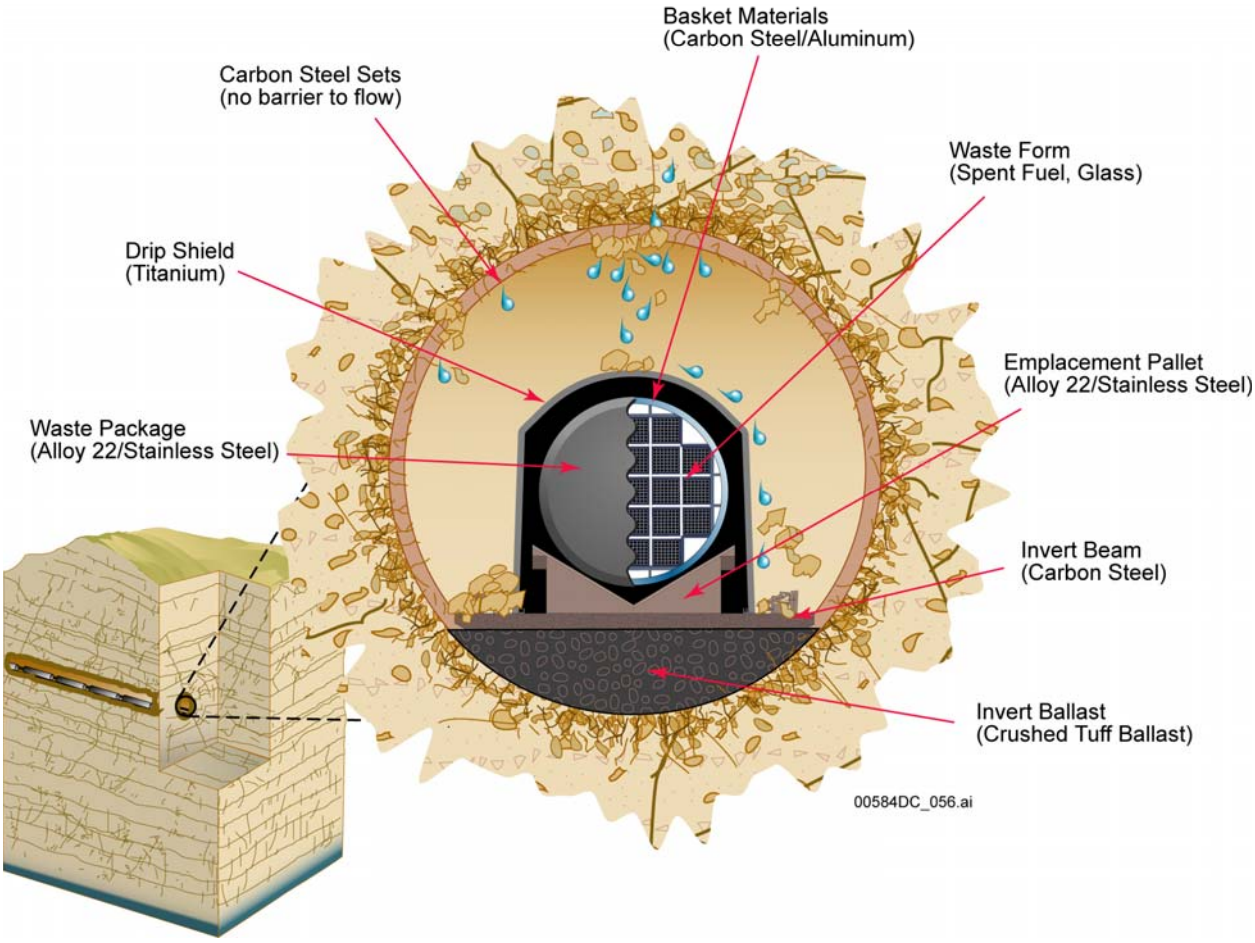

Figure 5.1-1. Schematic Diagram of the Engineered Barrier System Components in a Typical Emplacement Drift

5.2 INPUT PARAMETERS

The input parameters used for this study include:

- Design specifications,
- Material properties, and
- Rubble loads on the drip shield.

These parameters are summarized in Table 5.2-1 and are described in the following subsections.

Table 5.2-1. Input Parameters

Input Parameters	Value	Source	Application
Design Specifications:			
Detailed dimensions for drip shield	See reference drawings	BSC 2005 [DIRS 173303], Directory, Interlocking Drip Shield, LA Drip Shield Assembly Drawings	Sections 5.4 and 5.5 and Attachment III
Titanium Material Properties:			
Density (at RT), SB-265 Ti-7 [UNS R52400]	4520 kg/m^3	DTN: MO0003RIB00073.000 [DIRS 152926]; Table S04197_001, p.1	Sections 5.4 and 5.5 and Attachments II, III and IV
Yield strength (at 150ºC), SB-265 Ti-7 [UNS R52400]	176 MPa	ASME 2001 [DIRS 158115]; Section II, Part D, Table Y-1	Sections 5.4 and 5.5 and Attachments I, II, II and IV
Yield strength (at RT), SB-265 Ti-7 [UNS R52400]	276 MPa	ASME 2001 [DIRS 158115]; Section II, Part D, Table Y-1	Sections 5.5 and Attachments I and IV
Poisson's ratio (at RT), SB-265 Ti-7 [UNS R52400]	0.32	DTN: MO0003RIB00073.000 [DIRS 152926]; Table S04197_001, Section "Mechanical Properties"	Sections 5.4 and 5.5 and Attachments II, III and IV
Modulus of elasticity (at 150ºC), SB-265 Ti-7 [UNS R52400]	101 GPa	DTN: MO0003RIB00073.000 [DIRS 152926]; Table S04197_001, p.3	Sections 5.4 and 5.5 and Attachments II, III and IV
Modulus of elasticity (at RT), SB-265 Ti-7 [UNS R52400]	107 GPa	DTN: MO0003RIB00073.000 [DIRS 152926]; Table S04197_001, p.3	Section 5.5 and Attachment IV
Density (at RT), SB-265 Ti-24 [UNS R56405]	4430 kg/m^3	ASM International. 1990 [DIRS 141615]; p.620	Sections 5.4 and 5.5 and Attachments II, III and IV
Yield strength (at 150ºC), SB-265 Ti-24 [UNS R56405]	683 MPa	Assumption 3.2.11	Sections 5.4 and 5.5 and Attachments II, III and IV
Yield strength (at RT), SB-265 Ti-24 [UNS R56405]	828 MPa	ASME 2001 [DIRS 158115]; Section II, Part B, SB-265, Table 1	Section 5.5 and Attachments I and IV
Poisson's ratio (at RT), SB-265 Ti-24 [UNS R56405]	0.34	ASM International. 1990 [DIRS 141615]; p.621	Sections 5.4 and 5.5 and Attachments II, III and IV
Modulus of elasticity (at 150ºC), SB-265 Ti-24 [UNS R56405]	108 GPa	BSC 2004 [DIRS 168993]; Section 5.1.1	Sections 5.4 and 5.5 and Attachments II, III and IV
Modulus of elasticity (at RT), SB-265 Ti-24 [UNS R56405]	113.8 GPa	ASM International 1990 [DIRS 141615], p.621	Section 5.5 and Attachment IIV

Table 5.2-1. Input Parameters (Continued)

Input Parameters	Value	Source	Application
Contact Friction:			
Metal-to-rock	0.4	Assumption 3.2.2	Sections 5.4 and 5.5 and Attachment III
Rubble Loads on the Drip Shield:			
Six load realizations of the rubble	See source file "final drip shield quasi-static pressure.xls" for data	DTN MO0407MWDDSLCR.000 [DIRS 170873]	Section 5.4 and Attachment III

NOTE: There are discrepancies between some of the numbers listed in this Table and the actual numbers used in the input files for the calculations. The differences, which are consequences of rounding errors, are almost always less than 1 percent. The effects of these differences on the calculation results are inconsequential.

Normal and shear stiffnesses (equal to 914 GPa/m) of the contacts between the drip shield and the invert, and the drip shield and the pallet were also used in the calculations as the input parameters of the calculation. In this case, these parameters do not represent actual material properties. They are numerical tools used to generate the contact force which prevents overlapping of the contacting surfaces. Therefore it is only important that contact stiffness is sufficiently large to make contact overlap insignificant compared to other dimensions of the problem. Calculation shows that for average vertical pressure on the drip shield of approximately 150 kPa (listed in Table 5.2-2) and normal stiffness of 914 GPa/m, the overlap at the contact at the drip shield base would be of the order of 10 μm.

5.2.1 Design Specifications

The development of the numerical representation of the drip shield is based on the current design configuration (BSC 2004 [DIRS 168275]). The dimensions were obtained from the detailed design drawings (BSC 2005 [DIRS 173303]).

5.2.2 Titanium Material Properties

The material properties used in the numerical analyses include those for SB-265 Ti-7 (UNS R52400) and SB-265 Ti-24 (UNS R56405). Titanium was represented as a visco-elasto-plastic material. The material properties of titanium, listed in Table 5.2-1, include elastic properties (i.e., Young's modulus and Poisson's ratio) and the yield stress as a plasticity property. The elastic properties that were used in the calculations are bulk, K, and shear, G, moduli, calculated (Timoshenko and Goodier 1970 [DIRS 121096], pp. 10 and 11) as follows:

$$K = \frac{E}{3(1-2\nu)}$$
$$G = \frac{E}{2(1+\nu)} \qquad \text{(Eq. 5.2-1)}$$

where E is the Young's modulus, and ν is the Poisson's ratio. The Tresca yield criterion was used to represent the plastic deformation of titanium (Assumption 3.2.16). This criterion is very similar to the von Mises criterion, commonly used for metals. The von Mises criterion predicts that the pure-shear yield stress is approximately 15 percent greater than that predicted by the

Tresca criterion. The Tresca yield criterion is a special case of the Mohr-Coulomb yield criterion, when the friction angle is zero. Because FLAC3D is often used for simulation of geomaterials, it also has tension cut-off superimposed to the shear criterion (i.e., Mohr-Coulomb shear criterion). The default value (if not specified) for the tensile strength (i.e., tension cut-off) in FLAC3D is zero. The tensile strength of the metals is governed by the shear failure only. The tension cut-off does not exist. Therefore, the tensile strength of titanium (i.e., the tension cut-off) was set to a large value, greater than the yield strength of titanium. Although titanium exhibits hardening when strained beyond yield, the hardening rate is relatively small (BSC 2004 [DIRS 169753], Section 5.2.1.2.3); thus, in the calculations reported here, titanium was represented as a perfectly plastic material (Assumption 3.2.16).

Creep properties, which characterize the viscous behavior of titanium, and their derivation are discussed in more detail in Section 5.3 and Attachment I.

5.2.3 Contact Friction

The drip shield rests by its own weight on the crushed tuff in the invert of the emplacement drift. The only force that resists sliding of the drip shield on the invert is the frictional force. In the numerical representation, the invert is a rigid flat surface (Assumption 3.2.17). The friction coefficient of 0.4 (Assumption 3.2.2) is assigned to the interface between the invert and the drip shield.

5.2.4 Rubble Loads on the Drip Shield

The rock block shapes in the lithophysal rock mass and the manner in which they fall and compact around the drip shield is a random process. The rubble will consist of blocks of irregular shapes and a size distribution with a mean block size of approximately 0.2 m (BSC 2004 [DIRS 166107], Section 6.4). The static load of the rubble will be transferred to the drip shield through Hertzian contacts among the rocks and between the rocks and the drip shield (a large number of localized contacts that are nearly point loads).

The distribution of the point loads in the cross-Section and along the drip shield, as well as their magnitudes will vary significantly. This is illustrated by the distribution of the loads shown in Figure 5-33 of *Mechanical Assessment of the Drip Shield Subject to Vibratory Ground Motion and Dynamic and Static Rock Loading* (BSC 2004, [DIRS 169753]), obtained from 6 realizations of rock collapse simulation. There is also almost 50 percent variability of the average drip shield applied rubble pressures calculated for different realizations (Table 5.2-2). The pressure variability is due to the stochastic nature of the drift degradation (i.e., formation of the rock blocks of irregular shapes and different sizes, and their fall and compaction). The average pressures on the top and the sides of the drip shield for 6 realizations are listed in Table 5.2-2. Although obtained from a two-dimensional model, the pressure distribution for each realization is representative of the load on the drip shield for a finite length along the drip shield. The exact correlation between the results of the two-dimensional model and the actual three-dimensional load distribution cannot be established. However, it is reasonable to apply the pressure distribution from a particular realization over a drip shield axial length approximately equal to the average block size (i.e., 0.2 m as discussed in Section 6.4.2.5.3 of Drift Degradation Analysis BSC 2004 [DIRS 166107]). Considering the entire length of one drip shield (5.81 m) (BSC 2005

[DIRS 173303]), or even spacing of the bulkheads and support beams (1.07 m) (BSC 2005 [DIRS 173303]), compared to the length over which the loads of one realization are representative (~0.2 m), the average load (represented as a continuous line load in Figure 5.2-1) of a number of different realizations controls the overall stability of each structural frame and the drip shield.

Table 5.2-2. Average Pressure Values on the Drip Shield for Quasi-Static Drift Degradation (0.2 m Rock Size)

Realization	Pressure (kPa)		
	Left	Top	Right
1	41.54	108.92	58.76
2	19.15	147.07	19.33
3	31.35	154.80	6.69
4	57.23	129.76	128.82
5	69.69	112.73	105.43
6	32.97	113.87	52.19
Average	41.99	127.86	61.87

Source: DTN MO0407MWDDSLCR.000 [DIRS 170873], file "final drip shield quasi-static pressure.xls"

To account for variability in the loads (in one cross-Section and between different cross-sections), a drip shield stability analysis was conducted for all six realizations in which the pressure in a particular segment (Figure 5.2-1) is obtained from a two-dimensional model and acts along entire length of the drip shield that is analyzed in the three-dimensional model. If stability of the drip shield is demonstrated for all 6 realizations using this line-loading application, then it is also certain that the drip shield would be stable for the combined or average load resulting from those 6 realizations.

For the purpose of this calculation, the pressure distribution along the drip shield surface is discretized over 30 segments of approximately equal length, as indicated in Figure 5.2-1. Note that the even-numbered segments are omitted from Figure 5.2-1 to improve visibility. The pressure distribution does not vary in the longitudinal (z) direction in this calculation.

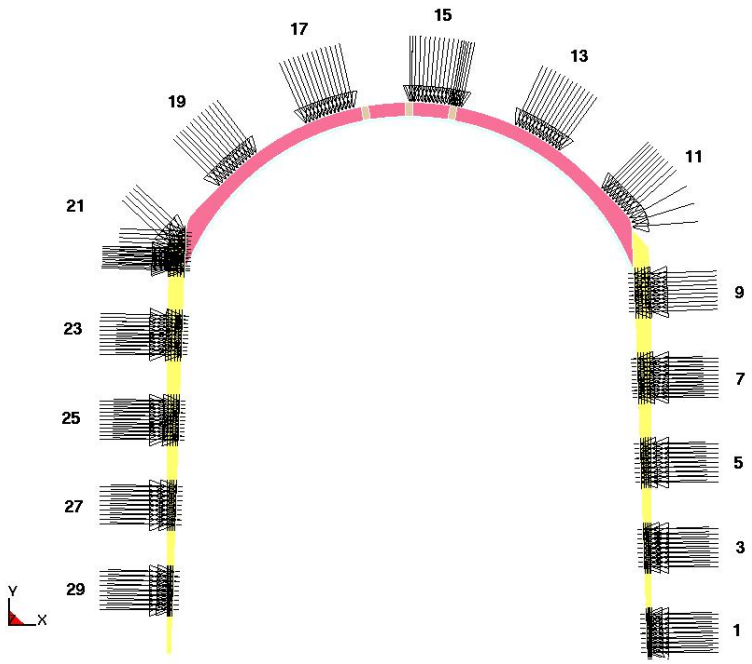

Source: BSC 2004 [DIRS 170791], Figure 5.

NOTE: The pressure applied to even numbered segments is removed for purposes of clarity.

Figure 5.2-1. Application of the Static Pressure of the Rubble on the Drip Shield

The six load realizations of the rubble on the drip shield were calculated from the analysis that simulated collapse of the emplacement drift and settlement of the rubble around the drip shield, coupled with deformation of the drip shield. The coupled analysis was two-dimensional. The drip shield was represented as a two-dimensional structure (i.e., no variation of geometry in the direction normal to the calculation plane), calibrated to the true bending and axial stiffnesses of the drip shield. Coupled three-dimensional analysis of the emplacement drift collapse and deformation of the drip shield was beyond the computational capabilities available at the time the calculation was conducted. One consequence of the two-dimensional approximation is that the rubble load variation along the drip shield could not be captured; therefore, the pressures were assumed to be uniform along the drip shield. The loads were then applied on a detailed, three-dimensional representation of the drip shield for analysis of drip shield stability. Loads applied to the drip shield are the result of the coupled mechanical interaction between the rubble and the drip shield—in other words, there is "sharing" of the rubble gravitational load between the drip shield and the surrounding rubble that depends on the deformability of the drip shield and the ability of the rubble to carry load via arching to the tunnel invert and walls. The deformability of the drip shield has a significant effect on the loads the rubble exerts on the drip shield. For example, a more compliant drip shield structure would cause more stress arching and load "sharing" in the rubble and, consequently, less load on the drip shield. A stiff drip shield, on the other hand, would be subjected to greater rubble loads. Although short-term (i.e., no creep) stability of the drip shield was analyzed in the uncoupled three-dimensional calculation, in which the loads were applied as dead loads, those loads were calculated from the coupled analysis that accounted for deformation of the drip shield (see *Structural Stability of a Drip Shield Under Quasi-Static Pressure* (BSC 2004 [DIRS 170791]). The initial quasi-static rubble

load, used in the short-term deformation of the drip shield, will change as a result of creep deformation of the drip shield. Evolution of those loads could be assessed in a coupled analysis of deformation of the rubble and creep of the drip shield. Instead, in a simple approach, the initial rubble pressures were applied as dead loads, and interaction between the drip shield and rubble was accounted for by using elastic springs to represent the reactive pressure of the rubble induced by creep deformation of the drip shield (Section 5.4.1.3).

5.3 CREEP PROPERTIES OF TITANIUM

The drip shield plates will be constructed of Ti-7. The main structural elements (i.e., the bulkheads and the support beams) will be constructed of Ti-24, which is a higher strength alloy. Creep equations at different temperatures were developed for the Ti-7 and Ti-24 (Attachment I) by fitting the power law shown in Equation (5.3-1) to published experimental creep testing results (Drefahl et al. 1985, Figures 3 and 10, [DIRS 174820]; Kiessel and Sinnottt 1953, Figure 12 [DIRS 174853]; Odegard and Thompson 1974, Figure 3 [DIRS 174818]; and Thompson and Odegard 1973, Figure 4 [DIRS 174852]) for commercially-pure, titanium Grade 2 and Grade 5 (Ti-6Al-4V) (Assumptions 3.2.13 and 3.2.14). The published experimental data are obtained from outside sources that are not established facts. They are considered as suitable for their intended use based on the reasoning provided in Table 5.3-1 based on LP-3.12Q-BSC, Section 5.2, Paragraph [12], Bullet number 8.

An expression for the creep strain of titanium at constant stress can be written as follows (Dutton 1996 [DIRS 174750], Section 5.1),

$$\varepsilon = A\sigma^n t^m \qquad \text{(Eq. 5.3-1)}$$

the creep rate (i.e., derivative of creep strain with respect to time), which is a form used to specify creep of a material in FLAC3D, can also be written equivalently (Assumption 3.2.10) in the following form:

$$\dot{\varepsilon} = B\sigma^n t^p \qquad \text{(Eq. 5.3-2)}$$

where $B = mA$, and $p = m - 1$.

Different creep equations were used in the analysis of drip shield creep under the static load of rubble (Section 5.4) and in the analysis of relaxation of residual stresses after impact by the rock block (Section 5.5). The reason for doing so is that creep equations that overestimate creep deformation (i.e., predicting large creep strains and deformations) also overpredict rate of stress relaxation in impact dent-induced residual stress relaxation analysis (i.e., predicting relatively fast stress relaxation). Conversely, creep equations that underpredict rate of residual stress relaxation (i.e., predicting slow stress relaxation) also underpredict creep deformation (i.e., predicting relatively small creep strains and deformation). The equations used in the analysis of drip shield creep deformation and stability are discussed in Section 5.3.1; the equations used in the analysis of impact dent-induced residual stress relaxation are discussed in Section 5.3.2.

Table 5.3-1. Qualification of Titanium Creep Data Sources

Data Source			
Drefahl et al. (1985), Figures 3 and 10, [DIRS 174820]	Availability of corroborating inputs: The results obtained from this source were corroborated with results by Teper (1991) [DIRS 174819] and Kissel and Sinnott (1953) [DIRS 174853].	Prior uses of the inputs: Data published in this article were used and referenced in the report by Dutton (1996) [DIRS 174750].	Conservative and bounding: The creep equations used in the calculations (either creep deformation or stress relaxation) are selected to be conservative or to bound response in the particular application.
Dutton (1996) [DIRS 174750]	Reliability: The information used (i.e., 15 percent creep strain is required for creep failure of titanium alloys) is based on experimental results published in an Atomic Energy of Canada Limited (AECL) report (number 11544). AECL is a prestigious institution in Canada so that results obtained by scientists working for it and published in its reports are reliable.	Qualification: The information was generated and published by R. Dutton, who is famous in the scientific community for his scholarly researches on titanium metal and its alloys. Based on the qualifications of the researcher and the reputation of the organization generating data (i.e., Atomic Energy of Canada Limited), the use of this information in this document is appropriate.	
Kiessel and Sinnott, Figure 12 (1953) [DIRS 174853]	Reliability: The information used is in the article published in a peer reviewed journal (*Journal of Metals*).	Prior uses of the inputs: Data published in this article were used and referenced in the report by Dutton (1996) [DIRS 174750].	
Odegard and Thompson (1974), Figure 3 [DIRS 174818]	Reliability: The information used is in the article published in a peer reviewed journal (*Metallurgical Transactions)*.	Prior uses of the inputs: Data published in this article were used and referenced in the report by Dutton (1996) [DIRS 174750].	
Thompson and Odegard (1973) , Figure 4 [DIRS 174852]	Reliability: The information used is in the article published in a peer reviewed journal (*Metallurgical Transactions)*.	Prior uses of the inputs: Data published in this article were used and referenced in the report by Dutton (1996) [DIRS 174750].	Conservative and bounding: Published data are for Ti-5Al-2.5Sn that creeps more than Ti-24. The creep equations fitted to the results published in this article overestimate creep deformation of the Ti-24 used for the drip shield.

5.3.1 Equations for Analysis of Creep of the Drip Shield

A power law formulation was used to represent the creep constitutive material behavior of Ti-7 and Ti-24. Different coefficients for the power law were derived (Attachment I, Equations I-25 and I-27) by fitting the power law to experimental creep test results for titanium. The equations that predict creep deformation greater than that measured in laboratory experiments at relevant stress levels are used in the simulation of drip shield creep. Titanium creep at 150°C was assumed (Assumption 3.2.4). The following relation [also given in Equation (I-25)] represents the creep strain rate of Ti-7 in the calculations[1]:

$$\dot{\varepsilon} = 2.87 \cdot 10^{-21} \sigma^{8.81} t^{-0.72} \quad \text{(Eq. 5.3-3)}$$

The creep rate of Ti-24 [also given in Equation (I-27)] is represented by

$$\dot{\varepsilon} = 8.51 \cdot 10^{-36} \sigma^{12.15} t^{-0.75} \quad \text{(Eq. 5.3-4)}$$

In creep equations throughout this document, unless noted otherwise, the creep rate, $\dot{\varepsilon}$, is in 1/h, stress, σ, is in MPa, and time, t, is in h.

Only the primary and secondary phases of the creep deformation were simulated as represented by Equations 5.3-3 and 5.3-4. These equations show a monotonically decreasing creep rate as a function of time. Although tertiary creep is not explicitly represented by these equations, the onset of tertiary creep, considered to coincide with localized drip shield rupture or a drip shield collapse, is assumed to occur when approximately 10 percent creep strain is reached (Assumption 3.2.9). The accumulated creep strains throughout the drip shield structure at the end of simulation (at 10,000 years) are compared with this tertiary creep threshold. If the strains are less than the threshold everywhere, the structure is considered to be stable; otherwise, it is considered to be unstable.

5.3.2 Equation for Analysis of Impact Dent-Induced Residual Stress Relaxation

A potential rock block impact into the drip shield was previously analyzed (BSC 2005 [DIRS 174052]) for non-time-dependent titanium properties assuming a drip shield temperature of 150ºC. Even if the drift collapses immediately after the closure of the repository, resulting in a rubble-covering of the drip shield, the temperature of the drip shield will be equal to or greater than 150ºC for only approximately 350 years, which is about 3.5 percent of the total duration of the regulatory period (Assumption 3.2.4). The decreased temperature of the drip shield has two competing effects on the time required for impact-related residual stresses to relax below the assumed stress corrosion cracking threshold (Assumption 3.2.12): (a) it decreases the stress relaxation rate, and (b) it increases the yield strength and, thus, the stress-corrosion cracking threshold. The simple calculations of stress relaxation in a beam of uniform cross-section, presented in Attachment IV, indicate that, at lower temperatures, the time required for residual

[1] There are discrepancies between some of the numbers in the equations listed in Section 5.3 and Attachment I and the actual numbers used in the input files for the calculations. The differences, which are consequences of rounding errors, are almost always less than 1 percent. The effects of these differences on the calculation results are inconsequential.

stresses to relax below the assumed stress corrosion cracking threshold is shorter than at higher temperatures. The creep equations (below) were developed and calculations of stress relaxation (Section 5.5) were conducted for two temperatures (i.e., RT and 150°C), but the results obtained at 150°C provide a longer estimate of the stress relaxation time.

The following equations (which can also be found as Equations I-8 and I-9 of Attachment I) approximate the creep of commercially-pure titanium (Ti-2), which is assumed to be mechanically-analogous to Ti-7 (Assumption 3.2.13), at RT, measured in constant-stress creep tests lasting 27 years. As described in Attachment I, these two equations provide upper and lower bounds to the creep strains at all stress levels.

$$\varepsilon = 4.87 \cdot 10^{-24} \sigma^{8.81} t^{0.28} \quad \text{(Eq. 5.3-5)}$$

$$\varepsilon = 2.86 \cdot 10^{-30} \sigma^{11.48} t^{0.28} \quad \text{(Eq. 5.3-6)}$$

Equations (5.3-7) and (5.3-8) (also listed as Equations (I-13) and (I-14) in Attachment I) which predict creep strain as a function of time and stress level at a temperature of 150ºC, are estimated using the methodology described in Attachment I. These equations correspond to their RT equivalents given in Equations (5.3-5) and (5.3-6), respectively:

$$\varepsilon = 2.15 \cdot 10^{-22} \sigma^{8.81} t^{0.28} \quad \text{(Eq. 5.3-7)}$$

$$\varepsilon = 1.26 \cdot 10^{-28} \sigma^{11.48} t^{0.28} \quad \text{(Eq. 5.3-8)}$$

The creep rate coefficients for Ti-7, which correspond to Equations (5.3-5) through (5.3-8), are listed in Table 5.3-2.

Table 5.3-2. Creep Rate Coefficients for Ti-7

Case	Equation	B	n	p
RT-1	(5.3-5)	$1.36 \cdot 10^{-24}$	8.81	-0.72
RT-2	(5.3-6)	$8.00 \cdot 10^{-31}$	11.48	-0.72
150ºC-1	(5.3-7)	$6.02 \cdot 10^{-23}$	8.81	-0.72
150ºC-2	(5.3-8)	$3.53 \cdot 10^{-29}$	11.48	-0.72

The following equation is developed (Attachment I, Equation I-19) as an estimate of Ti-24 creep strain as a function of applied stress and time at RT:

$$\varepsilon = 7.31 \cdot 10^{-38} \sigma^{12.15} t^{0.25} \quad \text{(Eq. 5.3-9)}$$

The creep strain of Ti-24 at 150ºC is approximated by the following equation (Attachment I, Equation I-21):

$$\varepsilon = 3.22 \cdot 10^{-36} \sigma^{12.15} t^{0.25} \quad \text{(Eq. 5.3-10)}$$

The creep rate coefficients for Ti-24, which correspond to Equations 5.3-9 and 5.3-10, are listed in Table 5.3-3.

Equation (5.3-9) was obtained based on experimental results obtained on Ti-6Al-4V, which is similar to Ti-24 (Assumption 3.2.14). However, it generally overpredicts creep deformation measured in the experiments. Consequently, creep Equation (5.3-9) were used in the calculation of overall drip shield creep under static loads. However, since the issue of enhanced stress corrosion cracking of the drip shield is concerned with the Ti-7 plates, creep residual stress accumulation and relaxation in the structural elements (i.e., bulkheads and support beams) designed of Ti-24 will not have a significant effect on stress relaxation in the plates.

Table 5.3-3. Creep Rate Coefficients for Ti-24

Case	Equation	B	n	p
RT	(5.3-9)	$1.83 \cdot 10^{-38}$	12.15	-0.75
150ºC	(5.3-10)	$8.06 \cdot 10^{-37}$	12.15	-0.75

5.4 CREEP DEFORMATION UNDER RUBBLE LOAD

For the drip shield to function as a shield for the waste packages against seepage water or mechanical load (either static or dynamic) resulting from rubble, it is essential that its structural integrity be maintained throughout the regulatory period. Collapse of the emplacement drift located in lithophysal rock units is expected when the drift is subjected to strong seismic ground motions that have peak ground velocity (PGV) greater than approximately 2 m/s. Consequently, the drip shield is expected to be completely or partially covered after such events by the rubble and subjected to the static load of the rubble on the top and along the sides of the drip shield. Collapse of the emplacement drift and the loads of rubble on the drip shield are investigated and reported in Section 6.4.2.5.4 of *Drift Degradation Analysis* AMR (BSC 2004 [DIRS 166107]). In this analysis, the rock mass was represented as an assembly of polygonal blocks that was calibrated to the stiffness and strength of the lithophysal rock mass. The results of the calculations (including the loads of rubble on the drip shield) are functions of a particular realization of the geometry of the blocks that compose the initially-intact rock mass surrounding the emplacement drift. The dimension and shape of the rock blocks are random in nature and controlled by the in situ fracture geometry of the rock mass. To investigate variability of load, six different realizations (Section 5.2.4) of initial rock block geometry were simulated, resulting in six different static loads on the drip shield. The analysis of "short-term" (i.e., not considering the creep of titanium) deformation and the stability of the drip shield for static load of the rubble demonstrated that the drip shield remains stable for all six load realizations [Section 6 of *Structural Stability of a Drip Shield under Quasi-Static Pressure* (BSC 2004 [DIRS 170791])]. The calculations indicate that the drip shield has an approximate safety margin against collapse of greater than 2.5 with respect to static load. The FLAC3D simulation begins by conducting the short-term static loading simulations for each of the six load realizations. Once the static equilibrium state is achieved under rubble loading, the creep constitutive material behavior of titanium is invoked for T-7 and Ti-24. The simulation is then run as a transient creep problem for the length of the 10,000 year period. During the simulation, the deformation of the drip

shield structure is recorded and examined to determine if excessive deformation or creep rupture leads to a loss of functionality as a seepage or mechanical shield.

Verification of the proper functioning of the FLAC3D code in representing the creep response of titanium is performed through comparison of the code output to the results of creep experiments on titanium rods. The power law fits representing Ti-7 and Ti-24 derived from laboratory uniaxial creep tests (Equations 5.3-3 and 5.3-4) are compared to FLAC3D simulations which exercise the creep constitutive laws via the numerical code. Attachment II shows that the agreement between the power law fits and the numerical implementation is very good (Figures II-1 and II-2).

5.4.1 Numerical Representation

5.4.1.1 Geometry

The geometry of the drip shield in the initial configuration is shown in Figure 5.4-1. Only one segment of the drip shield (associated with one frame formed by support beams and bulkhead) was included in the calculation due to the repetitive nature of the drip shield design. Different structural components are assigned different "group" names in the FLAC3D mesh and colored differently in the figure. The plates, designed of Ti-7, are group1, group2 and group7; the invert is group9; group11 represents the emplacement pallets. All other groups represent the load-bearing structural components designed of Ti-24. In the initial configuration, the drip shield rests on the invert under its own weight. The invert and the emplacement pallet are fixed and rigid in all calculations. Initially, the drip shield is not in contact with the two vertical, planar surfaces that represent the physical restraint of the emplacement pallet; however, sufficient deformation of the legs either under short-term static conditions or during creep can cause interaction between the drip shield and the emplacement pallet. Symmetry boundary conditions were imposed on the drip shield segment boundaries.

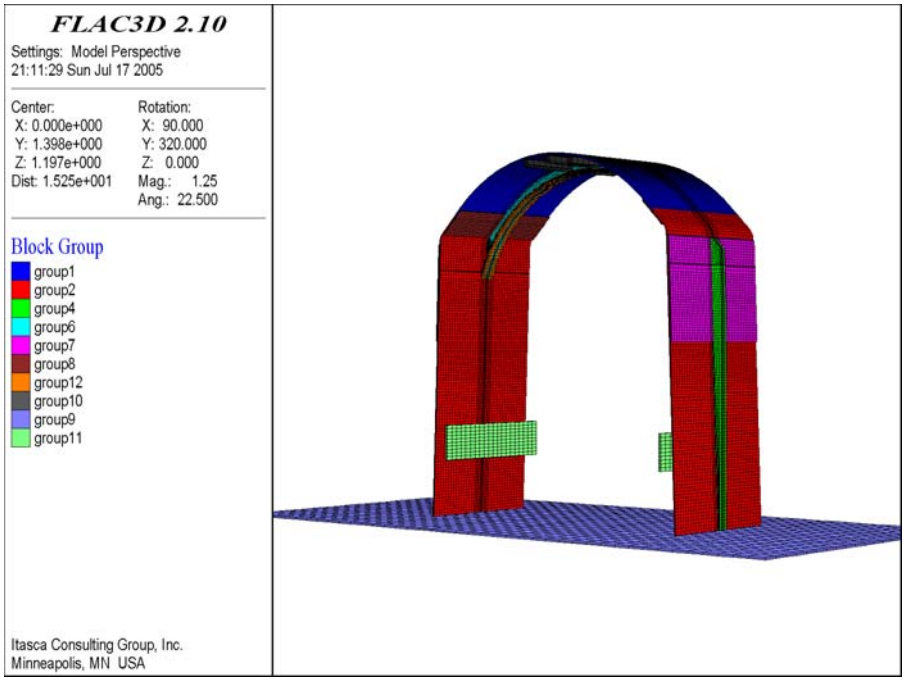

NOTE: The small, green vertical panels represent the emplacement pallet.

Figure 5.4-1. Geometry of the Numerical Representation of the Drip Shield Showing Groups of Elements Representing Different Parts of the Structure

In Figure 5.4-2, which shows the detail of drip shield crown, group1 is the drip shield plate 1, group6 and group12 represent the bulkhead, and group10 represents the longitudinal stiffeners. This mesh has two layers of elements per thickness of the plate, which is insufficient to accurately represent bending of the drip shield plates between the bulkheads. To investigate whether bending of the plates between the bulkheads and the support beams is the critical mode of deformation that could affect functionality of the drip shield, the effect of plate discretization was investigated (Attachment III) by conducting a simulation in which there were five elements per thickness of the drip shield plate. The majority of the calculations were carried out with a coarser mesh because: (a) the significant increase in simulation time for the refined mesh compared to that for the coarse mesh; (b) the same mode of deformation occurs for the drip shield for different discretizations (see Attachment III); (c) the extent by which the creep equations used exceed creep measured in laboratory tests (see Attachment I) is such that the mesh discretization effects do not appear to be significant; and (d) the large factor of safety (e.g., the creep strain at the onset of tertiary creep compared to the maximum predicted creep strains) of the results obtained with the coarse mesh (Section 5.4.3), again, makes the mesh discretization of lesser relative importance to the overall conclusions.

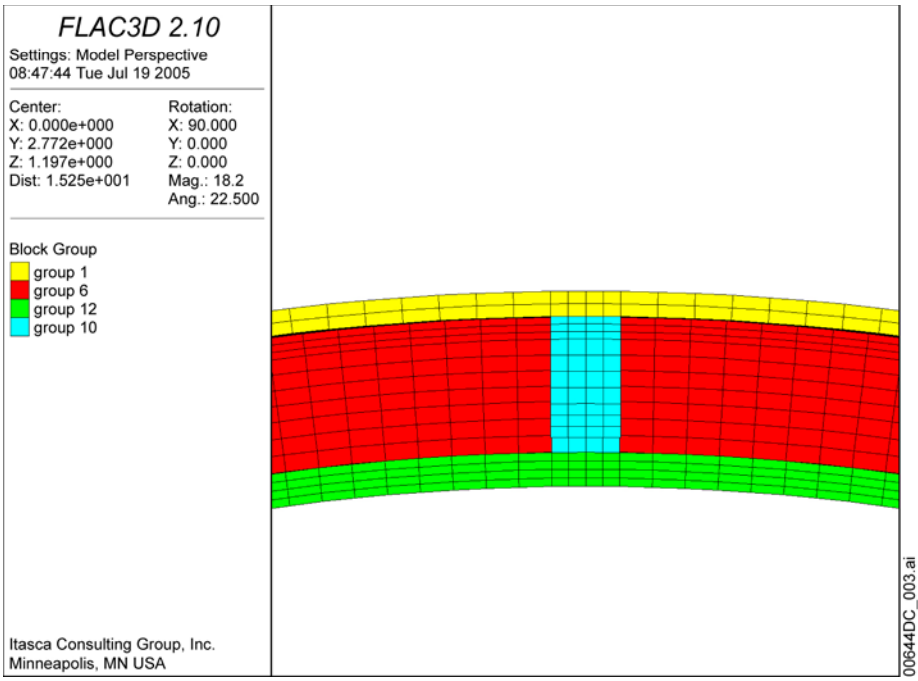

Figure 5.4-2. Geometry of the Numerical Representation of the Drip Shield Showing Groups of Elements Representing Different Parts of the Structure: Crown Detail

5.4.1.2 Stability Criterion

The stability of the structure and the potential for components of the drip shield entering a tertiary creep phase were assessed at the end of the simulation by inspection of the accumulated creep strain. The scalar measure of strain (because strain is a tensor) used in assessing the potential for entering the tertiary creep phase is

$$\varepsilon = \sqrt{\frac{4}{3} J_2(\varepsilon_{ij}^d)} = \sqrt{\frac{2}{3} \varepsilon_{ij}^d \varepsilon_{ij}^d} \qquad \text{(Eq. 5.4-1)}$$

where ε_{ij}^d is the deviatoric part of the strain tensor, and $J_2(\varepsilon_{ij}^d) = \varepsilon_{ij}^d \varepsilon_{ij}^d / 2$ (Equation (2.85) of Optional Features volume of FLAC3D manual, Itasca 2002 [DIRS 160331]) is the second invariant of the deviatoric strain. For a creep strain of ε^{cr} related to a uniaxial stress state, the measure in Equation (5.4-1) is equal to the creep strain (i.e., $\varepsilon = \varepsilon^{cr}$). The development of this scalar measure of creep strain is presented in Attachment V. The structure is considered stable if the creep strain measure does not exceed the threshold for onset of tertiary creep anywhere in the structure. The onset of tertiary creep is set at 10 percent (Assumption 3.2.9).

5.4.1.3 Interaction between the Drip Shield and the Rubble

The loads of the rubble on the drip shield are not simply the dead weight of the rubble, but are the consequence of the mechanical interaction between the drip shield and the rubble accumulated along the sides and on top of the drip shield. Due to the shear resistance of the rubble (mostly caused by friction among the rough rubble particles) coupled with the

deformation of the drip shield, some of the weight of the rubble located above the drip shield is transferred to the invert and the drift walls by stress arching through the rubble. Some of the loads on the sides of the drip shield are passive loads caused by lateral deformation of the legs of the drip shield under vertical load on the crown. These passive loads tend to provide a confinement to the legs of the drip shield, preventing lateral deformation or "leaning" of the structure. Six load realizations (Section 5.2.4) were calculated for static, short-term deformation of the drip shield. As the drip shield deforms during the creep of titanium, the loads will change (due to interaction with surrounding rubble). Deformation of the drip shield will alter both active and passive loads (pressures) of the rubble on the drip shield. The active pressure (when the rubble is moving toward the structure) will most likely decrease due to increased stress arching in the rubble. The passive pressure (when the structure is moving toward the rubble) will increase, in general. To account for the interaction between the drip shield and the surrounding rubble, and the change of load on the drip shield during creep, it is necessary, in general, to simulate concurrently (i.e., fully coupled) the three-dimensional deformation of the drip shield and the surrounding rubble. Because such an analysis would be very time consuming, two approximate sets of calculations were conducted. In the first, coupling between the drip shield and the rubble was not considered. The loads on the drip shield after static deformation were assumed to act as dead loads on the drip shield during creep deformation. The loads do not change, irrespective of the resulting creep deformation of the drip shield. As the drip shield deforms or translates in space, no reinforcement is provided back to the drip shield by the surrounding rubble. Clearly, such an approach is unrealistic resulting in very severe loading conditions. In the second approach, coupling between the drip shield and the rubble is represented in a simple fashion. The reactive pressures of the rubble, resulting from creep deformation of the drip shield, are generated and applied on the sides of the drip shield in locations where the drip shield is moving toward the rubble. The pressures on the crown of the drip shield do not change in this calculation, irrespective of the deformation of the drip shield. This approximation overestimates the vertical load on the drip shield, as the expected downward movement of the drip shield due to creep would tend to increase stress arching in the rubble and reduce the overall load of the rubble applied to the top of the drip shield. The pressures, generated by creep-related interaction between the drip shield and the rubble, were applied on the side of the drip shield (and superimposed on the initial pressures) only where the drip shield moved toward the rubble; elsewhere, the pressure did not change. The mechanical interaction between the rubble and the drip shield is represented by elastic springs (Figure 5.4-3) that act in compression only and are calibrated to simulate the approximate deformability of the rubble. The springs are connected to every node of the drip shield legs. The stiffness of the springs is calculated using the following relation:

$$k_n = E\,A / w \qquad \text{(Eq. 5.4-2)}$$

where E is the approximate Young's modulus of the rubble (taken to be 50 MPa in the calculations); w is the distance between the drip shield leg and the intact drift wall (assumed to be 2.5 m, Assumption 3.2.8); and A is the interacting drip shield surface area associated with the node. The effective elastic modulus of the rubble was estimated by conducting confined numerical compression tests of rubble generated during the six realizations of drift collapse and drip shield rubble loading (BSC 2004 [DIRS 166107], Section 6.4]). These numerical compression tests were supplemented by literature on elastic properties estimates of rockfill.

The analysis of rubble properties is reported in Attachment IX of *Mechanical Assessment of the Waste Package Subject to Vibratory Motion* (BSC 2005 [DIRS 173172]). The value of 50 MPa represents the lower bound of the initial tangent Young's modulus of the rubble at confinement greater than 100 kPa. Analysis of drift collapse shows (e.g., Figure 6-171 of the *Drift Degradation Analysis*, BSC 2004 [DIRS 166107]) that most of the rockfall comes from the drift crown. The rubble fills the space between the drip shield and the drift wall, reducing—or even preventing—deterioration of the walls. The maximum initial (before rockfall) horizontal distance from the drip shield to the drift wall is approximately 1.5 m. Accounting for some rockfall from the walls, the distance between the drip shield and the stable drift wall is taken to be 2.5 m (Assumption 3.2.8).

The force in a spring representing rubble is given by:

$$F = \begin{cases} -k_n u_h & \text{if } x_p\, u_h > 0 \\ 0 & \text{otherwise} \end{cases} \qquad \text{(Eq. 5.4-3)}$$

where x_p is the x coordinate of the node, and u_h is the horizontal displacement of the node. The practical interpretation of this equation shows that when the drip shield moves toward rubble, a compressive interaction force is developed, but when the drip shield and rubble move apart, no force is developed.

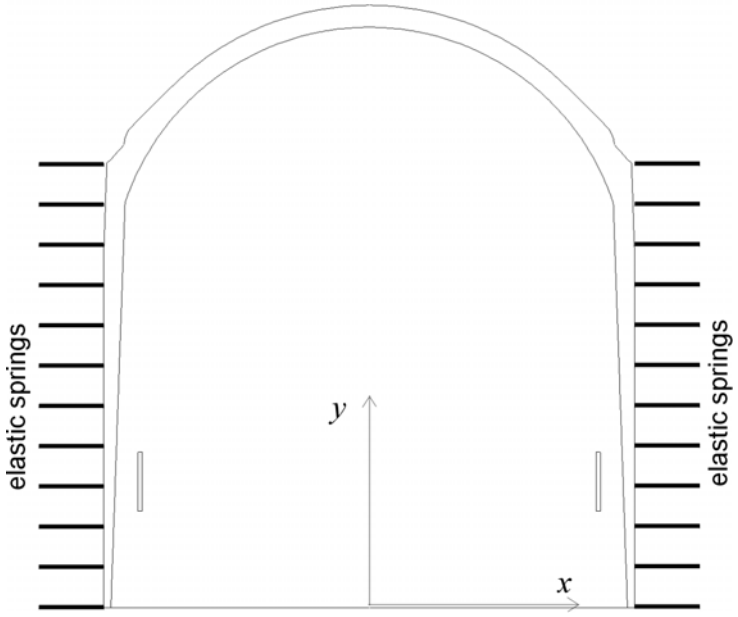

Figure 5.4-3. Interaction between the Drip Shield and the Rubble along the Sides of the Drip Shield is Represented by a Series of Elastic Springs that Represent the Rubble and its Connection to the Drip Shield

5.4.2 Results of Creep Deformation for Dead Load of Rubble (Without Drip Shield and Rubble Coupling)

The initial simulation of creep deformation was carried out for severe loading conditions in which the rubble load applied to the drip shield is considered to be a dead load—— i.e., the load never changes, irrespective of the drip shield deformation. This assumption does not consider the passive reactive pressure of the rubble along the sides of the drip shield generated when the drip shield deforms against the rubble. The results of the simulations indicate that, even for the severe dead load case, the drip shield will remain stable for load realizations 1, 3 and 5 (Table 5.2-2). Displacement time histories of a point in the middle of the crown and the associated drip shield geometry and displacement vector field after 10,000 years are superimposed in Figure 5.4-4 for load realization 3. The maximum displacement is approximately 0.13 m. The main mechanism of deformation is "leaning" of the drip shield on one side. This "leaning" mechanism is the result of the imbalance of lateral forces supplied to the sides of the drip shield, and points out the unrealistic consequences of ignoring the interaction of the rubble and the drip shield deformation. In reality, as the drip shield tends to deform in one direction, the interaction with the rubble would supply a reinforcing boundary pressure opposing the motion, which would tend to confine and stabilize the drip shield movement. The contours of the creep strain [i.e., the scalar measure expressed by Equation (5.4-1)] for realization 3 are shown in Figure 5.4-5. The maximum creep strain is of the order of 3.5 percent, which is much less than the 10-percent threshold (Assumption 3.2.9) for onset of tertiary creep. For realizations 2, 4 and 6, the drip shield collapses under the dead load of the rubble. The results for realization 2 are shown in Figures 5.4-6 and 5.4-7. Although the creep equation does not include tertiary creep (the creep rate actually is decaying continuously as a function of time), the structural response indicates creep acceleration because of the large deformation and the localization of strains in the thin portion of the drip shield legs as a plastic hinge is formed. The creep strain in the lower part of one leg after 10,000 years exceeds 30 percent (Figure 5.4-7)—well above the threshold for the onset of tertiary creep. (If deformation shown in Figure 5.4-6 would take place, the interaction between the drip shield and the waste package, which is not considered in these calculations, would become important. The waste package would reduce the deformation of the drip shield, and as a consequence the waste package would be subjected to the load by the drip shield and rubble.)

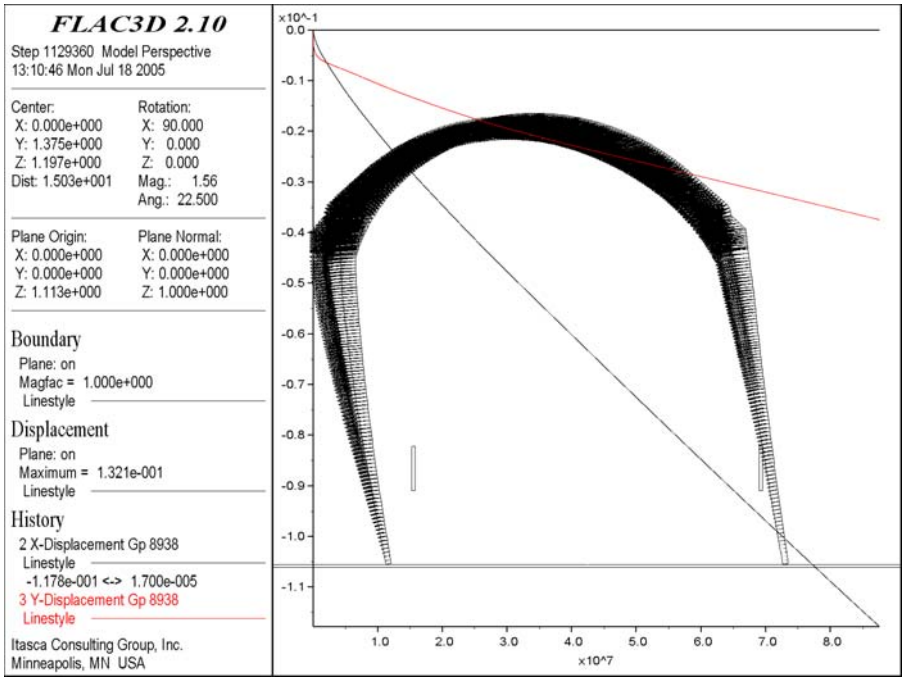

NOTE: The plot of displacement vector field overlies the plot of the displacement histories. Two thin vertically oriented rectangles inside the drip shield represent the emplacement pallet. Displacements are on the vertical axis; time is on the horizontal axis.

Figure 5.4-4. Realization 3: Creep Displacement Vector Field (m) after 10,000 Years and Horizontal (Black) and Vertical (Red) Displacement (m) Histories of the Middle of the Crown versus Time (h)

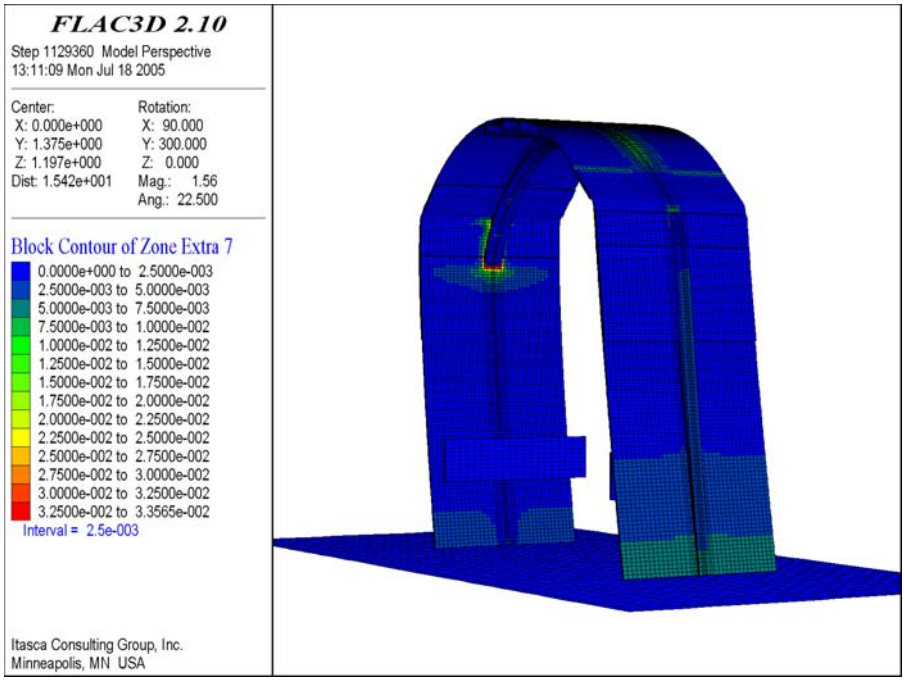

Figure 5.4-5. Realization 3: Contours of Creep Strain after 10,000 Years

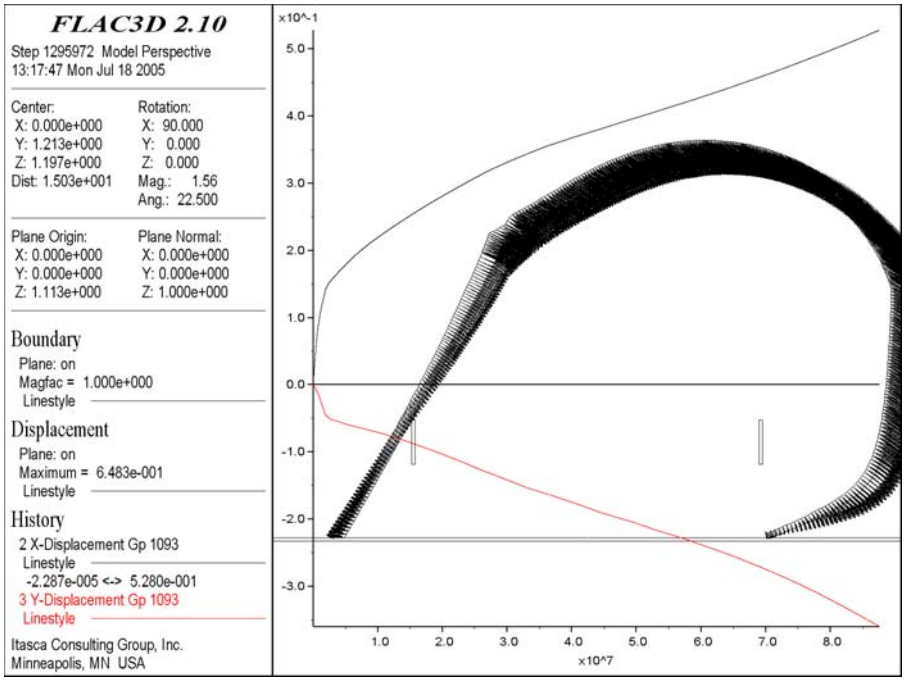

NOTE: The plot of displacement vector field overlies the plot of the displacement histories. Two thin vertically oriented rectangles inside the drip shield represent the emplacement pallet. Displacements are on the vertical axis; time is on the horizontal axis.

Figure 5.4-6. Realization 2: Creep Displacement Vector Field (m) after 10,000 Years and Horizontal (Black) and Vertical (Red) Displacement (m) Histories of the Middle of the Crown versus Time (h)

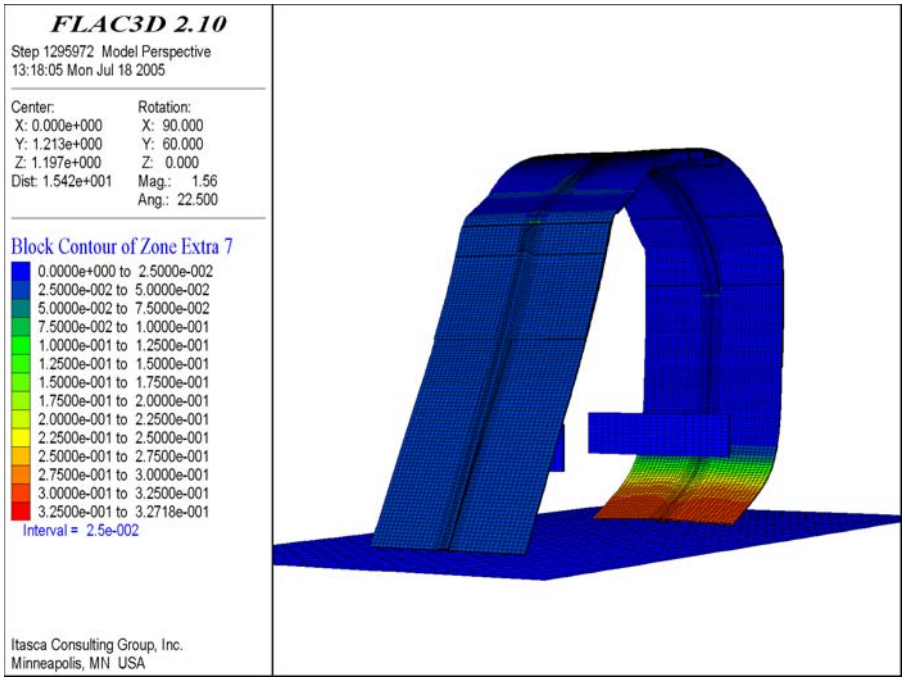

Figure 5.4-7. Realization 2: Creep Strain after 10,000 Years

5.4.3 Results of Creep Deformation Taking into Account Interaction between the Drip Shield and the Rubble

Neglecting the interaction of the drip shield with the rubble, particularly the backpressure that will be generated when the drip shield leans to one side or the other (which is the main mechanism of drip shield deformation, as illustrated in Figure 5.4-6, when collapses occur in the uncoupled analysis for three load realizations), is unrealistic and leads to very unfavorable loading conditions from the perspective of drip shield stability. The effect of the interaction between the drip shield and the rubble is accounted for in these analyses using springs that generate the reactive forces corresponding to the stiffness of the rubble when the drip shield leans to one side (discussed in Section 5.4.1.3). The effect of the change in vertical loads acting on the crown of the drip shield as a function of creep-related drip shield deformation is not considered.

The results of the simulations in which interaction between the drip shield and the rubble along its sides is represented with springs are shown in Figures 5.4-8 through 5.4-15. Again, these Figures show the deformed shape of the drip shield superimposed on time histories of the vertical and horizontal displacement of the drip shield crown. The maximum deformation of the drip shield in the 10,000 year period for all six rubble load realizations is approximately 5.5 cm. The maximum creep strains (listed in Table 5.4-1) are less than 5 percent. The contours of creep strains for load realization 2 are shown in Figure 5.4-14. The drip shield clearly remains stable for all load realizations. The deformation rates, indicated in the displacement history plots, are very small after 10,000 years. The rubble that surrounds the drip shield and acts as a load on the drip shield also provides confinement to the structure, preventing asymmetric deformation by leaning to one side or the other (which is the main mode of deformation during collapse of the drip shield if coupling between the drip shield and the rubble is not considered). The reaction forces of the rubble (in addition to the forces applied on the drip shield in the initial equilibrium state before creep deformation) for load realization 3 after 10,000 years of creep are shown in Figure 5.4-15. It is apparent, from comparison of Figures 5.4-10 and 5.4-15, that reaction forces are generated only on the portion of the drip shield legs where deformation of the drip shield occurs in the direction toward the rubble.

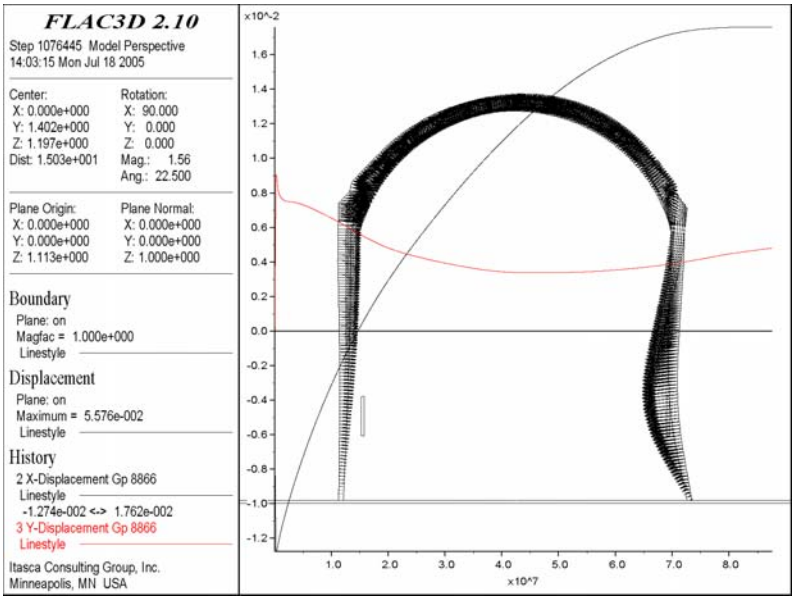

NOTE: The plot of displacement vector field overlies the plot of the displacement histories. Two thin vertically oriented rectangles inside the drip shield represent the emplacement pallet. Displacements are on the vertical axis; time is on the horizontal axis.

Figure 5.4-8. Coupled Realization 1: Creep Displacement Vector Field (m) after 10,000 Years and Horizontal (Black) and Vertical (Red) Displacement (m) Histories of the Middle of the Crown versus Time (h)

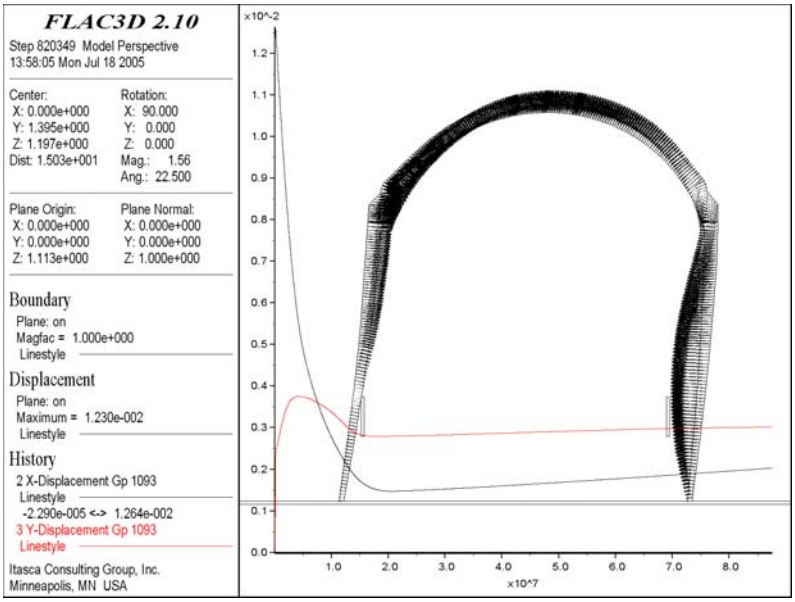

NOTE: The plot of displacement vector field overlies the plot of the displacement histories. Two thin vertically oriented rectangles inside the drip shield represent the emplacement pallet. Displacements are on the vertical axis; time is on the horizontal axis.

Figure 5.4-9. Coupled Realization 2: Creep Displacement Vector Field (m) after 10,000 Years and Horizontal (Black) and Vertical (Red) Displacement (m) Histories of the Middle of the Crown versus Time (h)

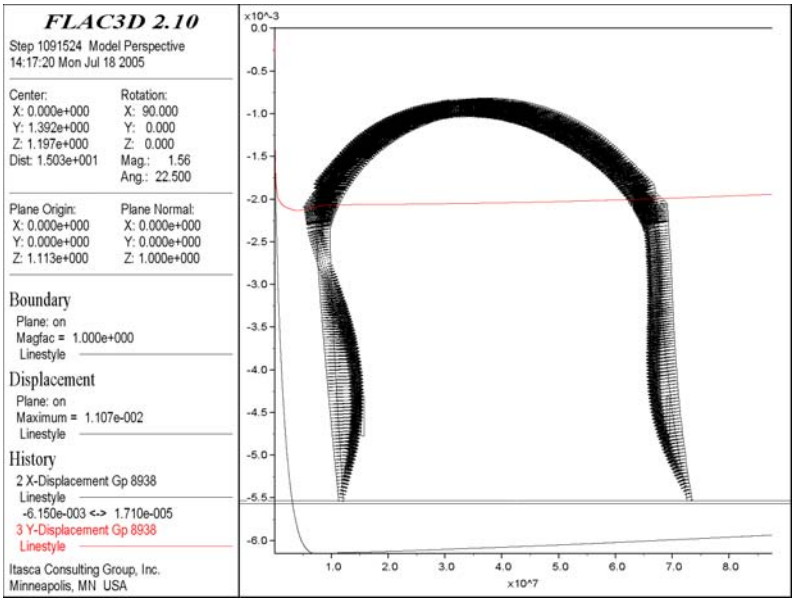

NOTE: The plot of displacement vector field overlies the plot of the displacement histories. Two thin vertically oriented rectangles inside the drip shield represent the emplacement pallet. Displacements are on the vertical axis; time is on the horizontal axis.

Figure 5.4-10. Coupled Realization 3: Creep Displacement Vector Field (m) after 10,000 Years and Horizontal (Black) and Vertical (Red) Displacement (m) Histories of the Middle of the Crown versus Time (h)

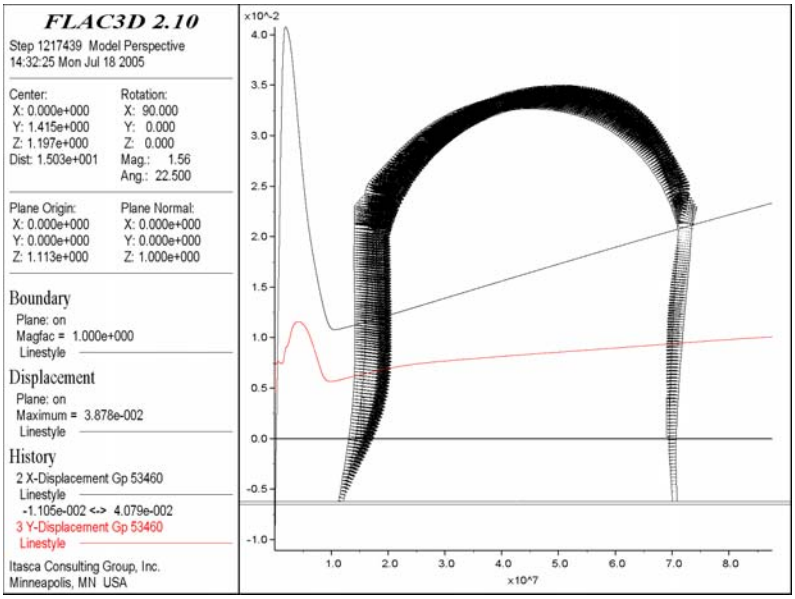

NOTE: The plot of displacement vector field overlies the plot of the displacement histories. Two thin vertically oriented rectangles inside the drip shield represent the emplacement pallet. Displacements are on the vertical axis; time is on the horizontal axis.

Figure 5.4-11. Coupled Realization 4: Creep Displacement Vector Field (m) after 10,000 Years and Horizontal (Black) and Vertical (Red) Displacement (m) Histories of the Middle of the Crown versus Time (h)

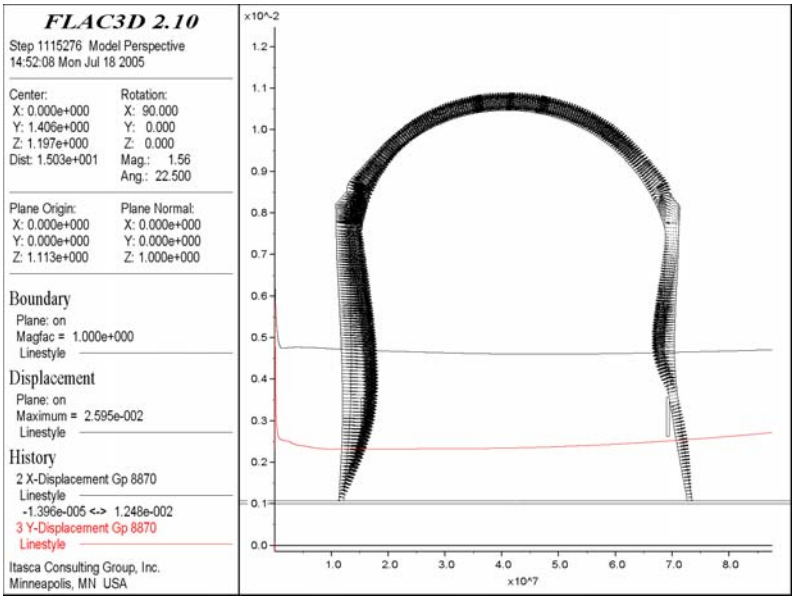

NOTE: The plot of displacement vector field overlies the plot of the displacement histories. Two thin vertically oriented rectangles inside the drip shield represent the emplacement pallet. Displacements are on the vertical axis; time is on the horizontal axis.

Figure 5.4-12. Coupled Realization 5: Creep Displacement Vector Field (m) after 10,000 Years and Horizontal (Black) and Vertical (Red) Displacement (m) Histories of the Middle of the Crown versus Time (h)

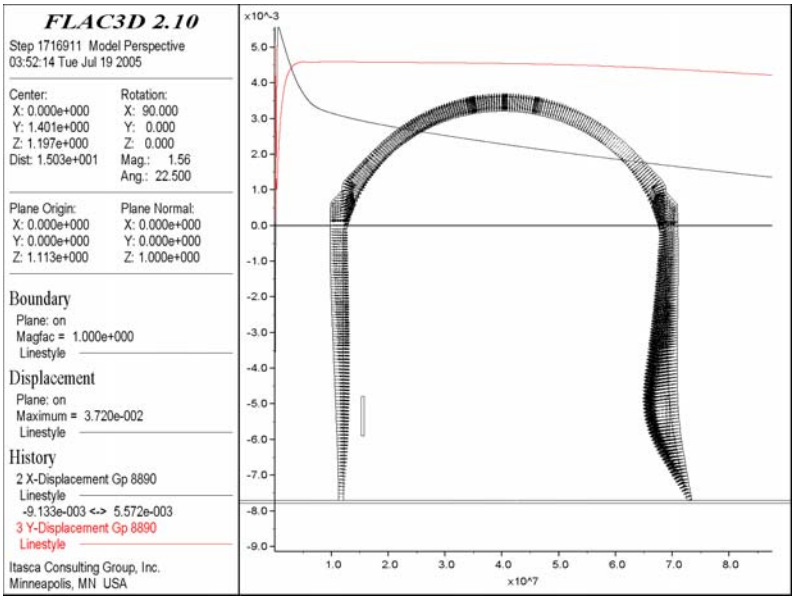

NOTE: The plot of displacement vector field overlies the plot of the displacement histories. Two thin vertically oriented rectangles inside the drip shield represent the emplacement pallet. Displacements are on the vertical axis; time is on the horizontal axis.

Figure 5.4-13. Coupled Realization 6: Creep Displacement Vector Field (m) after 10,000 Years and Horizontal (Black) and Vertical (Red) Displacement (m) Histories of the Middle of the Crown versus Time (h)

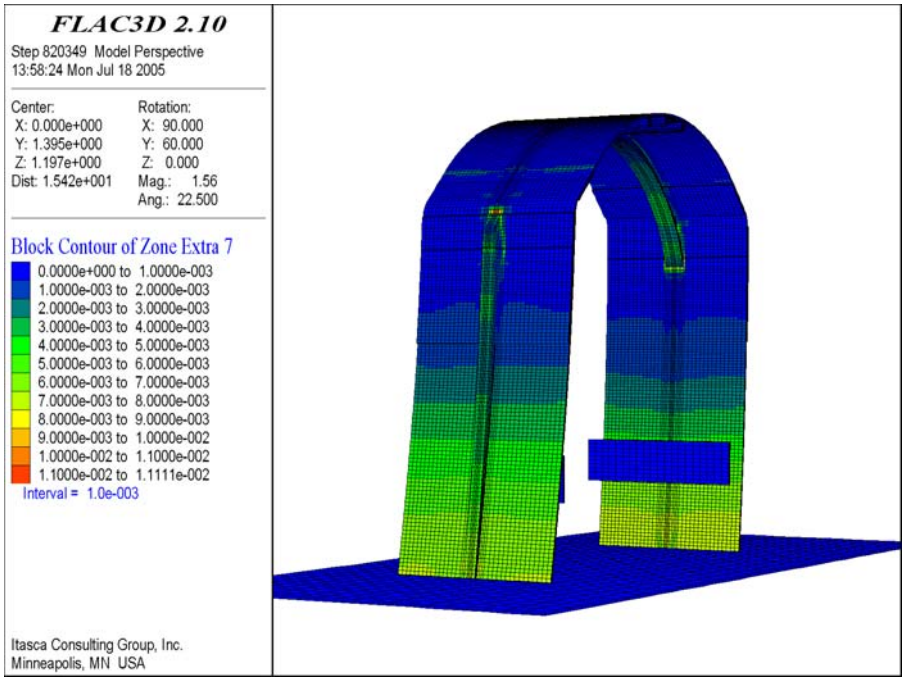

Figure 5.4-14. Coupled Realization 2: Contours of Creep Strain after 10,000 Years

Table 5.4-1. Maximum Creep Strains after 10,000 Years

Realization	Creep Strain (%)
1	4.20
2	1.74
3	2.01
4	3.11
5	1.28
6	2.95

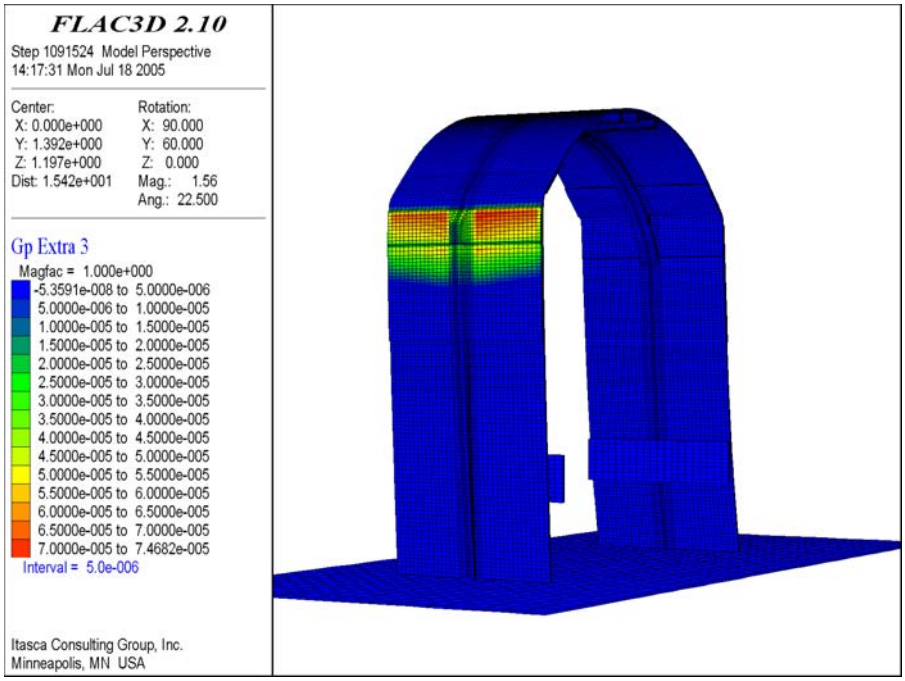

Figure 5.4-15. Coupled Realization 3: Contours of Reaction Forces (MN) after 10,000 Years

5.5 ANALYSIS OF CREEP-RELAXATION OF RESIDUAL STRESSES INDUCED BY IMPACT DENTING OF THE DRIP SHIELD PLATES FROM ROCK BLOCKS

Analysis (reported in *Drip Shield Structural Response to Rock Fall Supplemental Calculation* BSC 2005 [DIRS 174052]) of impact of a large rock block falling from the crown of the emplacement drift onto the drip shield has shown that the drip shield remains permanently deformed after the impact (see Figure 5.5-3). In other words, impact from large rock blocks falling either under gravity or from seismic shaking can result in dents to the drip shield plates. The residual stresses associated with the irreversible deformation of the plates could adversely affect the drip shield as an engineered barrier designed to, among other things, prevent seepage ground water from reaching the waste packages. Permanent tensile residual stresses in the structure that exceed a certain stress threshold will trigger a time-dependent process of stress corrosion cracking that may eventually form continuous cracks through the thickness of the drip shield plates and a pathway for ground water through the drip shield. Although a yield-stress initiation threshold is defined as 50 percent of the Ti-7 yield strength at 140ºC, i.e., as 110.5 MPa (BSC 2004 [DIRS 172203], Section 6.2.1), it is more realistic to use the 50 percent of actual yield strength for the temperature of interest (i.e., RT and 150ºC) (Assumption 3.2.12). Because titanium is a metal that exhibits creep at relatively low deviatoric stresses and temperatures (Dutton 1996, Section 2 [DIRS 174750], Kissel and Sinnott 1953 [DIRS 174853]), the residual, locked-in stresses in the drip shield structure after impact by a rock block will decrease gradually with time as a result of the creep-induced stress relaxation process. After sufficient time, the stresses will relax below the stress corrosion cracking threshold. The purpose of the following calculation is to examine the time-related stress relaxation process for dented Ti-7 plates.

The relaxation of stresses in the drip shield plates as a function of time, after impact by 28.29 MT block with energy of 706,914 J (BSC 2005 [DIRS 174052])[2], was analyzed for different assumed creep equations (at RT and 150ºC) and is discussed in this section. The effect of temperature on the time scale during which the major principal stress decays below the stress-corrosion cracking threshold is not obvious. For example, increase in temperature accelerates stress relaxation, but it also lowers the stress corrosion threshold. The critical (i.e., longest) time required for the major (maximum) principal stress to decay below the stress corrosion cracking threshold was determined for different temperatures (i.e., RT and 150ºC) and creep equations (Section 5.3.2). The temperature of the drip shield during postclosure most likely (at least 96.5 percent of time as discussed in *Multiscale Thermohydrologic Model,* BSC 2005 [DIRS 173944], Section 6.3.7 and Table 6.3-42) will be between RT and 150ºC. Analysis of stress relaxation at these two temperatures will provide the bounding time of stress relaxation below the stress corrosion cracking threshold. The mass and impact energy, which created the dent and the residual stresses in the drip shield analyzed here, represent the rare event of maximum impact energy calculated for the 5.35 m/s PGV level[3] (Assumption 3.2.2 in BSC 2005 [DIRS 174052]).

5.5.1 Transfer of Geometry and Stresses between LS-DYNA and FLAC3D

Analysis of a rock block hitting the drip shield, the resultant drip shield plate deformation and development of residual stresses was carried out in *Drip Shield Structural Response to Rock Fall Supplemental Calculation* (BSC 2005 [DIRS 174052]) with the LS-DYNA code. The subsequent creep-relaxation of the residual stresses in the drip shield structure after impact was calculated with FLAC3D. The equilibrium state of stress and deformation of the dented drip shield at the end of the LS-DYNA simulation was transferred to FLAC3D for the creep analysis. There is a one-to-one correspondence of the nodal points and calculation elements between the two numerical codes, i.e., the initial geometry and element stresses of the FLAC3D simulation are identical to the deformed element geometry and stresses at the end of the LS-DYNA simulation. Equivalence between the LS-DYNA final and FLAC3D initial states is illustrated in Figures 5.5-1 and 5.5-2, which show the geometry and contours of major principal stress in the drip shield after impact.

---

[2] The Drift Degradation Analysis (BSC 2004 [DIRS 166107], Section 6.3) determined this rock block, dislodged during seismic shaking, to have the greatest energy produced from all three-dimensional discontinuum analyses.

[3] Ground motions are identified by the appropriate value of PGV because the value of PGV provides a unique and unambiguous identifier for each set of ground motions, even if multiple hazard curves have been developed for a site. For the reader's convenience, the following list identifies the correspondence between the values of annual exceedance frequency at the emplacement drifts and the values of PGV (BSC 2005 [DIRS 173172], Section 1.3.3):

PGV of 0.19 m/s corresponds to the 5×10^{-4} per year exceedance frequency;
PGV of 0.384 m/s corresponds to the 10^{-4} per year exceedance frequency;
PGV of 1.05 m/s corresponds to the 10^{-5} per year exceedance frequency;
PGV of 2.44 m/s corresponds to the 10^{-6} per year exceedance frequency; and
PGV of 5.35 m/s corresponds to the 10^{-7} per year exceedance frequency.

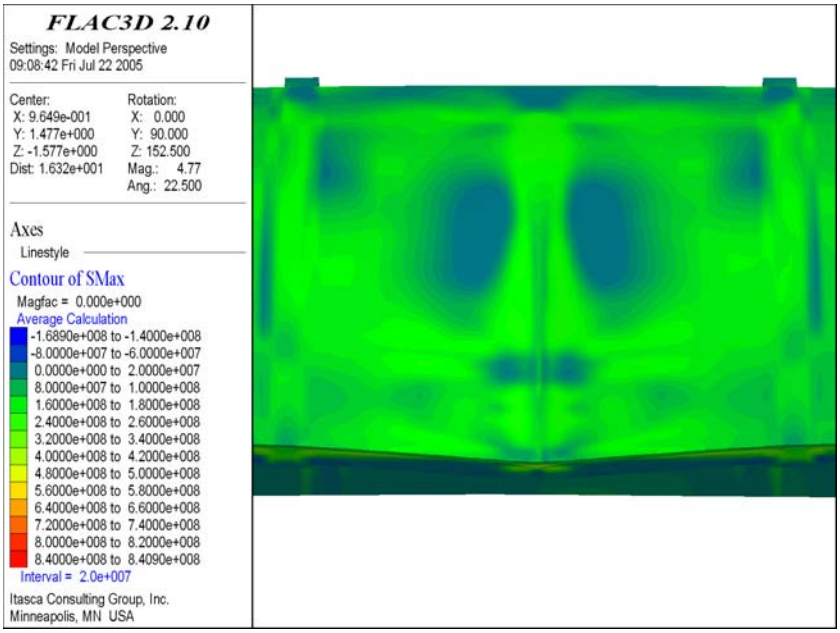

NOTE: The Figure includes a view of the drip shield structure from above. It is not directly downward, but slightly inclined from vertical. Consequently, a small portion of the leg is shown at the bottom part of the figure. The majority of Figure shows the plate of the drip shield crown.

Figure 5.5-1. Contours of the Residual Major Principal Stress (Pa) and Geometry of the Drip Shield Structure after Impact by Rock Block Imported in FLAC3D

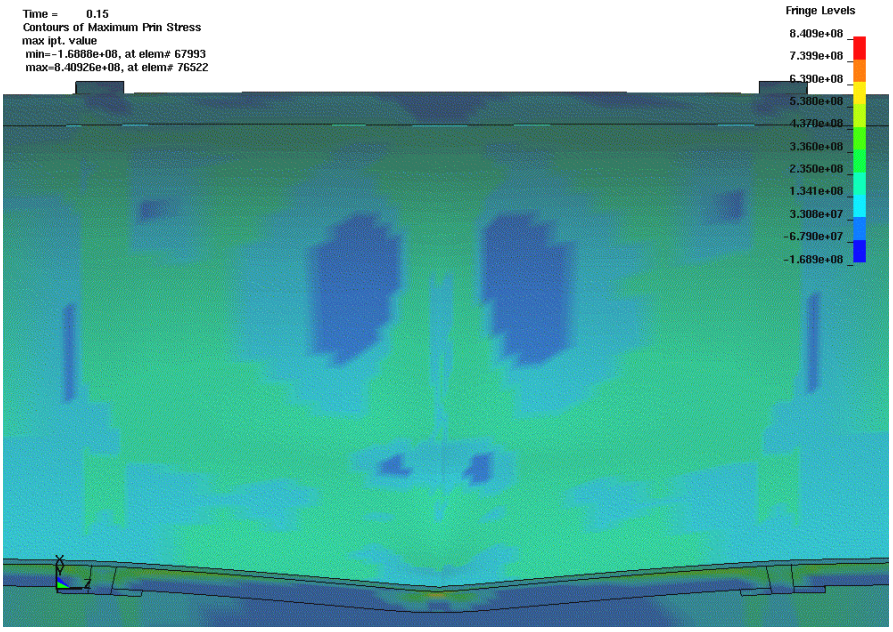

Source: Figure 7-59 (BSC 2005 [DIRS 174052]).

Figure 5.5-2. Contours of the Residual Major Principal Stress (Pa) and Geometry of the Drip Shield Structure after Impact by Rock Block Calculated in LS-DYNA

5.5.2 Numerical Representation

Permanent deformation of the drip shield and residual stresses are localized around the point of impact (e.g., Figure 5.5-1). In order to optimize the calculation execution time, stress relaxation was simulated in FLAC3D for the portion of the drip shield surrounding the location of the impact. The geometries of the numerical representation of the entire drip shield and the portion for which stress relaxation was simulated are shown in Figure 5.5-3. Symmetry of the drip shield was used in the calculations to reduce the size of the analyzed domain. "Roller" boundary conditions were applied along the vertical symmetry plane of the drip shield. Three boundaries, along which the portion of the grid analyzed in FLAC3D was extracted from the numerical representation of the entire drip shield, are fixed (i.e., no displacements or rotations) in the stress relaxation calculation. Reduction of the simulated domain and fixed outer boundaries lead to predictions of stress relaxation at slower rate because boundary displacements and rotations that could reduce residual stresses are restrained.

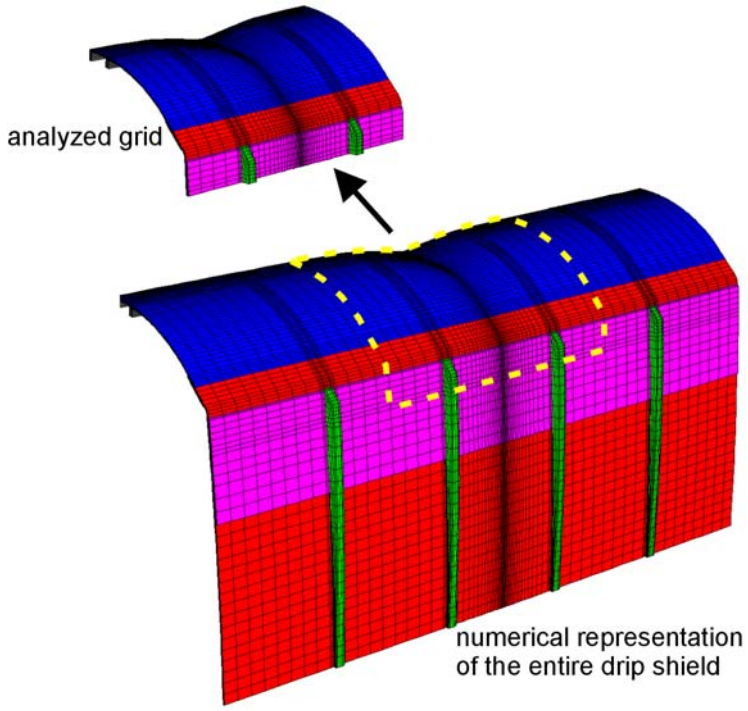

Figure 5.5-3. The Geometry of the Numerical Representation of the Drip Shield and Part of the Grid used in the Analysis of Stress Relaxation

Although the residual stresses and deformation of the drip shield were calculated at 150°C, the stress relaxation was carried out assuming titanium creep properties at RT and 150°C. (The residual stresses for the RT will be smaller than for 150°C. The moduli of elasticity of titanium [both Ti-7 and Ti-24] at the RT and 150°C are practically the same [Table 5.2-1]. The yield strength of titanium is 20 percent and 50 percent greater at the RT than at 150°C, for Ti-7 and Ti-24, respectively. In the limit, if the structure were elastic during impact there would be no residual stresses. If the structure is stronger (with practically the same pre-yield stiffness), it will undergo less inelastic deformation and consequently have less residual stresses.) Two sets of creep properties (listed in Table 5.3-2), at RT and 150ºC, were considered for Ti-7. Because of

less importance of structural components designed of Ti-24 for stress relaxation in the plates, only one set of creep properties (listed in Table 5.3-3), at RT and 150ºC, was considered for Ti-24. The original LS-DYNA analysis used the von Mises yield criterion for titanium. Because this yield condition is not available in FLAC3D, the Tresca yield criterion (Assumption 3.2.16) was used instead.

5.5.3 Results

The results of the calculations are presented in 12 vertical cross-sections through the drip shield indicated in Figure 5.5-4. Only stresses in the plates are shown. Stresses are contoured only if they exceed a value greater than 50 percent of the yield strength at the given temperature for which the analysis was carried out (Assumption 3.2.12). The regions that are below 50 percent of the yield strength are left white in the contour plots (i.e., outside the contouring range).

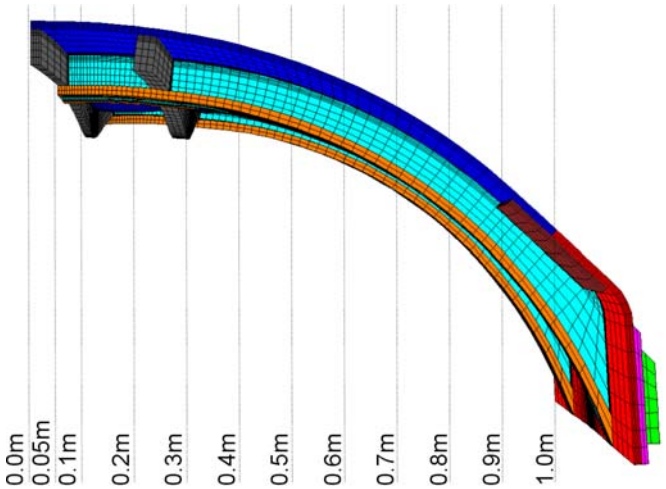

NOTE: The dent is centered along the axis of symmetry, corresponding to 0.0m coordinate.

Figure 5.5-4. Locations of Vertical Sections where the Major Principal Stress Contours are Presented

The major principal stresses, contoured based on the Ti-7 yield strength of 276 MPa at RT (Table 5.2-1), after rock block impact are shown in Figure 5.5-5 in the 12 cross-sections through the drip shield. Clearly, there is a significant area of the drip shield plates in which the residual major principal stresses are in excess of the stress corrosion cracking threshold at RT. Relaxation of the stresses as a function of time up to 100 years for the case RT-1 (the creep coefficients corresponding to this case are listed in Table 5.3-2) is illustrated in Figures 5.5-6 through 5.5-8. In one year (Figure 5.5-6), most of the stresses relax below 50 percent of the yield strength, leaving no continuous stress path with stresses exceeding 50 percent of the yield strength between two sides (outside and inside) of the plates. Stress relaxation in the case RT-2 is slower (Figures 5.5-9 through 5.5-11). In this case, it takes 100 years to reach the stress state that is approximately the same as the state after one year of stress relaxation in the case RT-1.

The major principal stresses, contoured based on the Ti-7 yield strength of 176 MPa at 150ºC, after impact by the rock block are shown in Figure 5.5-12 in the 12 cross-sections through the drip shield. Although the stresses decay faster at elevated temperatures, it takes longer for stresses to fall below the stress corrosion cracking threshold, which is lower at elevated

temperatures. In the case 150ºC-1 (the creep coefficients are listed in Table 5.3-2), for which the results are shown in Figures 5.5-13 through 5.5-15, takes approximately five years to reach the state at which there is no continuous path between two sides of the drip shield plate through the regions with major principal stress in excess of 50 percent of the yield strength. Stress decay for the case 150ºC-2 is much slower (Figures 5.5-16 through 5.5-19). Although it takes more than 1,000 years for stresses to decay sufficiently so that there is no continuous path between the two sides of the plate through the regions with major principal stress in excess of 50 percent of the yield strength, the stresses are less than 65 percent of the yield strength throughout the plate after 10 years (Figure 5.5-17). Consequently, it is expected that the propagation rate of any stress corrosion cracking that may initiate on the upper surfaces of the drip shield, in areas where the stress exceeds 50 percent of the yield strength at given temperature, would arrest before the cracking was through-wall.

The above discussion regarding the time required for stresses to relax below the stress corrosion threshold considers almost the entire surface of the drip shield crown. However, on a large portion of the crown plate there is no potential for accumulation of water even after denting. Particularly on the sloping surfaces there is more potential for water to be diverted by flowing on the surface of the drip shield plate instead of percolating through the relatively tight cracks. It seems reasonable that formation of stress corrosion cracks on those surfaces will not result in seepage of water through the drip shield. The water could pond inside the dent formed by the block impact. If cracks are formed below the surface where water can pond, water can percolate through the drip shield and drip on the waste package. The maximum size (in plan view) of the portion of the drip shield plate where ponding of water is possible is indicated in Figure 5.5-20. The Figure shows the horizontal cross-Section through the drip shield plate at the highest elevation where the contour of the inside surface created by denting is closed. The maximum horizontal dimensions of the dent are approximately 0.20 m by 0.07 m. These results are in excellent agreement with the dimensions reported in Section 7.2 and Figure 7-20 of *Drip Shield Structural Response to Rock Fall Supplemental Calculation* (BSC 2005 [DIRS 174052], p. 36). If stress contour plots are investigated limiting the search for stress values above the stress corrosion cracking threshold only to areas where ponding is possible (i.e., in Figures 5.5-5 through 5.5-19, sections marked as 0.05 m, 0.1 m and 0.2 m and approximately 35 mm left and right from the impact location), it appears that a continuous path does not exist even immediately after the impact irrespective of the temperature considered (i.e., RT or 150ºC). At 150ºC, in the Section that is in the axis of symmetry (i.e., 0.0 m in Figure 5.5-12), there is a continuous path between outside and inside surfaces. However, as shown in Figure 5.5-20, the axis of symmetry is above the area where water can pond. The nonexistence of a continuous path between the outside and inside surfaces of the drip shield plates is a good argument that stress corrosion cracking will not propagate through the thickness of the plate. However, the argument may not be sufficient because either areas on the outer surface of the drip shield plate with stresses above the threshold could initiate cracks, and/or rubble loading could exist, which could change the stress state. This will change the conditions for crack propagation compared to the conditions existing before onset of cracking or rubble loading.

Stress relaxation will make stress corrosion crack initiation and propagation less likely and occurring at a slower rate. Stress corrosion crack growth rate in Ti-7 has been measured in laboratory experiments (BSC 2004 [DIRS 171564]). It was determined (Figure 1-9 in BSC 2004 [DIRS 171564]) that the crack growth rate at 110ºC for loading which maintained a stress

intensity factor of 30 MPa × $m^{1/2}$ was $1.25 \cdot 10^{-8}$ mm/s. The stress intensity factor in a plate of uniform thickness, h, at an edge crack of length, a, loaded by a uniform tensile stress, σ, can be expressed by the following formula (Section 6.4.1 of BSC 2004 [DIRS 172203]):

$$K_I = \beta\sigma\sqrt{\pi a} \qquad \text{(Eq. 5.6-1)}$$

where

$$\beta = 1.12 - 0.231\left(\frac{a}{h}\right) + 10.55\left(\frac{a}{h}\right)^2 - 21.72\left(\frac{a}{h}\right)^3 + 30.95\left(\frac{a}{h}\right)^4 \qquad \text{(Eq. 5.6-2)}$$

For the maximum possible tensile stress of 176 MPa (equal to yield strength of Ti-7 at 150ºC, see Table 5.2-1), the stress intensity factor becomes equal to 30 MPa × $m^{1/2}$ when the edge crack length is approximately 4 mm. Based on the crack velocity measured in the laboratory at 30 MPa × $m^{1/2}$ of $1.25 \cdot 10^{-8}$ mm/s, it will take longer than 10 years for the stress corrosion crack to propagate to achieve a length of 4 mm. Inspection of stress contours after 10 years of stress relaxation and within the area where ponding of water is possible shows that the residual stresses still above the stress corrosion cracking threshold are very limited on the outside surface. It is very likely that any stress corrosion cracks will be arrested before propagating through the thickness of the drip shield plate.

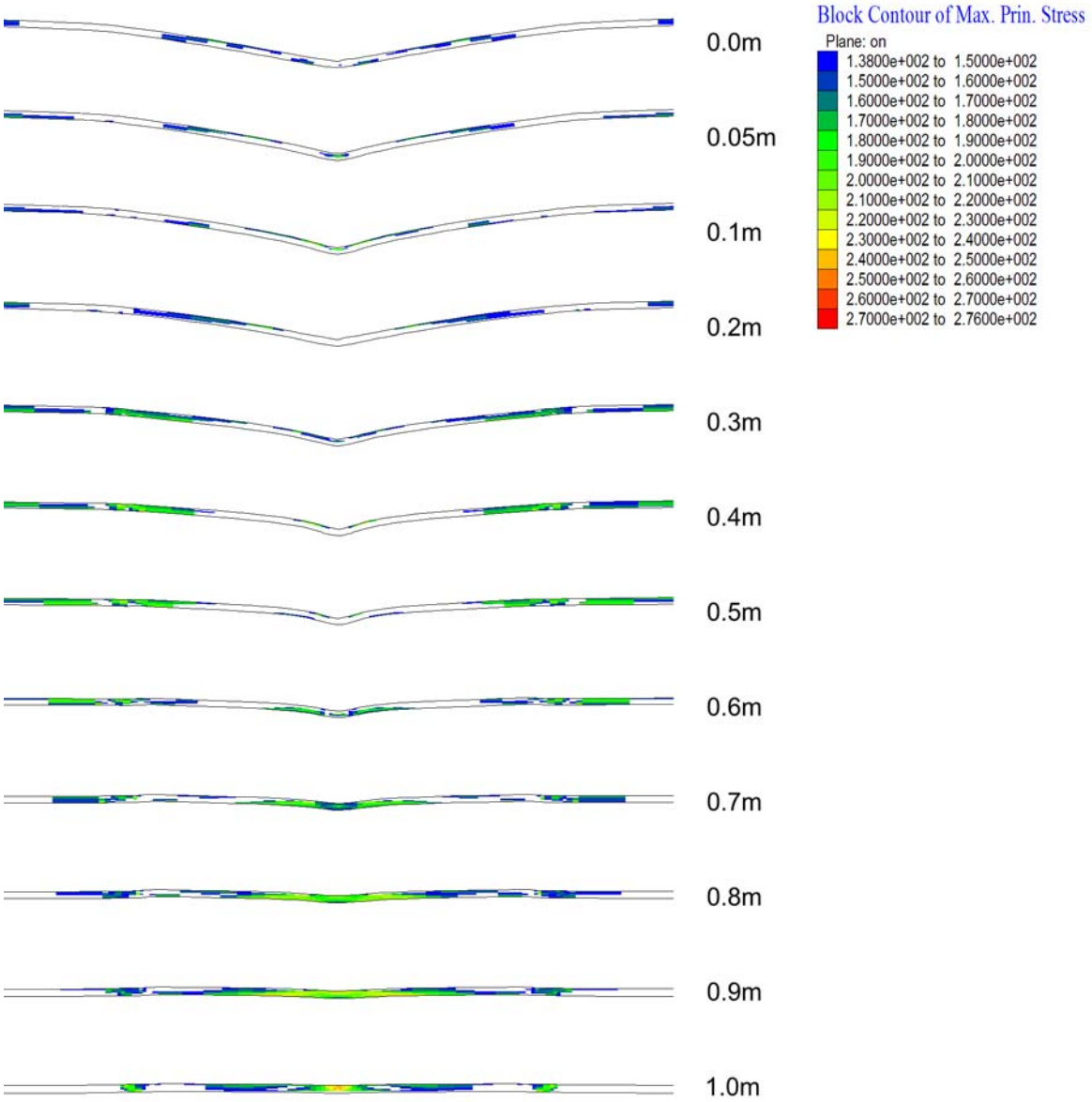

Figure 5.5-5. Major Principal Stress Contours (MPa) in Drip Shield Plates Greater than 138 MPa (50 Percent of the Yield Strength at Room Temperature) after Impact by a Rock Block

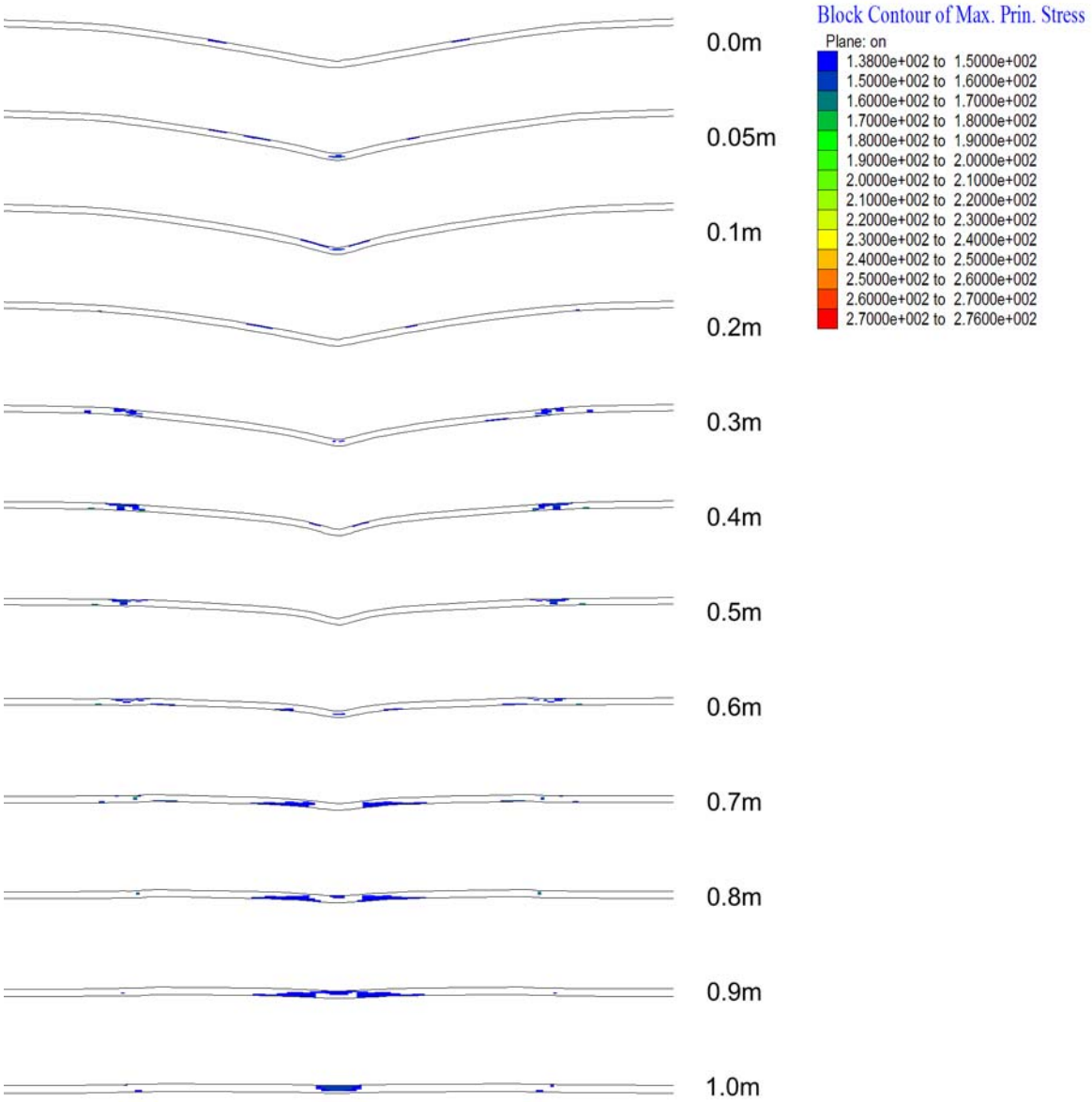

Figure 5.5-6. Major Principal Stress Contours (MPa) in Drip Shield Plates Greater 138 MPa (50 Percent of the Yield Strength at Room Temperature) after 1 y of Stress Relaxation Calculated for the Case RT-1

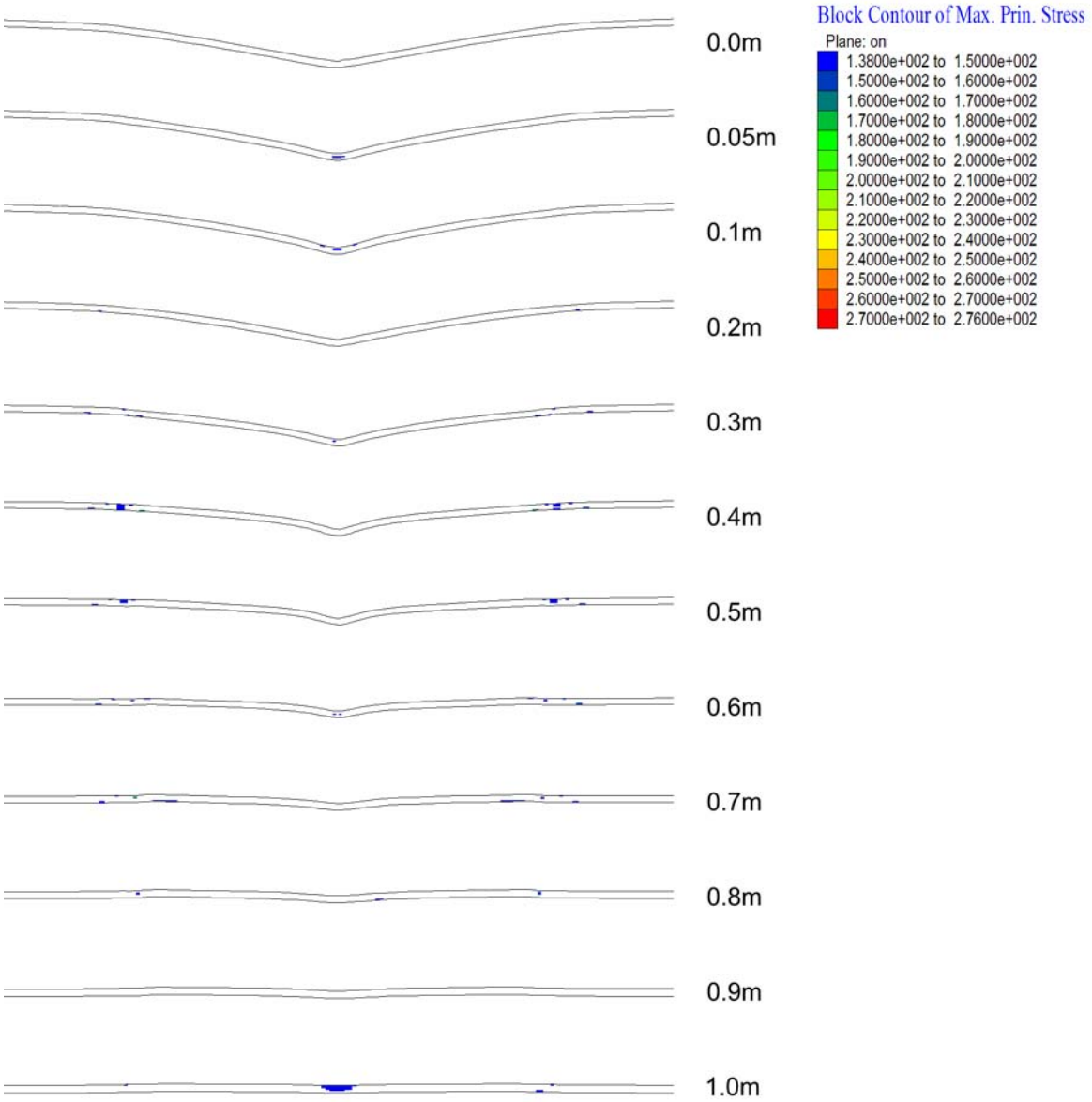

Figure 5.5-7. Major Principal Stress Contours (MPa) in Drip Shield Plates Greater than 138 MPa (50 Percent of the Yield Strength at Room Temperature) after 10 y of Stress Relaxation Calculated for the Case RT-1

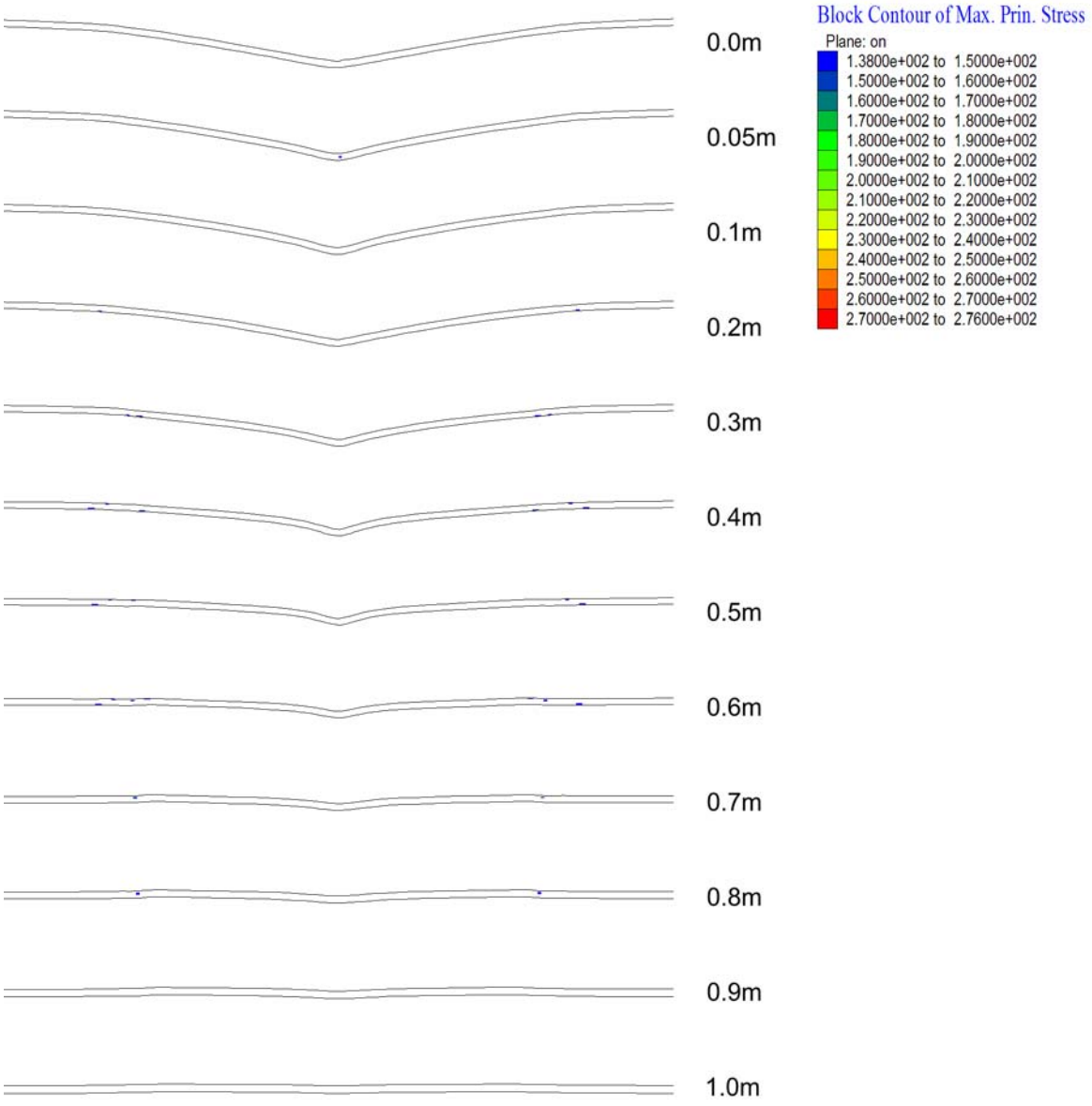

Figure 5.5-8. Major Principal Stress Contours (MPa) in Drip Shield Plates Greater than 138 MPa (50 Percent of the Yield Strength at Room Temperature) after 100 y of Stress Relaxation Calculated for the Case RT-1

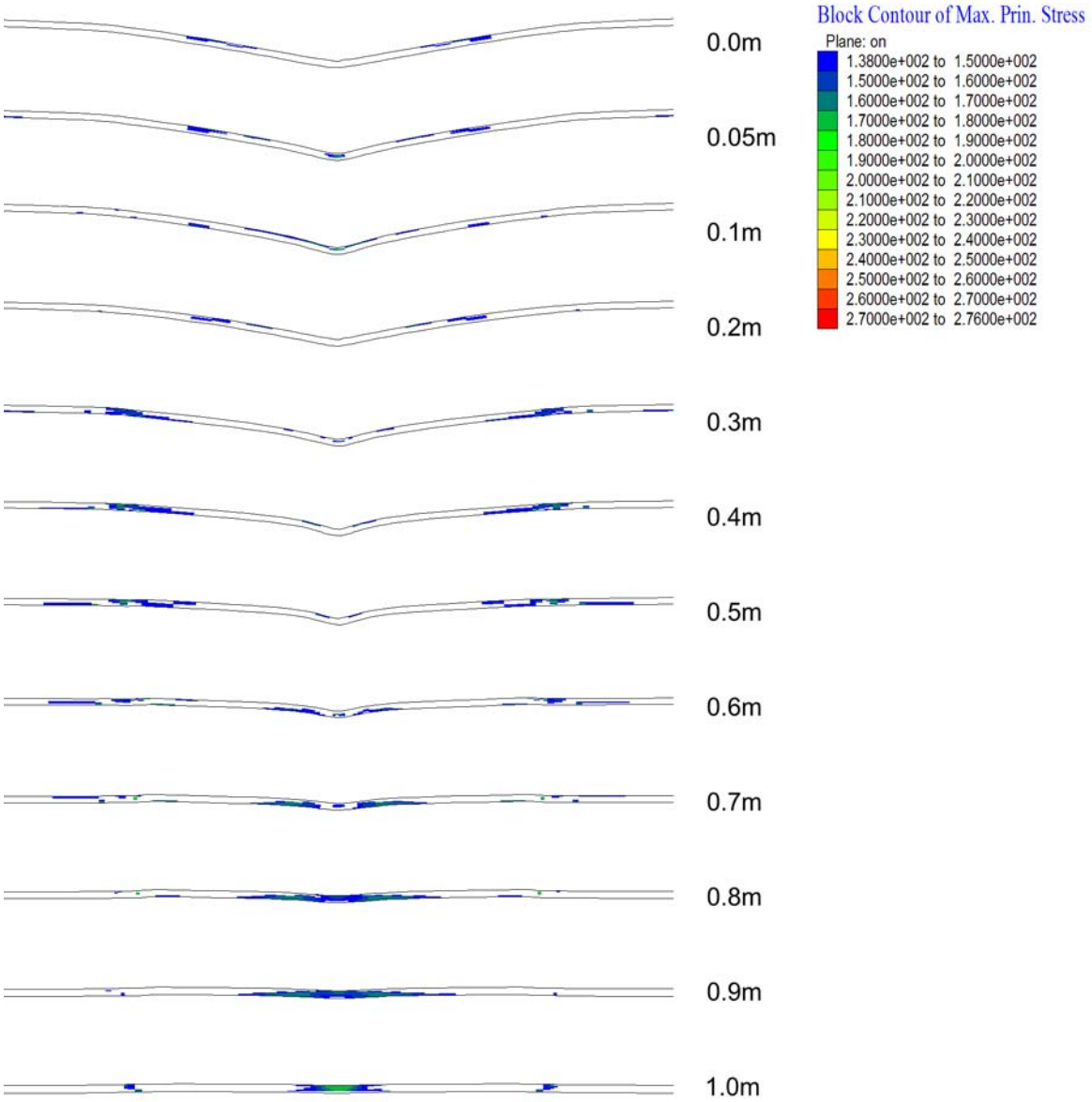

Figure 5.5-9. Major Principal Stress Contours (MPa) in Drip Shield Plates Greater than 138 MPa (50 Percent of the Yield Strength at Room Temperature) after 1 y of Stress Relaxation Calculated for the Case RT-2

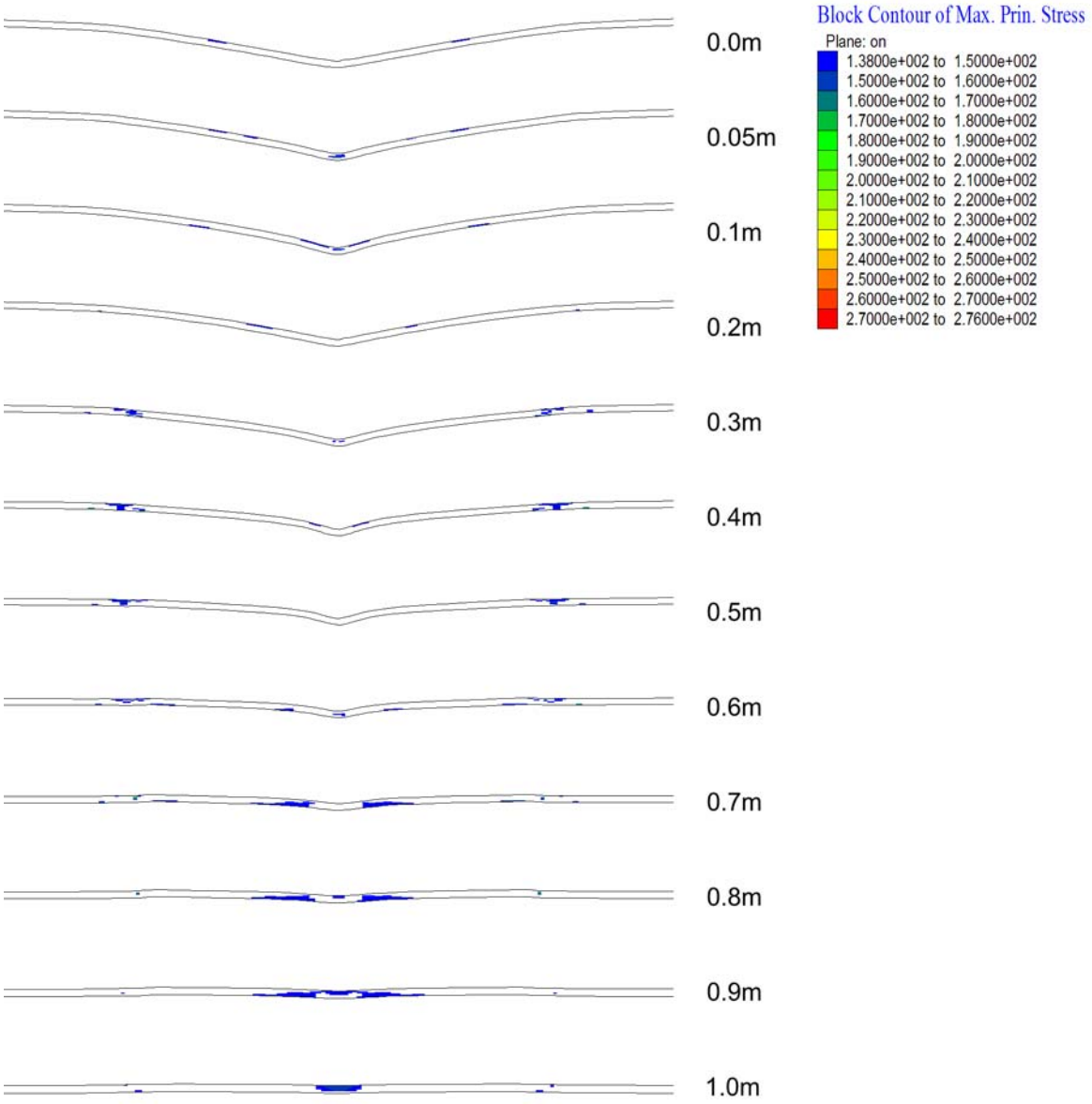

Figure 5.5-10. Major Principal Stress Contours (MPa) in Drip Shield Plates Greater than 138 MPa (50 Percent of the Yield Strength at Room Temperature) after 100 y of Stress Relaxation Calculated for the Case RT-2

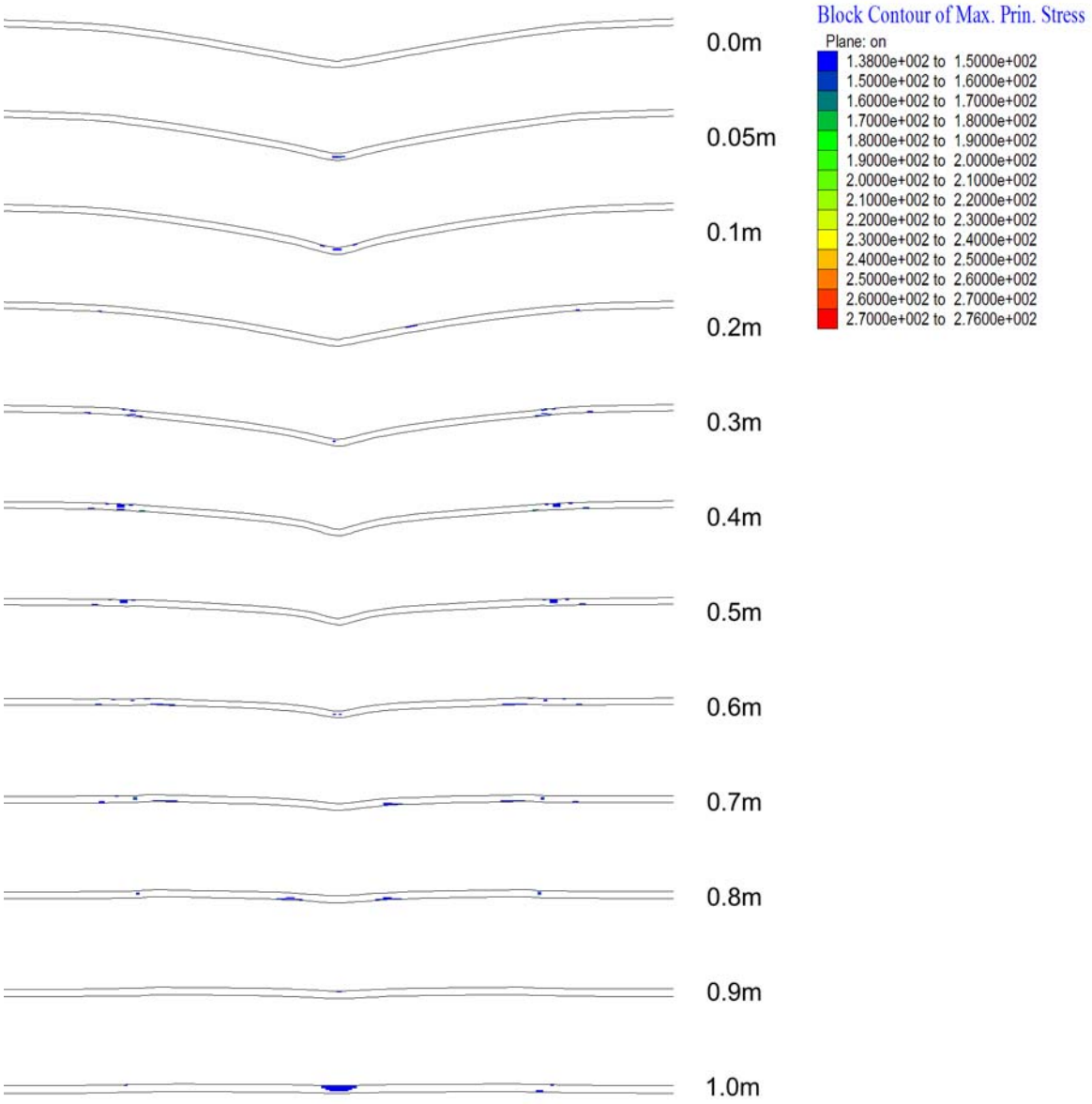

Figure 5.5-11. Major Principal Stress Contours (MPa) in Drip Shield Plates Greater 138 MPa (50 Percent of the Yield Strength at Room Temperature) after 1,000 y of Stress Relaxation Calculated for the Case RT-2

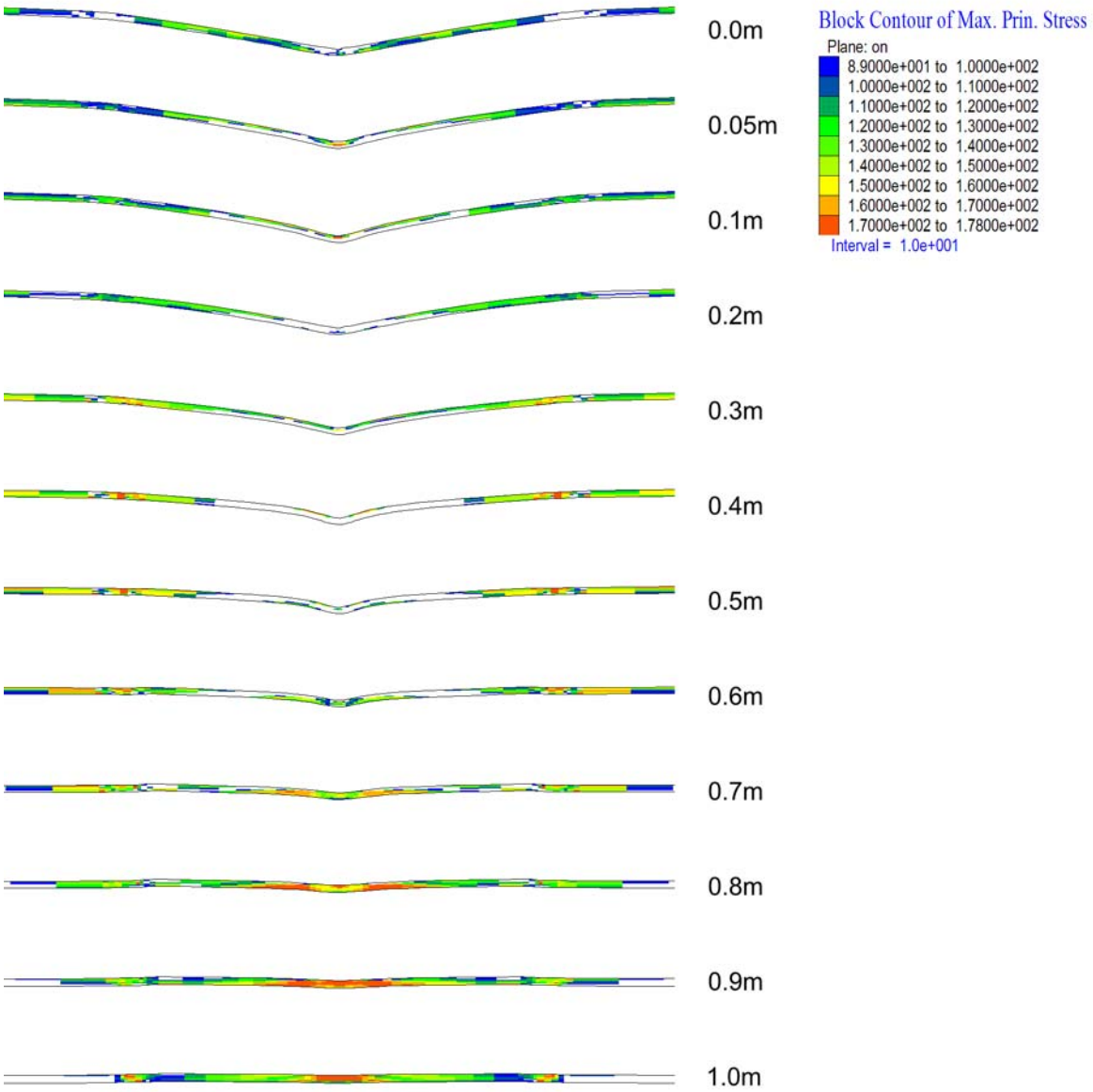

Figure 5.5-12. Major Principal Stress Contours (MPa) in Drip Shield Plates Greater than 89 MPa (50 Percent of the Yield Strength at 150ºC) after Impact by a Rock Block

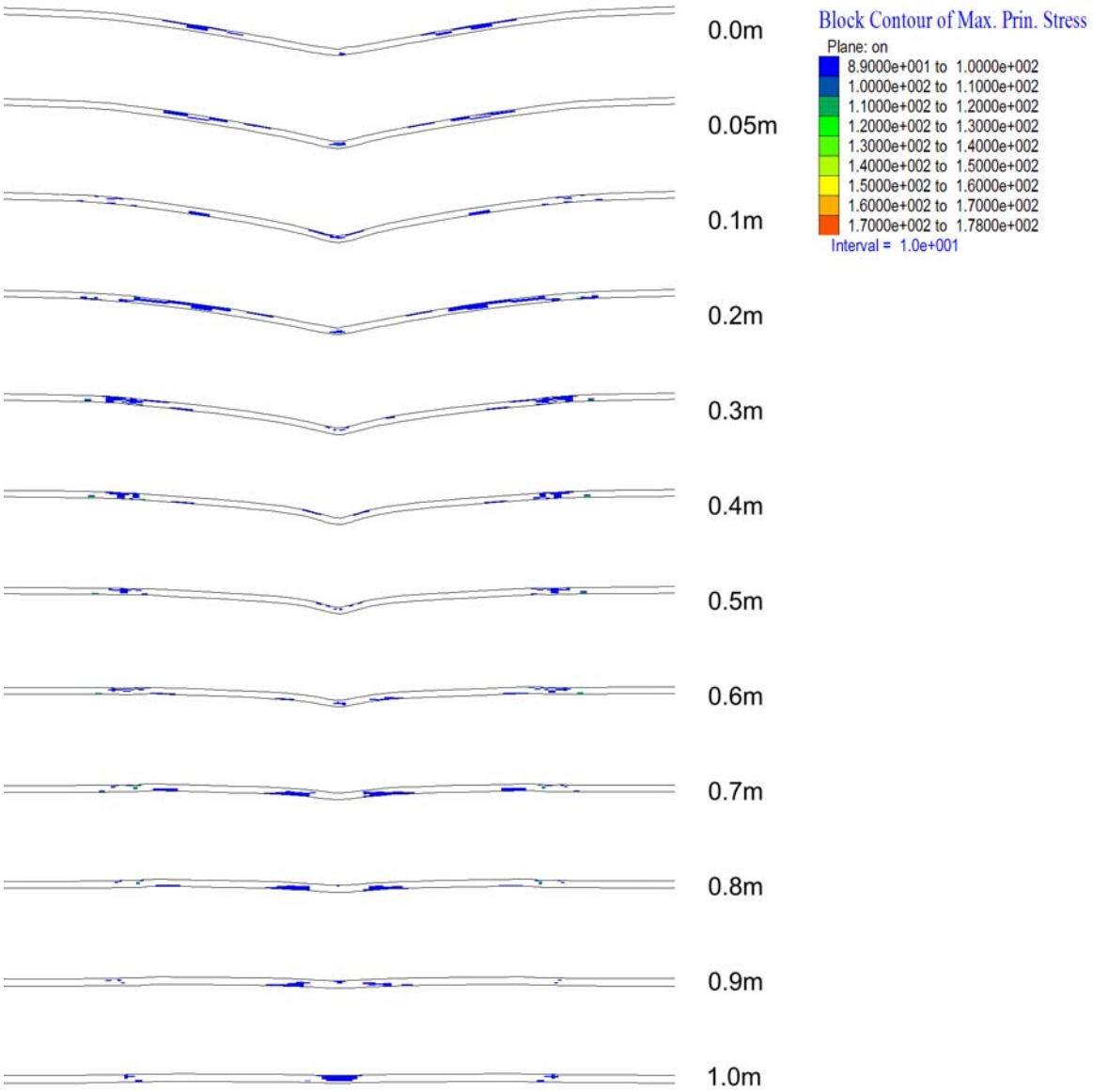

Figure 5.5-13. Major Principal Stress Contours (MPa) in Drip Shield Plates Greater than 89 MPa (50 Percent of the Yield Strength at 150ºC) after 1 y of Stress Relaxation Calculated for the Case 150ºC-1

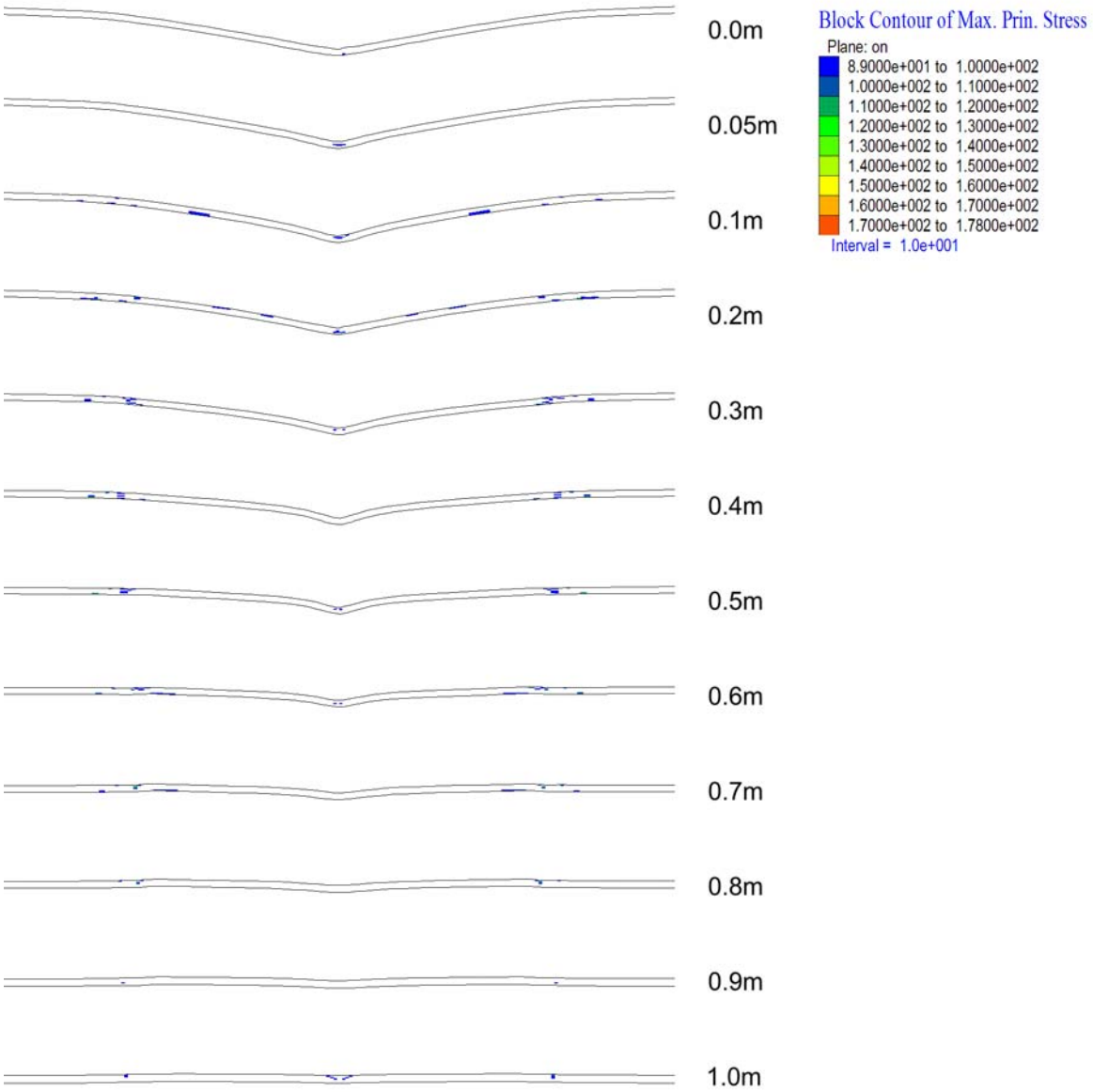

Figure 5.5-14. Major Principal Stress Contours (MPa) in Drip Shield Plates Greater than 89 MPa (50 Percent of the Yield Strength at 150ºC) after 5 y of Stress Relaxation Calculated for the Case 150ºC-1

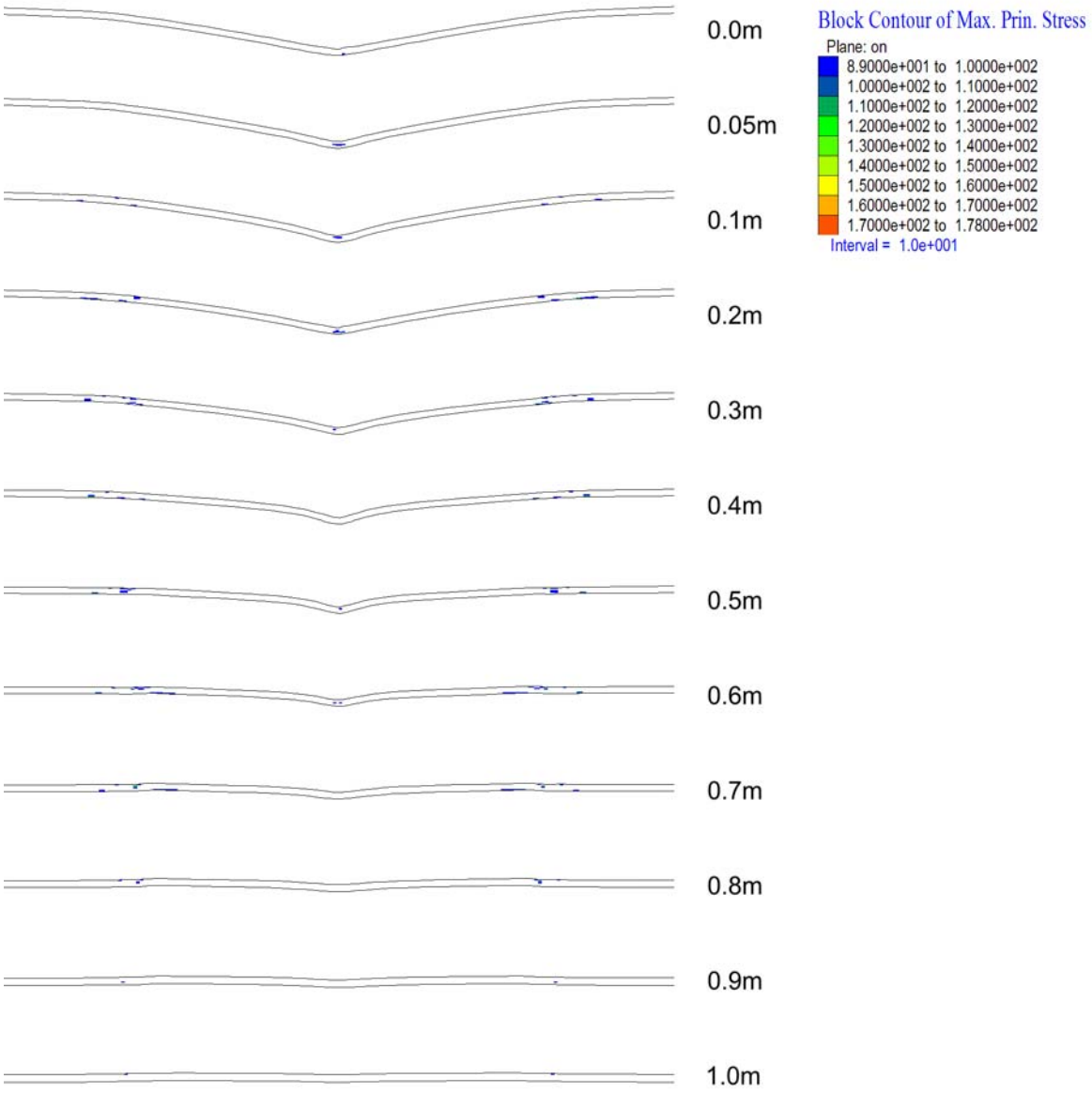

Figure 5.5-15. Major Principal Stress Contours (MPa) in Drip Shield Plates Greater than 89 MPa (50 Percent of the Yield Strength at 150ºC) after 10 y of Stress Relaxation Calculated for the Case 150ºC-1

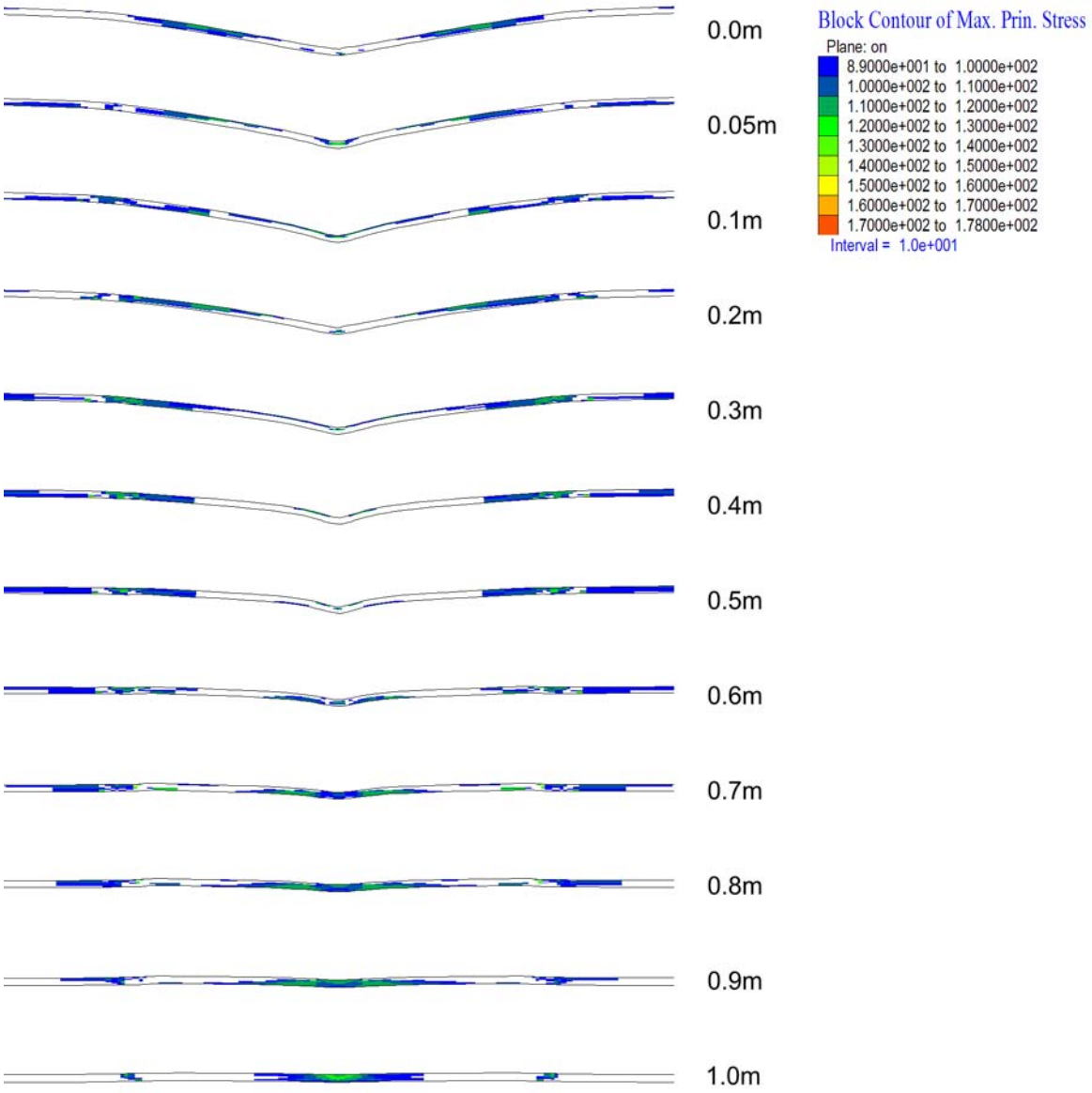

Figure 5.5-16. Major Principal Stress Contours (MPa) in Drip Shield Plates Greater than 89 MPa (50 Percent of the Yield Strength at 150ºC) after 1 y of Stress Relaxation Calculated for the Case 150ºC-2

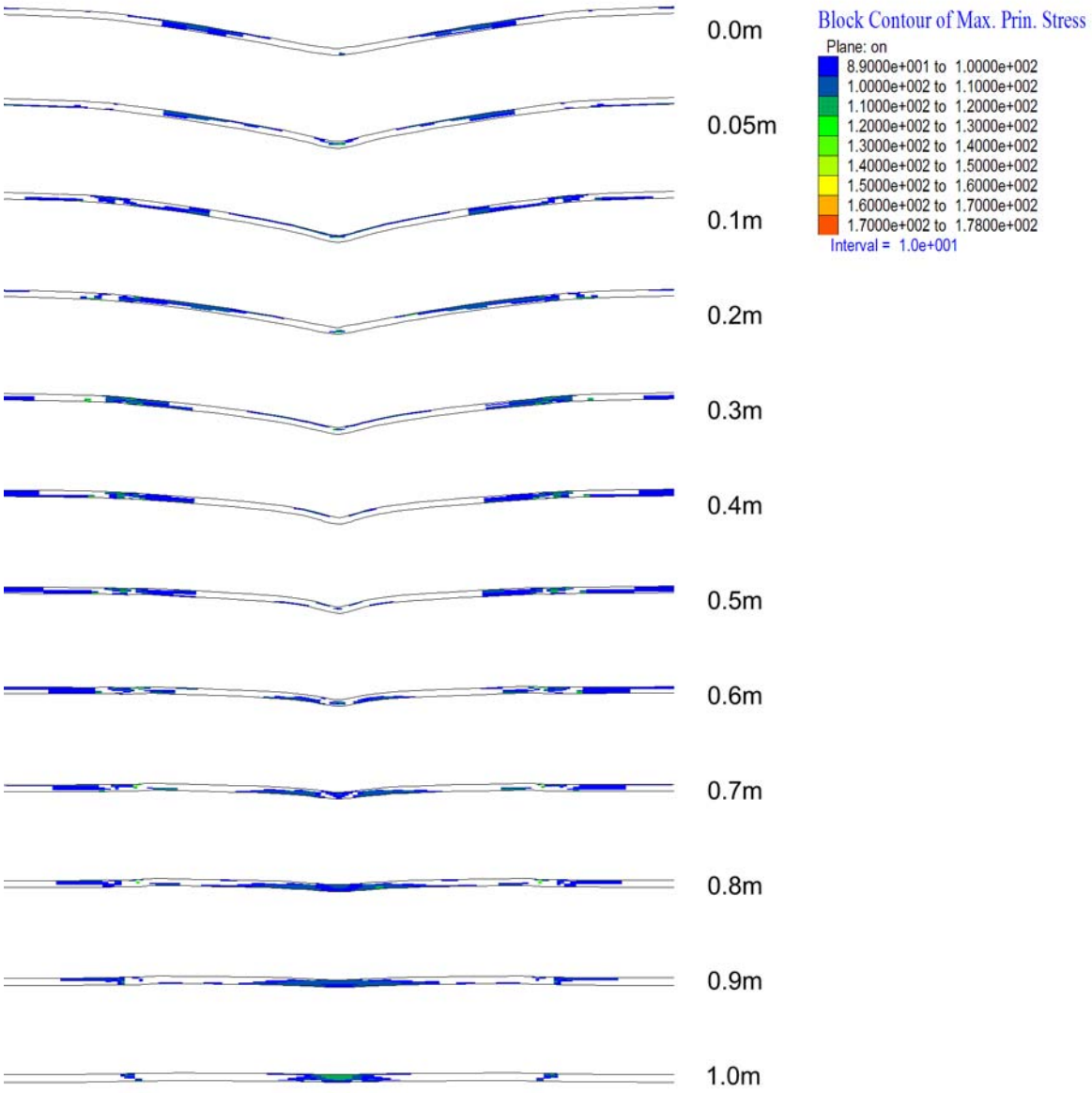

Figure 5.5-17. Major Principal Stress Contours (MPa) in Drip Shield Plates Greater than 89 MPa (50 Percent of the Yield Strength at 150ºC) after 10 y of Stress Relaxation Calculated for the Case 150ºC-2

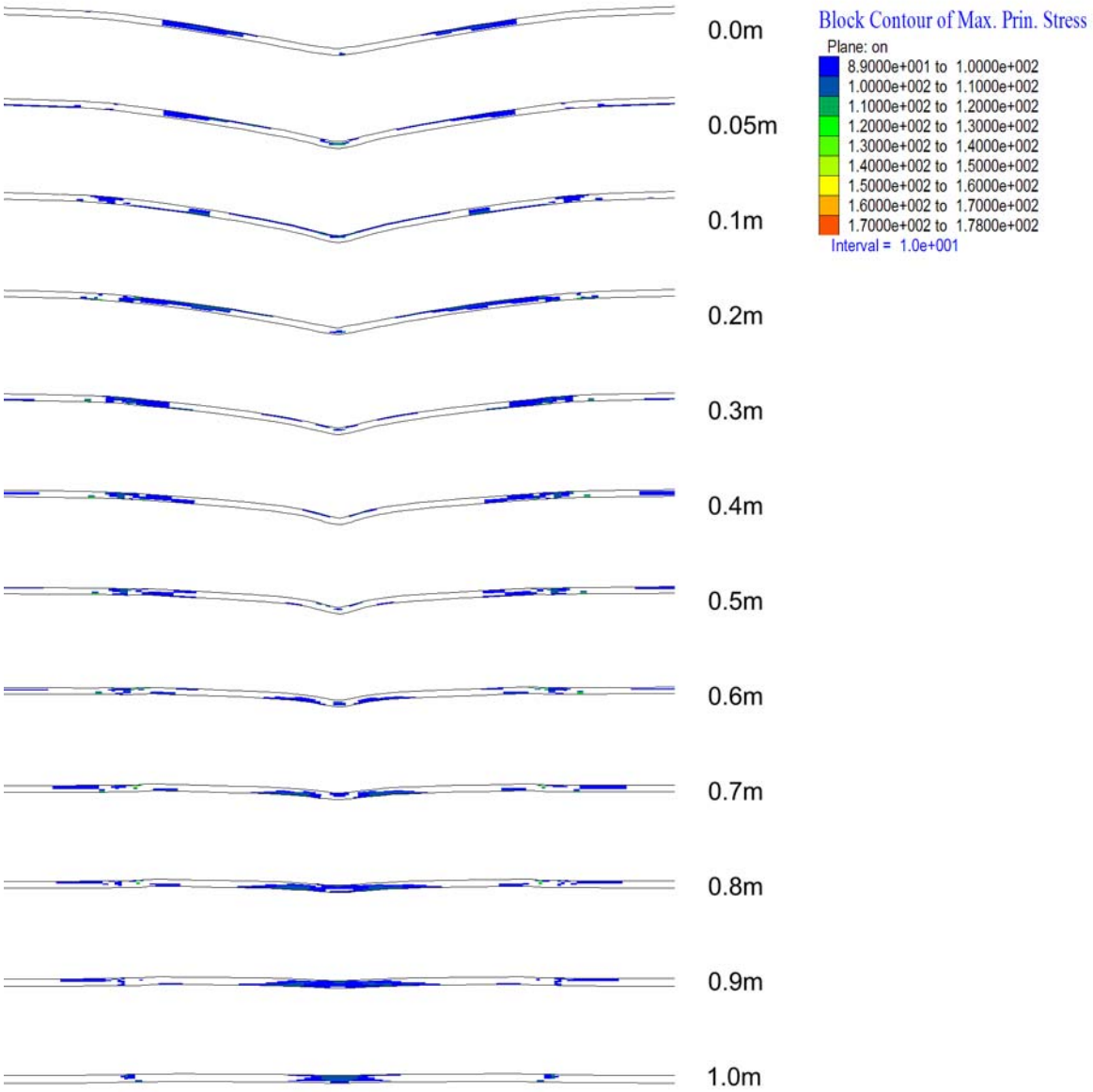

Figure 5.5-18. Major Principal Stress Contours (MPa) in Drip Shield Plates Greater than 89 MPa (50 Percent of the Yield Strength at 150ºC) after 100 y of Stress Relaxation Calculated for the Case 150ºC-2

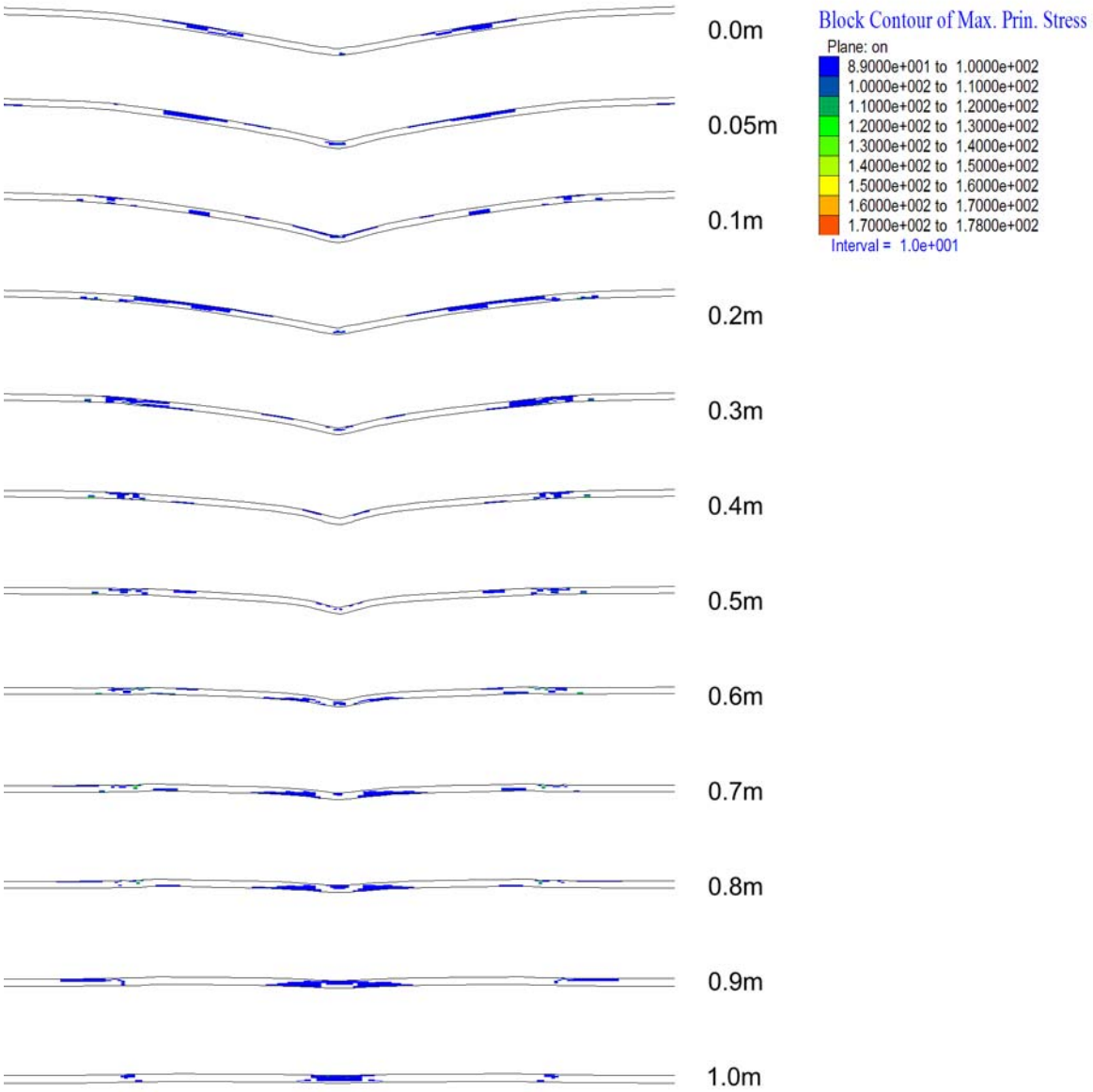

Figure 5.5-19. Major Principal Stress Contours (MPa) in Drip Shield Plates Greater than 89 MPa (50 Percent of the Yield Strength at 150ºC) after 1,000 y of Stress Relaxation Calculated for the Case 150ºC-2

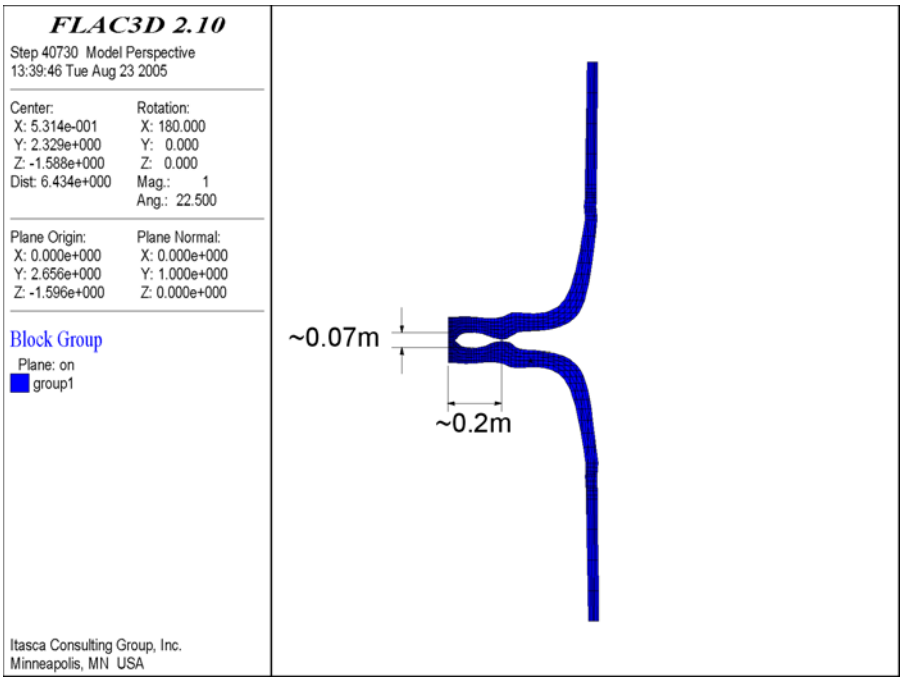

Figure 5.5-20. Horizontal Cross-Section Through the Drip Shield Plate Indicating the Maximum Area where Ponding of Water is Possible

5.6 CONCLUSIONS

Creep of the drip shield structure was analyzed for six realizations of static load by the rubble covering the drip shield after simulation of collapse of the emplacement drift. Creep response of titanium was simulated using a power law representation in which the coefficients of the power law were derived from curve fits that bound laboratory creep tests on titanium samples. The selected coefficients in the creep equations (i.e., power law) represent creep of Ti-7 and Ti-24 at the RT and 150ºC, resulting, at some stress levels and times, in creep predictions that are more than one order of magnitude greater than creep measured in laboratory.

An initial set of calculations were performed in which the coupling of the deformation of the drip shield to reinforcing back-pressures from the rubble was not considered. In these initial, simple calculations, the rubble loads are dead loads—i.e., they do not change with time and drip shield deformation, and any arching of load through the rubble to the rock mass is not considered. The approach of applying the dead load of the rubble is unfavorable from the perspective of drip shield stability and is considered unrealistic. These simulations showed that, if the reinforcing pressures of the rubble back to the drip shield are not considered, instability resulting from a "leaning" of the drip shield is predicted. This "leaning" mode of creep deformation is the result of initial imbalance in the lateral dead loads obtained directly from rubble collapse simulations and applied to the sidewalls of the drip shield. However, it is obvious that, in reality, once the "leaning" mechanism initiates, the rubble will provide a reactive backpressure that will tend to reinforce the drip shield and prevent this mechanism.

The presence of rubble and the mechanical interaction with the drip shield creep deformation was represented by using elastic springs that connect the drip shield legs to the intact

emplacement drift wall. The stiffness of the springs is determined from the estimated elastic modulus of the rubble. When the drip shield deforms toward the rubble, a reactive backpressure will be developed and is applied to the drip shield. When the reactive pressures due to leaning of the drip shield on the rubble are taken into account and applied to its sides (legs), the drip shield is stable for all six load realizations. The maximum displacement after 10,000 years resulting from creep deformation is approximately 5.5 cm, and the maximum creep strain is less than 5 percent. It is assumed (Assumption 3.2.9) that onset of tertiary creep rupture occurs at creep strains greater than 10 percent. Thus, it is concluded that instability (collapse) of the drip shield from creep of titanium is highly unlikely during the 10,000-year period.

Stress relaxation in the drip shield plates after an unlikely event of impact denting by a 28.29 MT block with energy of 707 kJ was analyzed at RT and at 150ºC. The time required for residual stresses in the plates to decay (relax) in such a way that there is no continuous path of the major (maximum) principal stress exceeding the stress-corrosion threshold between the outer and inner surfaces of the plate is determined. The stress-corrosion threshold is assumed to be 50 percent of the yield strength of Ti-7 (Assumption 3.2.12). Two sets of Ti-7 creep equations, fitted to experimental results, at RT and 150ºC were used in the calculations. At RT, the stresses relax below the threshold at a time scale between 1 year and 100 years, depending on the applied creep equations. The stresses relax below the threshold more slowly at 150ºC. Strictly, depending on the creep equation used, it takes between 5 years and 1,000 years for stresses to relax below the threshold. However, even in the case in which it takes 1,000 years for stresses to relax below the 50 percent of yield strength threshold, the stresses are less than 65 percent of the yield strength throughout the plate after 10 years of stress relaxation. The above discussion regarding the time required for stresses to relax below the stress corrosion threshold considers almost entire surface of the drip shield crown. However, on large portion of the crown plate there is no potential for accumulation of water even after denting. Considering the potential for stress corrosion cracking inside the dent where water ponding is possible, the stresses never exceed the stress corrosion threshold in a continuous path which connects outside and inside surface of the drip shield plate for both RT and 150ºC (e.g., see Figures 5.5-5 and 5.5-12). After 10 years, which is a considerable underestimate of the time required for the stress corrosion cracks to propagate through the thickness of the drip shield plate, the stresses above the stress corrosion cracking threshold become very limited within the area where the water can pond, making propagation of stress corrosion cracks through the thickness of the drip shield plates very unlikely.

The main limitation of the analysis is the fact that creep and stress relaxation of the drip shield structure were analyzed for period of 10,000 years based on experimental results obtained from tests which lasted for much sorter period of time, at most 27 years. Extrapolation (from the time scale for which data are available to 10,000 years) was carried out using functional forms widely used to represent creep of titanium and other metals. The effect of uncertainty of extrapolation is reduced (and probably eliminated) by using creep equations in the analysis that bound (in case of creep deformation overestimate creep strain measured in the laboratory by more than one order of magnitude) observed behavior within the time scale of the laboratory tests.

The data developed and documented in this calculation report have been entered into DTN: MO0508SPACREEP.000 in the Technical Data Management System.

INTENTIONALLY LEFT BLANK

6. INPUTS AND REFERENCES

6.1 DOCUMENTS CITED

Andresen, P.L. 2005. *Stress Corrosion Crack Initiation & Growth Measurements in Environments Relevant to High Level Nuclear Waste Packages.* [Schenectady, New York]: General Electric Global Research Center. ACC: MOL.20050608.0317. 173867

ASM International. 1990. *Properties and Selection: Nonferrous Alloys and Special-Purpose Materials.* Volume 2 of *ASM Handbook.* Formerly Tenth Edition, Metals Handbook. 5th Printing 1998. Materials Park, Ohio: ASM International. TIC: 241059. 141615

ASME (American Society of Mechanical Engineers) 2001. *2001 ASME Boiler and Pressure Vessel Code (includes 2002 addenda).* New York, New York: American Society of Mechanical Engineers. TIC: 251425. 158115

ASTM B 265-99. 1999. *Standard Specification for Titanium and Titanium Alloy Strip, Sheet, and Plate.* West Conshohocken, Pennsylvania: American Society for Testing and Materials. TIC: 246708. 132376

Beer, F.P. and Johnston, E.R., Jr. 1977. *Vector Mechanics for Engineers, Statics.* 3rd Edition. New York, New York: McGraw-Hill Book Company. TIC: 247391. 145138

BSC (Bechtel SAIC Company) 2001. *Repository Multiple Waste Package Thermal Calculation.* CAL-WIS-TH-000010 REV 00. Las Vegas, Nevada: Bechtel SAIC Company. ACC: MOL.20010814.0330. 156276

BSC 2002. *Software Implementation Report for FLAC3D Version 2.1.* Document Number: 10502-SIR-2.1-00. Las Vegas, Nevada: Bechtel SAIC Company. ACC: MOL.20020730.0346. 168821

BSC 2004. *Aqueous Corrosion Rates for Waste Package Materials.* ANL-DSD-MD-000001 REV 01. Las Vegas, Nevada: Bechtel SAIC Company. ACC: DOC.20041012.0003. 169982

BSC 2004. *Design and Engineering, Interlocking Drip Shield Configuration.* 000-M00-SSE0-00101-000-00B. Las Vegas, Nevada: Bechtel SAIC Company. ACC: ENG.20040305.0020. 168275

BSC 2004. *Drift Degradation Analysis.* ANL-EBS-MD-000027 REV 03. Las Vegas, Nevada: Bechtel SAIC Company. ACC: DOC.20040915.0010; DOC.20050419.0001. 166107

BSC 2004. *Drip Shield Structural Response to Rock Fall.* 000-00C-SSE0-00300-000-00A. Las Vegas, Nevada: Bechtel SAIC Company. ACC: ENG.20040405.0019; ENG.20050817.0026. 168993

BSC 2004. *General Corrosion and Localized Corrosion of the Drip Shield.* ANL-EBS-MD-000004 REV 02. Las Vegas, Nevada: Bechtel SAIC Company. ACC: DOC.20040921.0002. 169845

BSC 2004. *Mechanical Assessment of the Drip Shield Subject to Vibratory Motion and Dynamic and Static Rock Loading.* CAL-WIS-AC-000002 REV 00A. Las Vegas, Nevada: Bechtel SAIC Company. ACC: DOC.20041028.0004. 169753

BSC 2004. *Repository Subsurface Emplacement Drifts Steel Invert Structure Sect. & Committed Materials.* 800-SS0-SSE0-00102-000-00B. Las Vegas, Nevada: Bechtel SAIC Company. ACC: ENG.20040520.0005. 169776

BSC 2004. *Seismic Consequence Abstraction.* MDL-WIS-PA-000003 REV 01. Las Vegas, Nevada: Bechtel SAIC Company. ACC: DOC.20041025.0004. 169183

BSC 2004. *Stress Corrosion Cracking of the Drip Shield, the Waste Package Outer Barrier, and the Stainless Steel Structural Material.* ANL-EBS-MD-000005 REV 02. Las Vegas, Nevada: Bechtel SAIC Company. ACC: DOC.20041028.0008; DOC.20050621.0003. 172203

BSC 2004. *Structural Stability of a Drip Shield Under Quasi-Static Pressure.* 000-00C-SSE0-00500-000-00A. Las Vegas, Nevada: Bechtel SAIC Company. ACC: ENG.20040830.0032. 170791

BSC 2005. *Drip Shield Structural Response to Rock Fall Supplemental Calculation.* 000-00C-SSE0-00700-000-00A. Las Vegas, Nevada: Bechtel SAIC Company. ACC: ENG.20050707.0002. 174052

BSC 2005. *IED Interlocking Drip Shield and Emplacement Pallet [Sheet 1 of 1].* 800-IED-WIS0-00401-000-00E. Las Vegas, Nevada: Bechtel SAIC Company. ACC: ENG.20050301.0007. 173303

BSC 2005. *Mechanical Assessment of the Waste Package Subject to Vibratory Ground Motion.* CAL-WIS-AC-000001 REV 0B. Las Vegas, Nevada: Bechtel SAIC Company. ACC: DOC.20050823.0001. 173172

BSC 2005. *Multiscale Thermohydrologic Model.* ANL-EBS-MD-000049 REV 03. Las Vegas, Nevada: Bechtel SAIC Company. ACC: DOC.20050711.0001. 173944

BSC 2005. *Q-List.* 000-30R-MGR0-00500-000-002. Las Vegas, Nevada: Bechtel SAIC Company. ACC: ENG.20050805.0006. 174269

DOE (U.S. Department of Energy) 2004. *Quality Assurance Requirements and Description.* DOE/RW-0333P, Rev. 16. Washington, D.C.: U.S. Department of Energy, Office of Civilian Radioactive Waste Management. ACC: DOC.20040907.0002. 171539

Drefahl, K.; Wincierz, P.; Zwicker, U.; and Delarbre, P. [1985]. "230 000 h Creep Properties of Titanium Produced from Electrolytic and Sponge Material and TiAl6V4 Alloy at 20°C." *[Titanium Science and Technology Proceedings of the Fifth International Conference on Titanium, Congress-Center, Munich, FRG, September 10-14, 1984]. [4],* 2387-2394. [Oberrursel, West Germany: Deutsche Gesellschaft fur Metallkunde]. TIC: 257549. 174820

Dutton, R. 1995. *A Methodology to Analyze the Creep Behaviour of Nuclear Fuel Waste Containers.* AECL-11249. Pinawa, Manitoba, Canada: Whiteshell Laboratories, Atomic Energy of Canada Limited. TIC: 226154. 173919

Dutton, R. 1996. *A Review of the Low-Temperature Creep Behaviour of Titanium.* AECL-11544. Pinawa, Manitoba, Canada: Whiteshell Laboratories, Atomic Energy of Canada Limited. TIC: 231204. 174750

Itasca Consulting Group [2002]. *Itasca Software–Cutting Edge Tools for Computational Mechanics.* Minneapolis, Minnesota: Itasca Consulting Group. TIC: 252592. 160331

Kiessel, W.R. and Sinnott, M.J. 1953. "Creep Properties of Commercially Pure Titanium." *Journal of Metals, 5,* (2), 331-338. New York, New York: American Institute of Mining and Metallurgial Engineers. TIC: 257556. 174853

Odegard, B.C. and Thompson, A.W. 1974. "Low Temperature Creep of Ti-6 Al-4 V." *Metallurgical Transactions, 5,* (5), 1207-1213. New York, New York: Metallurgical Society of American Institue of Mining, Metallurgical, and Petroleum Engineers. TIC: 251481. 174818

Teper, B. 1991. "Activities Aimed at Qualification of a HLW Disposal Container." *High Level Radioactive Waste Management, Proceedings of the Second Annual International Conference, Las Vegas, Nevada, April 28-May 3, 1991. 2,* 961-967. La Grange Park, Illinois: American Nuclear Society. TIC: 204272. 174819

Thompson, A.W. and Odegard, B.C. 1973. "The Influence of Microstructure on Low Temperature Creep of Ti-5 Al-2.5 Sn." *Metallurgical Transactions, 4,* 899-908. [Warrendale, Pennsylvania]: Metallurgical Society of AIME and American Society for Metals. TIC: 257573. 174852

TIMET. 1993. First in Titanium Worldwide, Quality Products and Services. Denver, Colorado: [Titanium Metals Corporation]. TIC: 242692. 157726

Timoshenko, S.P. and Goodier, J.N. 1970. *Theory of Elasticity.* 3rd Edition. New York, New York: McGraw-Hill. TIC: 245469. 121096

6.2 CODES, STANDARDS, REGULATIONS, AND PROCEDURES

10 CFR 63. 2005 Energy: Disposal of High-Level Radioactive Wastes in a Geologic Repository at Yucca Mountain, Nevada. ACC: MOL.20050405.0118. 173273

LP-3.12Q-BSC. *Design Calculations and Analyses*. REV 00 ICN 00. Washington, D.C.: U.S. Department of Energy, Office of Civilian Radioactive Waste Management. ACC: DOC.20050518.0007.

LP-SI.11Q-BSC. *Software Management*. REV 00 ICN 01. Washington, D.C.: U.S. Department of Energy, Office of Civilian Radioactive Waste Management. ACC: DOC.20041005.0008.

6.3 SOURCE DATA, LISTED BY DATA TRACKING NUMBER

MO0003RIB00073.000. Physical and Chemical Characteristics of Ti Grades 7 and 16. Submittal date: 03/13/2000. 152926

MO0407MWDDSLCR.000. Drip Shield Load in Collapsed Lithophysal Rock. Submittal date: 07/21/2004. 170873

MO0408MWDGLCDS.002. General Corrosion and Localized Corrosion of the Drip Shield for LA. Submittal date: 08/27/2004. 171486

MO0409GE835924.000. Stress Corrosion Crack Initiation & Growth Measurements for C-22 and Ti-7 in Environments Relevant to High Level Nuclear Waste Packages. Submittal date: 09/09/2004. 171564

6.4 SOFTWARE CODES

BSC 2002. *Software Code: FLAC3D*. V2.1. PC WINDOWS 2000/NT 4.0. STN: 10502-2.1-00. 161947

ATTACHMENT I

DERIVATION OF CREEP EQUATIONS FOR TI-7 AND TI-24

I-1 INTRODUCTION

The mathematical characterization of the creep constitutive behavior of titanium used in the numerical analysis is provided in this Attachment. Based on the information provided in the literature, particularly by Dutton (1996) [DIRS 174750] (a comprehensive literature survey on titanium creep behavior) different creep equations for Ti-7 and Ti-24 are developed in this attachment. Creep predictions resulting from these equations are compared with experimental results in order to demonstrate their conservatism for use in further numerical analyses.

I-2 CREEP LAWS

Creep, which is a transient process, is a function (Dutton 1995, Equations 6 and 7 [DIRS 173919], Section 4.2 and Eq. 2) of stress, σ, and temperature, T—that is:

$$\varepsilon = \varepsilon(\sigma, t, T) \qquad \text{(Eq. I-1)}$$

The creep response (i.e., the creep strain expressed as a function of time under constant applied load) described by equation I-1 is typically subdivided into three parts: a) initial, primary or transient creep in which the creep rate changes rapidly as a function of time, b) secondary or steady state creep in which the creep rate is more or less constant, and, c) tertiary creep or creep rupture in which the creep rate rapidly accelerates, resulting in rupture and failure of the sample. Among the different functional forms representing the creep dependence on stress, temperature and time (during primary and secondary creep), the following is often used (Equations (5) and (7) in Dutton 1996 [DIRS 174750]):

$$\varepsilon = A\sigma^n t^m e^{-\frac{Q}{kT}} \qquad \text{(Eq. I-2)}$$

A, n and m are coefficients obtained by fitting the equation to the experimental results. Q is the activation energy, $k = 8.31\,\text{J/mol K}$ is the Boltzman constant, and T is the absolute temperature (in degrees K). This functional dependence of creep (and creep rate) on stress is termed Norton's power law. Different coefficients (A and n) often are used over different stress ranges to obtain better fits to the experimental data, leading to a two-component power creep law. As the creep changes from primary to secondary[1] and tertiary, it is clear that a single function describing creep and creep-rate dependence to time is an oversimplification. For example, Drefahl et al. (1985) [DIRS 174820] use a logarithmic function (Equation 1) to fit the creep strains for small values of stress and strain, and a power law (Equation 2), for large values of stress and strain.

The objective of this investigation of the titanium creep equations to be used in the analysis of the drip shield structure was to develop a relatively simple functional form of the creep law that will result in conservative estimates of: (a) the time-dependent deformation of the drip shield and potential for drip shield collapse and (b) the time required for relaxation of residual stresses in the drip shield plates resulting from impact denting.

[1] Some laboratory results (e.g., Drefahl et al. 1985) suggest that creep rate is always transient (i.e., the secondary or steady creep rate is an idealization that is dependent on test duration).

In the analyses discussed in this document (i.e., drip shield creep analysis in Section 5.4 and stress relaxation in Section 5.5) characterization of creep of Ti-7 and Ti-24 at RT and 150ºC at specific stress levels is required. Experimental data for those grades do not exist for all conditions of interest (i.e., stress and temperature ranges). The following approach is used in development of the creep equations that are used in the calculations. In the first step, creep equations are derived by fit to experimental data on similar materials (e.g., commercially-pure titanium for Ti-7, Assumption 3.2.13; or Ti-6Al-4V for Ti-24, Assumption 3.2.14), or on material that creeps more than the grades of interest (e.g., Ti-5Al-2.5Sn for Ti-24). In these equations, a single component power law represents dependence of creep to stress. Often this approximation does not provide at all stress levels a good fit to measured results. Instead, two (or more) different equations need to be used for approximation of creep within different stress intervals. To reduce uncertainty due to representation of creep by the single component creep law, two different equations are fitted to the experimental results of Ti-7 creep. These two equations bound experimental data in different stress intervals. Experimental data were obtained on titanium alloys that are mechanically similar to Ti-7 and Ti-24, but not the same. Consequently, their yield strengths are different from those of Ti-7 and Ti-24. Although creep of titanium (or other materials) is usually expressed as a function of stress, the ratio of stress to the yield strength is the factor that affects creep. In the second step, the creep equations are rescaled accounting for the yield strengths of Ti-7 and Ti-24, which are used in the calculations. The initial fit is obtained for RT, because most of available data are for RT. Finally, in the third steps, the creep equations are transformed (using the relation shown in Equation I-2) to attain predictions of creep at 150ºC. To account for temperature effect on creep predictions it is necessary to estimate creep activation energy, Q. The estimate is verified by comparison with experimental results obtained at different temperatures.

I-3 CREEP EQUATIONS FOR TI-7

I-3.1 FITTING A POWER LAW TO LONG-TERM CREEP DATA

Drefahl et al. (1985) [DIRS 174820] describe the results of creep tests, conducted on commercially-pure titanium at RT, which lasted for 27 years. These creep tests involved placing rods of commercially-pure titanium under constant uniaxial load while measuring the associated time-dependent uniaxial displacement (and, thus, strain) of the sample. Because the commercially-pure titanium, Ti-2, is analogous to Ti-7, and 27 years is the longest testing period for titanium noted in the literature, the results by Drefahl et al. (1985), Figure 3, [DIRS 174820] are used as the basis for development of the creep equations for Ti-7 (Assumption 3.2.13). The creep strains (as a percentage) measured in these tests as a function of time and applied stress are shown as solid lines in Figures I-1 and I-2. The curves indicate that if stresses are equal or larger than approximately 227 MPa, the strain is best represented by a power function of time. The strain is best represented as a logarithmic dependence of time if stresses are less than about 227 MPa. However, it is advantageous for the numerical analyses described in Section 5 of this calculation if the creep strain is described by a power law for the entire range of applied stresses. To this end, two different power laws are fitted to the experimental results for the entire stress range. Creep strains predicted by Equation (I-3) are compared with experimental results in Figure I-1:

$$\varepsilon = 2.71 \cdot 10^{-24} \sigma^{8.81} t^{0.28} \qquad \text{(Eq. I-3)}$$

In these equations and elsewhere in the document, unless stated otherwise, σ is stress in MPa, and t is time in h. This equation provides a reasonable fit that slightly overpredicts the measured strains for stresses equal to or less than about 251 MPa. For larger stresses (i.e., more than 85% of the yield strength for Ti-7), Equation (I-3) slightly underpredicts the creep strain. The underprediction is not significant, particularly before the onset of tertiary creep (which is not simulated explicitly in the calculations of drip shield creep in Sections 5.4 and 5.5); it shows a trend of decay with time, indicating that, at later times, the creep equation probably would overpredict creep strains from the experimental results (if they exist).

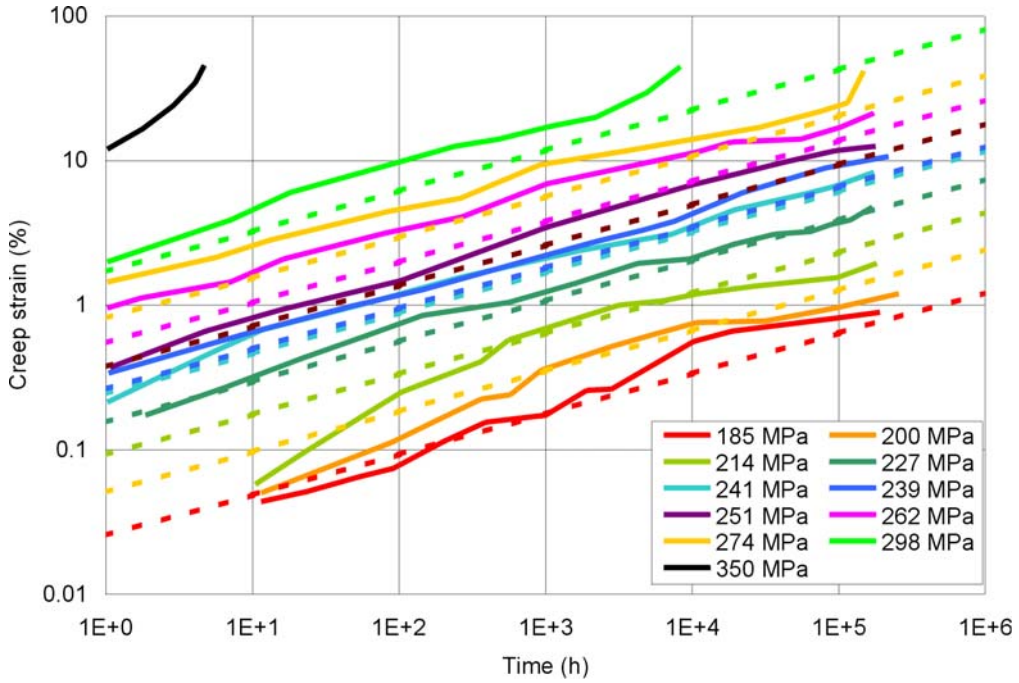

NOTE: The solid lines are experimental results digitized from the paper by Drefahl et al. (1985), Figure 3 [DIRS 174820]. The dashed lines are equations fitted to the experimental data.

Figure I-1. Fit of Equation (I-3) to the Experimental Creep Data by Drefahl et al. (1985), Figure 3 [DIRS 174820] for Commercially-Pure Titanium at RT

The second fit to the Drefahl et al. (1985), Figure 3 [DIRS 174820] data, given by Equation (I-4), is compared to the experimental results in Figure I-2:

$$\varepsilon = 1.33 \cdot 10^{-30} \sigma^{11.48} t^{0.28} \qquad \text{(Eq. I-4)}$$

Equation (I-4) provides a reasonable fit to the experimental data or overpredicts the measured creep strains for all stress levels equal to or larger than 200 MPa. The underprediction of the creep strain is indicated for 185 MPa, but the trend of the measured data indicates reduction of the difference for later times.

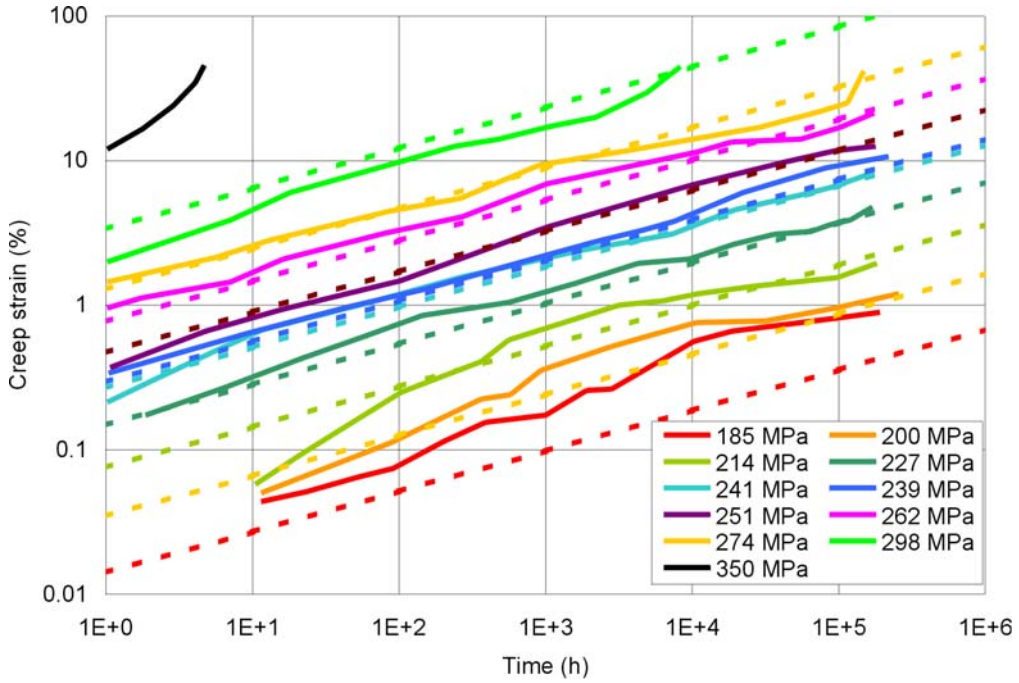

NOTE: The solid lines are experimental results digitized from the paper by Drefahl et al. (1985), Figure 3 [DIRS 174820]. The dashed lines are equations fitted to the experimental data.

Figure I-2. Fit of Equation (I-4) to the Experimental Creep Data by Drefahl et al. (1985), Figure 3 [DIRS 174820] for Commercially-Pure Titanium at RT

I-3.2 SCALING OF THE POWER LAW TO ACCOUNT FOR TITANIUM YIELD STRENGTH

Although commercially-pure Ti-2 titanium and Ti-7 alloy are considered to be mechanically-analogous (Assumption 3.2.13), there is a slight discrepancy between their yield strengths at RT. Dutton (1996) [DISR 174750] states (in Section 5.1) that the yield strength of the commercially-pure titanium used by Drefahl et al. (1985) [DIRS 174820] was 295 MPa. The yield strength of non-commercially-pure Ti-2 used in the analysis is 276 (ASME 2001 [DIRS 158115], Section II, Part D, Table Y-1). If the power law that describes creep of the material with yield strength σ_{y1} is known to be:

$$\varepsilon_{\sigma_{y1}} = A_{\sigma_{y1}} \sigma^n \qquad \text{(Eq. I-5)}$$

then the coefficient $A_{\sigma_{y2}}$, which describes creep of a similar material with yield stress σ_{y2}, e.g.,:

$$\varepsilon_{\sigma_{y2}} = A_{\sigma_{y2}} \sigma^n \qquad \text{(Eq. I-6)}$$

can be approximated using the following rescaling of stresses:

$$\varepsilon_{\sigma_{y2}} = A_{\sigma_{y1}} \left(\sigma \frac{\sigma_{y1}}{\sigma_{y2}} \right)^n$$
$$A_{\sigma_{y2}} = A_{\sigma_{y1}} \left(\frac{\sigma_{y1}}{\sigma_{y2}} \right)^n \quad \text{(Eq. I-7)}$$

Using that approach, Equations (I-3) and (I-4) can be transformed into Equations (I-8) and (I-9) to be consistent with the ASME code minimum (ASME 2001 [DIRS 158115], Section II, Part D, Table Y-1) yield strength of 276 MPa as follows:

$$\varepsilon = 4.87 \cdot 10^{-24} \sigma^{8.81} t^{0.28} \quad \text{(Eq. I-8)}$$

$$\varepsilon = 2.86 \cdot 10^{-30} \sigma^{11.48} t^{0.28} \quad \text{(Eq. I-9)}$$

Although there is a physically-based method to account for the effect of temperature on creep using the activation energy for creep, as shown in Equation (I-2) and used in Section I-3.3, the effect of temperature on creep law can be estimated by also rescaling the stresses, using the yield strength of Ti-7 at 150º of 178 MPa – approximately 1% higher than the values of 176 MPa listed in Table 5-2.1; this results in the following relation:

$$\varepsilon = 2.32 \cdot 10^{-22} \sigma^{8.81} t^{0.28} \quad \text{(Eq. I-10)}$$

I-3.3 SCALING OF THE POWER LAW TO ACCOUNT FOR TEMPERATURE EFFECT

Creep can be expressed, based on Equation (I-2), in the following form

$$\varepsilon(\sigma, t, T) = \varepsilon_o(\sigma, t) e^{-\frac{Q}{kT}} \quad \text{(Eq. I-11)}$$

Consequently, if the creep, $\varepsilon_{RT}(\sigma, t)$, at room temperature is known, the creep strain at any other temperature can be calculated using the following relation:

$$\varepsilon(\sigma, t, T) = \varepsilon_{RT}(\sigma, t) \frac{e^{-\frac{Q}{kT}}}{e^{-\frac{Q}{kT_{RT}}}} \quad \text{(Eq. I-12)}$$

where T_{RT} is RT in degrees K. The parameter that is needed to estimate creep strain as a function of temperature is the activation energy of creep, Q. This parameter varies depending on the type of material, but it also varies for a particular material as a function of temperature. Kiessel and Sinnott (1953) [DIRS 174853] investigated creep of commercially-pure titanium at elevated temperatures in tests that lasted approximately 1,000 hours. The results of their tests (relations between steady creep rate and stress at a given temperature) are shown in Figure I-3 as a solid

red line (at RT) and dots at elevated temperatures. Blue and green dashed lines are generated from the RT line using Equation (I-12) for an activation energy of creep, Q, equal to 30 kJ/mol (Assumption 3.2.15). The extrapolated lines and, consequently, use of the assumed value of Q, predict larger creep rates for the same stress levels. The agreement between the experimental results and the fit is reasonable at 99ºC, but there is significant disagreement at 204ºC. There is an anomaly in the temperature effect on the creep, manifested by a larger creep strain rate at 99ºC than at 204ºC. This effect also can be observed in the plot of the stress required to achieve a 10^{-4} /h creep strain rate in 1,000 h. The thermal anomaly is not properly accounted for by relation I-11, which will overpredict creep deformation at the temperature level of interest for $Q = 30$ kJ/mol. However, for residual stress relaxation predictions at 150ºC, associated with impact denting (Section 5.5), using the same equation and activation energy of creep value will overpredict stress relaxation rate. Two sets of creep equations (at 150ºC) were used in the stress relaxation analysis (Sections 5.3.2 and 5.5) to address this issue.

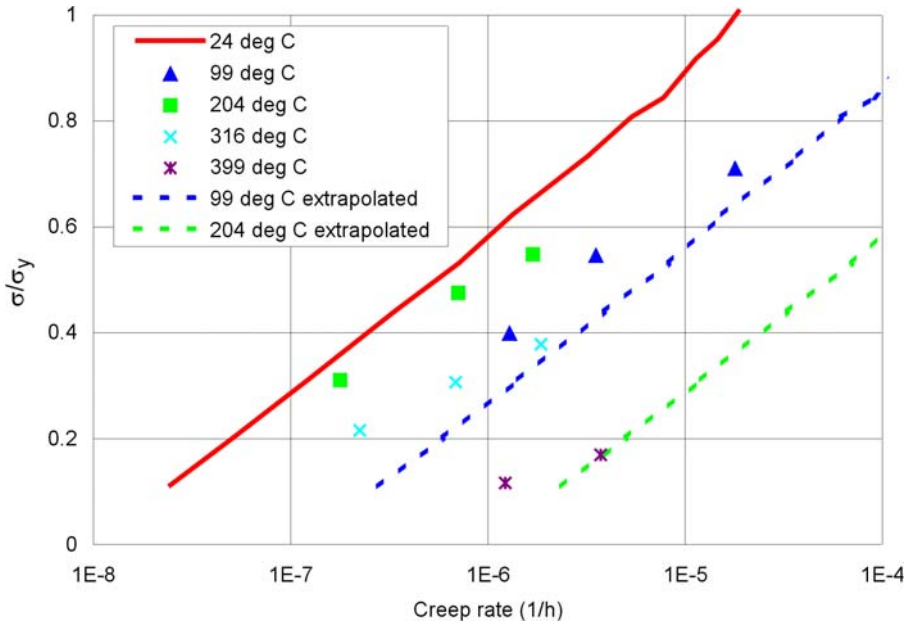

NOTE: The solid line and points are experimental results digitized from the paper by Kiessel and Sinnott (1953), Figure 12 [DIRS 174853]. The dashed lines are creep model predictions based on the assumed activation energy (Assumption 3.2.15).

Figure I-3. Effect of Temperature on Creep Rates Measured in the Laboratory by Kiessel and Sinnott (1953), Figure 12 [DIRS 174853] for Commercially-Pure Titanium Compared with Model Predictions for Activation Energy, Q, of 30 kJ/mol

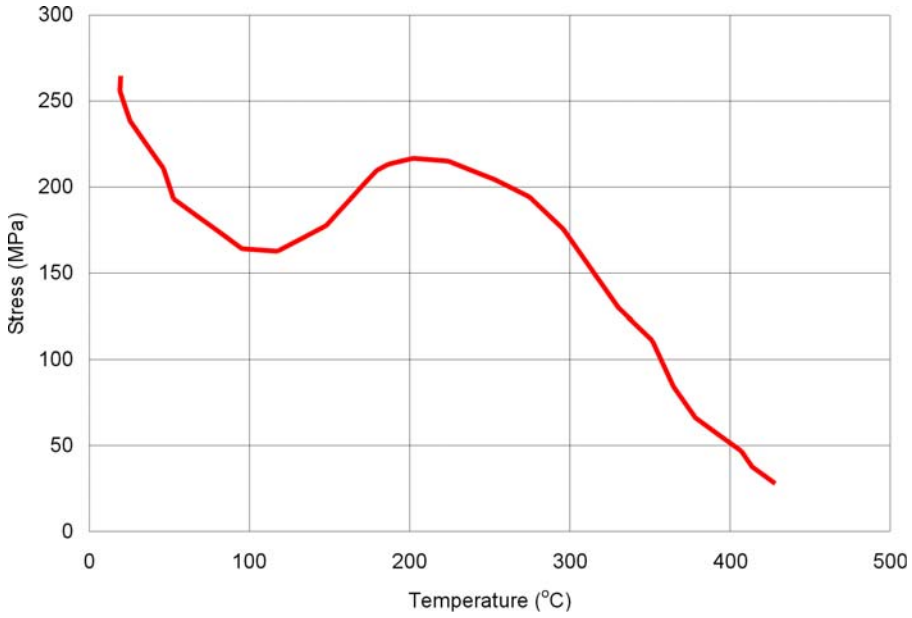

NOTE: The solid line is an experimental result digitized from the paper by Kiessel and Sinnott (1953), Figure 13 [DIRS 174853].

Figure I-4. Effect of Temperature on Stress Required to Achieve a 10^{-4} 1/h Creep Rate Measured in the Laboratory by Kiessel and Sinnott (1953), Figure 13 [DIRS 174853] for Commercially-Pure Titanium

The creep strains of Ti-7 at 150ºC, estimated from Equations (I-8) and (I-9) using relation (Equation I-12) for $Q = 30$ kJ/mol, are shown in Equations (I-13) and (I-14), respectively:

$$\varepsilon = 2.15 \cdot 10^{-22} \sigma^{8.81} t^{0.28} \quad \text{(Eq. I-13)}$$

$$\varepsilon = 1.26 \cdot 10^{-28} \sigma^{11.48} t^{0.28} \quad \text{(Eq. I-14)}$$

Equation (I-15) is derived as an overestimate of creep strain for Ti-7 at 150ºC by applying relation (I-12) to Equation (I-10), already rescaled by Ti-7 yield strength at 150ºC. Practically, this means that the temperature effect is accounted for twice:

$$\varepsilon = 1.02 \cdot 10^{-20} \sigma^{8.81} t^{0.28} \quad \text{(Eq. I-15)}$$

Equation (I-15) is used in the prediction of drip shield creep deformation (Sections 5.3.1 and 5.4). Equations (I-8) and (I-9), at RT, and Equations (I-13) and (Equation I-14), at 150ºC, are used for prediction of stress relaxation (Sections 5.3.2 and 5.5).

I-3.4 COMPARISON OF CREEP EQUATIONS WITH TEPER (1991) DATA

Teper (1991) [DIRS 174819] (in Figure 3 and equations 1 and 2) reported results of creep tests on Ti-2 (analogous to Ti-7, Assumption 3.2.13) at 125ºC, which is relatively close to temperature of interest for drip shield creep calculations. The test at stresses ranging between 50 and 95 percent of the yield strength lasted between 1,300 h and 6,300 h. The reason these data were not

used in this report for derivation of creep equations used in the analysis is that test duration is relatively short compared to 27 years duration of the tests by Drehafl et al. (1985 [DIRS 174820]). The creep equations derived for Ti-7 in the previous Sections are compared with the Teper (1991) [DIRS 174819] data.

Teper (1991) [DIRS 174819] proposed the following equations as a fit to the his test results:

$$\varepsilon = \begin{cases} 3.54 \cdot 10^{-13} \sigma^{4.92} \ln t & \sigma < 0.9\sigma_y \\ 3.1 \cdot 10^{-30} \sigma^{12.6} t^{0.1125} & \sigma > 0.9\sigma_y \end{cases} \quad \text{(Eq. I-16)}$$

Strains in Equation (I-16) are in percent. The proposed creep equations for Ti-7 given by relations (I-8), (I-9) and (I-10) are rescaled, using Equation (I-12) and $Q = 30\,\text{kJ/mol}$ (Assumption 3.2.15), for a temperature of 125ºC, at which the tests reported by Teper (1991) [DIRS 174819] were conducted. (Equations I-8, I-9 and I-10 are for RT; equations I-13, I-14 and I-15 are for 150ºC and cannot be directly compared with the Teper (1991) [DIRS 174819] data which were obtained at 125ºC.) The three rescaled equations are compared (in Figures I-5 through I-7) with the test results and creep equations reported by Teper (1991) [DIRS 174819]. Equation (I-10), which is the basis for equation (I-15) used in the analysis of creep of the drip shield (Section 5.3.1), predicts much larger creep strains at all stress levels and times (Figure I-7). This comparison provides additional confidence that the creep equations for Ti-7 used in the analysis of drip shield stability under the quasi-static load of the rubble will overpredict creep deformation. Equations (I-8) and (I-9), which are the basis for the equations used in stress relaxation (Section 5.3.2), predict greater creep strains at higher stress levels; however, when the stresses decay to 75 percent of yield stress or less, they match or underpredict (Figure I-6) the Teper (1991) [DIRS 174819] data.

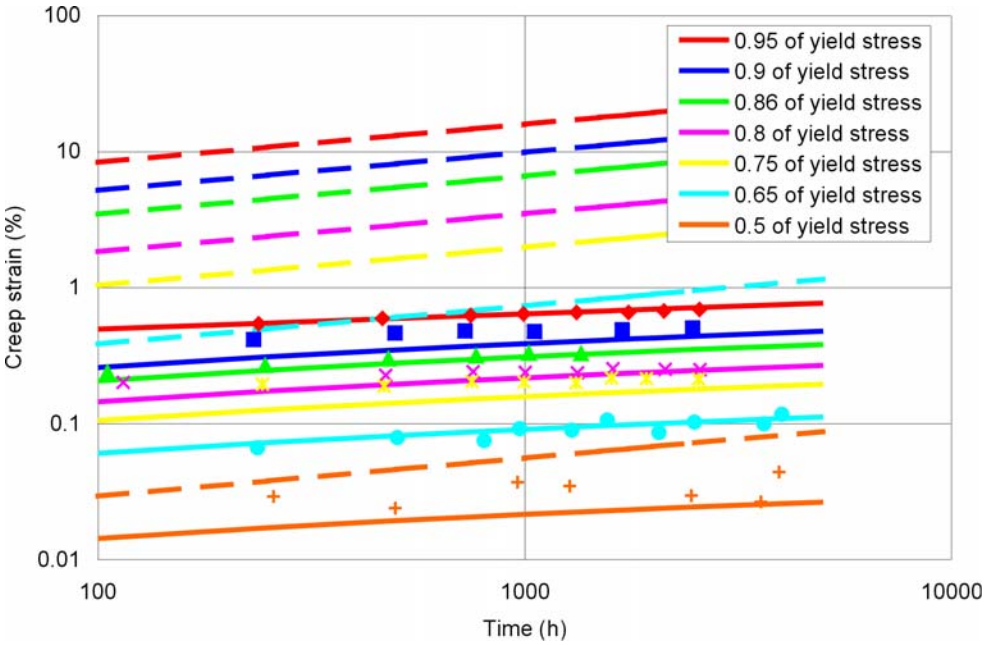

NOTE: The solid lines are creep Equations (I-16) proposed by Teper (1991) [DIRS 174819]. The points are digitized experimental data reported by Teper (1991) [DIRS 174819]. The dashed lines are predictions by Equation (I-8) rescaled to 125ºC.

Figure I-5. Comparison of Creep Predicted by Equation (I-8), Rescaled to 125ºC, with the Results of Teper (1991) [DIRS 174819]

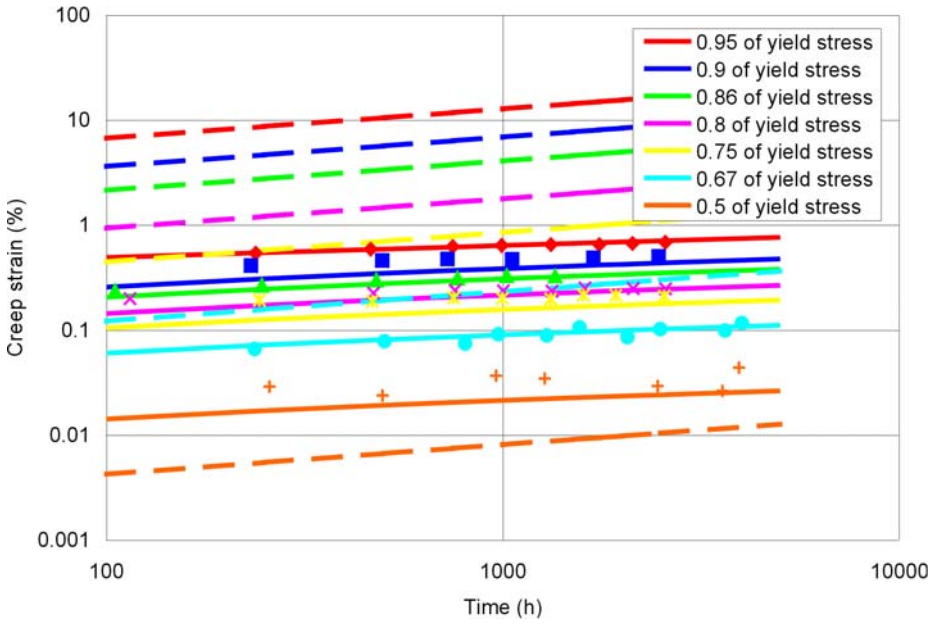

NOTE: The solid lines are creep Equations (I-16) proposed by Teper (1991) [DIRS 174819]. The points are digitized experimental data reported by Teper (1991) [DIRS 174819]. The dashed lines are predictions by Equation (I-9) rescaled to 125ºC.

Figure I-6. Comparison of Creep Predicted by Equation (I-9), Rescaled to 125ºC, with the Results of Teper (1991) [DIRS 174819]

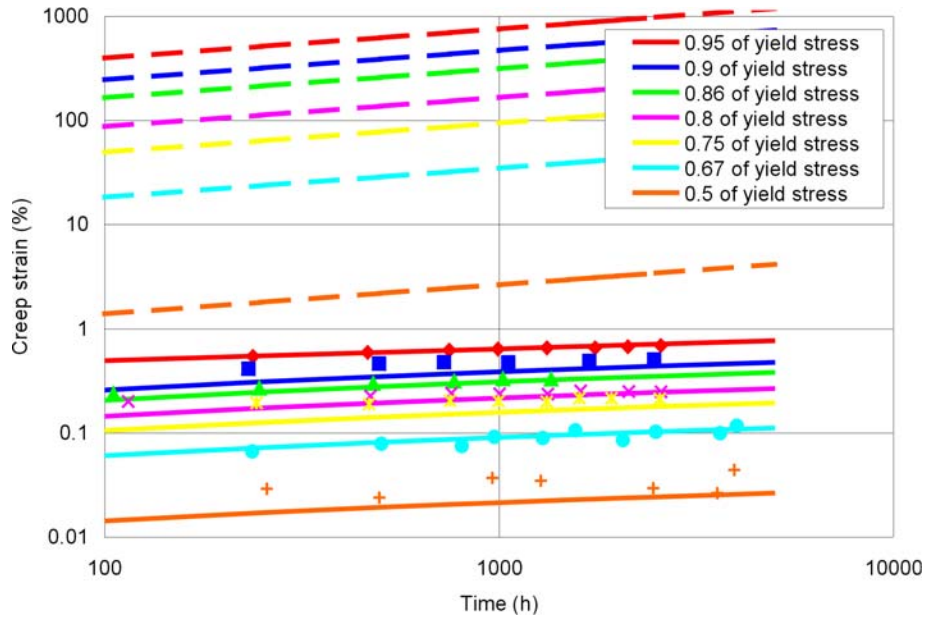

NOTE: The solid lines are creep Equations (I-16) proposed by Teper (1991) [DIRS 174819]. The points are digitized experimental data reported by Teper (1991) [DIRS 174819]. The dashed lines are predictions by Equation (I-10) rescaled to 125ºC.

Figure I-7. Comparison of Creep Predicted by Equation (I-10), Rescaled to 125ºC, with the Results of Teper (1991) [DIRS 174819]

I-4 CREEP EQUATIONS FOR TI-24

Experimental data obtained on Ti-6Al-4V (Odegard and Thompson 1974, Figure 3 [DIRS 174818]; Drefahl et al. (1985), Figure 10 [DIRS 174820]), which is mechanically similar to Ti-24 (Assumption 3.2.14), were used as a basis for derivation of creep equations for Ti-24 at RT. These equations are also compared with results of Thompson and Odegard (1973), Figure 4 [DIRS 174852] from tests on Ti-5Al-2.5Sn, which is an alloy that creeps more than Ti-24. Demonstration that the equations derived for Ti-24 predict greater creep than that observed in laboratory tests on Ti-5Al-2.5Sn confirms that the equations will overpredict the drip shield creep deformation. The experimental results for creep at elevated temperature are available for Ti-5Al-2.5Sn only (Thompson and Odegard 1973, Figure 4 [DIRS 174852]). Those results are compared with predictions of the creep equations for Ti-24 at elevated temperatures (obtained from the creep equations at RT using creep energy activation, Q, of 30 kJ/mol, Assumption 3.2.15).

I-4.1 FITTING A POWER LAW TO RT CREEP DATA

Odegard and Thompson (1974) [DIRS 174818] conducted RT creep tests on Ti-6Al-4V (Ti-5), which is mechanically-analogous to Ti-24 (Assumption 3.2.14). The results from the 1,000 h test are shown as dots in Figure I-8. The creep strains are bounded by creep law (i.e., the creep law predicts larger strains than those reported from the test) provided in Equation (I-17):

$$\varepsilon = 0.0208\left(\frac{\sigma}{\sigma_y}\right)^{12.15} t^{0.25} \qquad \text{(Eq. I-17)}$$

Thompson and Odegard's (1973), Figure 4 [DIRS 174852] test results and comparison with creep predictions by Equation (I-17) are shown in Figure I-9. Ti-5Al-2.5Sn exhibits more creep than Ti-6Al-4V. The creep equations that fit the test results for Ti-5Al-2.5Sn will overpredict creep strain for Ti-24. [Creep of Ti-24, used for structural elements (support beams and bulkheads) does not have a significant effect on stress relaxation of the drip shield plates. The structural elements are relatively rigid compared to the plates and stress relaxation or creep of these elements will not have considerable effect on stress relaxation in the plates. Therefore, the same equations derived to overestimation the creep deformation in Section 5.4 are also used in the analysis of impact dent-induced residual stress relaxation analysis in Section 5.5.] The creep test results shown in Figure I-9 are for bar stock titanium and lasted 1,000 h (the same as test results for Ti-6Al-4V, shown in Figure I-8). In the same paper, Thompson and Odegard (1973), Figure 4 [DIRS 174852] reported the results of creep tests for α- and β-forged titanium that lasted 10,000 h. Bar stock titanium shows smaller creep resistance than forged titanium, but the trend of creep to increase as a function of time is the same for all three sets of results (i.e., bar stock, α- and β-forged), providing additional confidence in extrapolation of the results obtained on bar stock beyond 1,000 h of testing. Drefahl et al. (1985), Figure 10 [DIRS 174820] reported creep results at RT conducted on Ti-6Al-4V that lasted 27 years. Unfortunately, the test was conducted for a single stress value of 723 MPa. The test results, as digitized from Drefahl et al. (1985), Figure 10 [DIRS 174820] are shown in Figure I-10 as a solid line. The creep strain predictions by Equation (I-17), shown in the same Figure as a dashed line, exceed the measured strains.

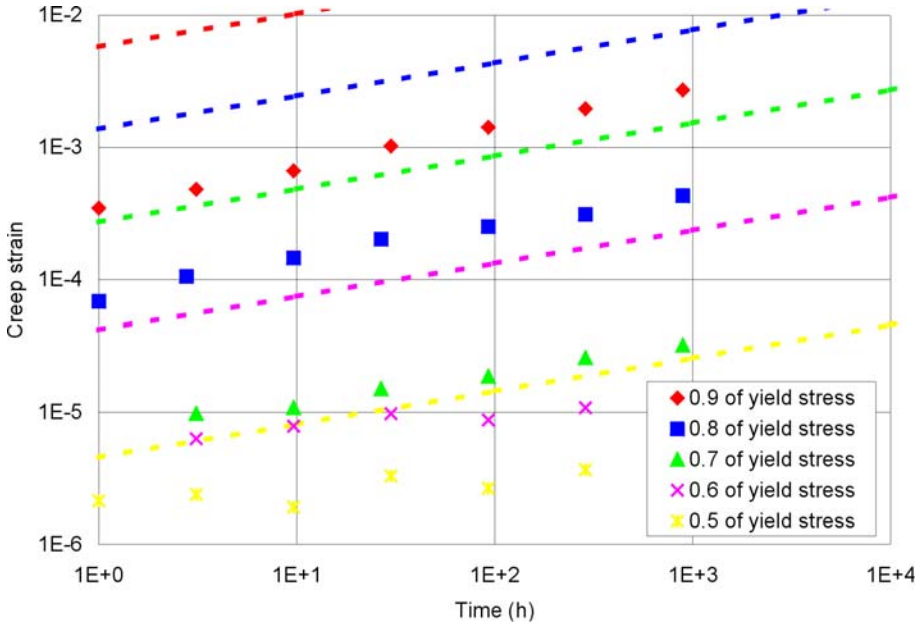

NOTE: The solid lines are experimental results digitized from the paper by Odegard and Thompson (1974), Figure 3 [DIRS 174818]. The dashed lines are model predictions.

Figure I-8. Comparison of Creep Strains Predicted by Equation (I-17) (Dashed Lines) to the Experimental Creep Data by Odegard and Thompson (1974), Figure 3 [DIRS 174818] for Ti-6Al-4V at RT

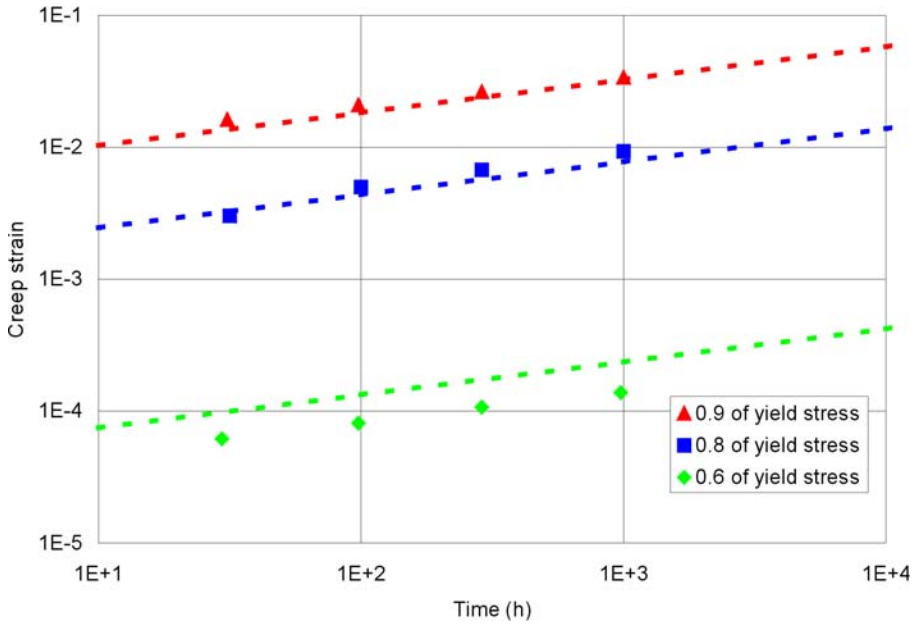

NOTE: The solid lines are experimental results digitized from the paper by Thompson and Odegard (1973), Figure 4 [DIRS 174852]. The dashed lines are model predictions.

Figure I-9. Comparison of Creep Strains Predicted by Equation (I-17) (Dashed Lines) to the Experimental Creep Data by Thompson and Odegard (1973), Figure 4 [DIRS 174852] for Ti-5Al-2.5Sn at RT

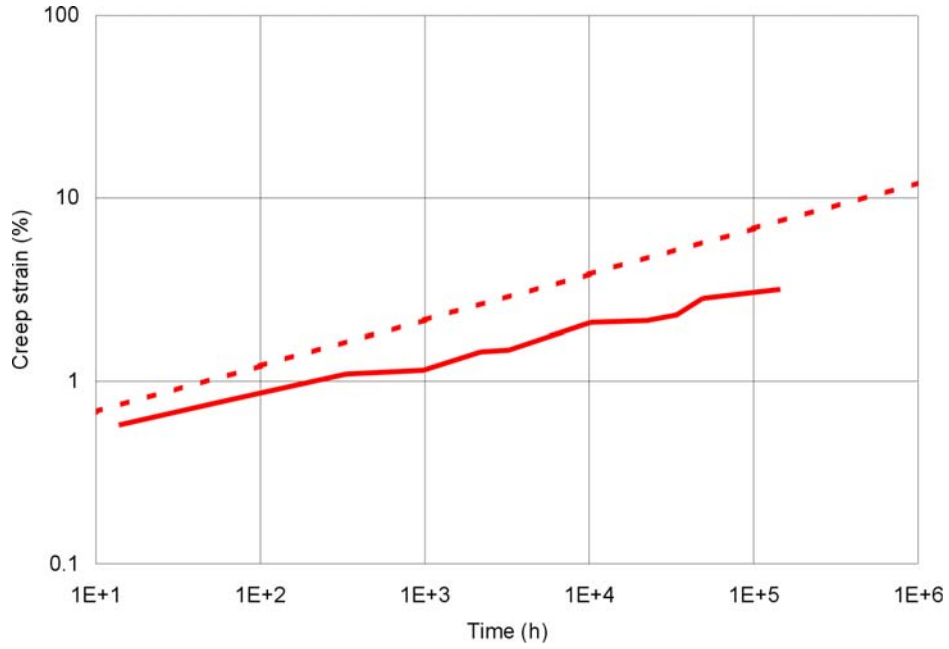

NOTE: The solid line is an experimental result digitized from the paper by Drefahl et al. (1985), Figure 10 [DIRS 174820]. The dashed line is the model prediction.

Figure I-10. Comparison of Equation (I-17) to the Experimental Creep Data by Drefahl et al. (1985), Figure 10 [DIRS 174820] for Ti-6Al-4V at RT

I-4.2 SCALING OF THE POWER LAW TO ACCOUNT FOR TEMPERATURE EFFECT

Thomson and Odegard (1973), Figure 4 [DIRS 174852] also reported results for Ti-5Al-2.5Sn at elevated temperatures (above RT) for different stress levels (shown as dots in Figure I-11). (Ti-5Al-2.5Sn is an alloy that exhibits more creep than Ti-24.) These results are used to estimate the activation energy of creep for Ti-24 (again, because Ti-5Al-2.5Sn has a lower resistance to creep than Ti-24, use of these data will overpredict creep deformation) using the functional relation shown in Equation (I-18):

$$\varepsilon = 0.0208\left(\frac{\sigma}{\sigma_y}\right)^{12.15} t^{0.25} \frac{e^{-\frac{Q}{kT}}}{e^{-\frac{Q}{kT_{RT}}}} \qquad \text{(Eq. I-18)}$$

The model predictions for $Q = 30$ kJ/mol (Assumption 3.2.15), shown in Figure I-11 as dashed lines, match or exceed the creep strains measured in the test for all loads and temperatures.

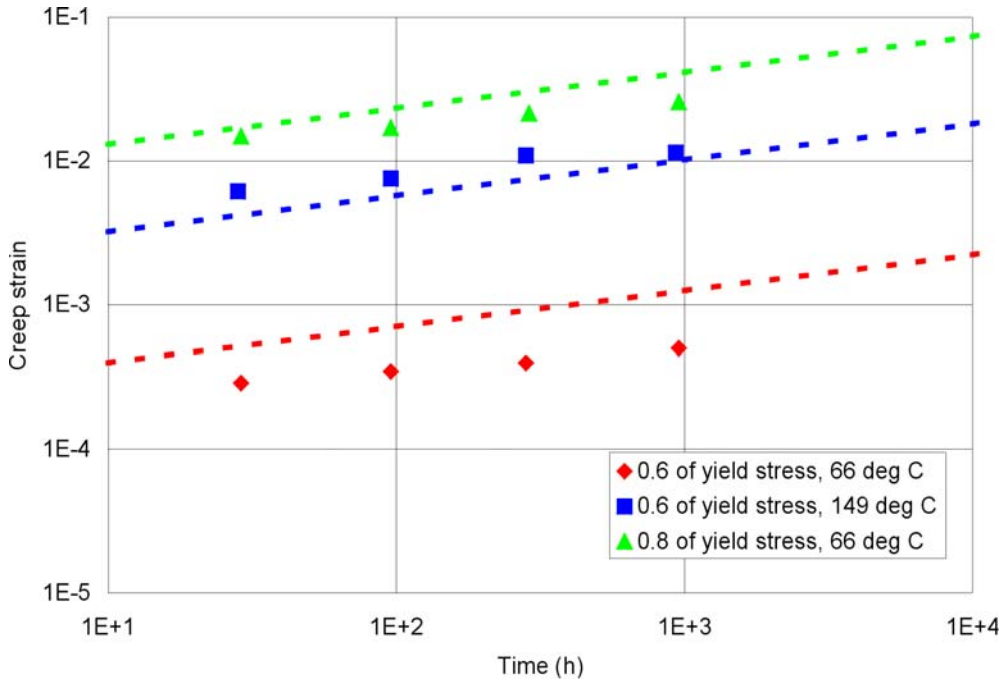

NOTE: The points are experimental results digitized from the paper by Thompson and Odegard (1973), Figure 4 [DIRS 174852]. The dashed lines are creep model predictions based on assumed activation energy (Assumption 3.2.15).

Figure I-11. Effect of Temperature on Creep Rates Measured in the Laboratory by Thompson and Odegard (1973), Figure 4 [DIRS 174852] for Ti-5Al-2.5Sn Compared with Model Predictions for Activation Energy, Q, of 30 kJ/mol

Using the yield strengths of 828 MPa and 682 MPa for Ti-24 at RT and 150ºC (Table 5.2-1), respectively, Equation (I-17) transforms into the following two relations:

$$\varepsilon = 7.31 \cdot 10^{-38} \sigma^{12.15} t^{0.25} \quad \text{(Eq. I-19)}$$

$$\varepsilon = 7.72 \cdot 10^{-37} \sigma^{12.15} t^{0.25} \quad \text{(Eq. I-20)}$$

Because the yield strength at 150ºC is used in rescaling the stresses, Equation (I-20) is an estimate of the creep strains of Ti-24 at 150ºC. The estimate of the creep strain at the elevated temperature also is derived using relation (I-18) for $Q = 30$ kJ/mol, as given in the following equation:

$$\varepsilon = 3.22 \cdot 10^{-36} \sigma^{12.15} t^{0.25} \quad \text{(Eq. I-21)}$$

Finally, an estimate of creep strain at an elevated temperature, shown in Equation (I-22), is derived by applying relation (I-18) to Equation (I-20)—i.e., accounting for the temperature effect on creep strain twice:

$$\varepsilon = 3.40 \cdot 10^{-35} \sigma^{12.15} t^{0.25} \quad \text{(Eq. I-22)}$$

Equation (I-22) is used in the prediction of drip shield creep deformation (Sections 5.3.1 and 5.4). Equations (I-19), at RT, and (I-21), at 150ºC, are used for prediction of stress relaxation (Sections 5.3.2 and 5.5).

I-5 CREEP RATES

The creep rates can be obtained by differentiating creep strains with respect to time. For example, creep rate predictions utilizing data from the various sources cited here for Ti-7 at 150ºC, obtained by differentiating Equations (I-13), (I-14) and (I-15), are shown in Equations (I-23), (I-24) and (I-25), respectively:

$$\dot{\varepsilon} = 6.02 \cdot 10^{-23} \sigma^{8.81} t^{-0.72} \quad \text{(Eq. I-23)}$$

$$\dot{\varepsilon} = 3.53 \cdot 10^{-29} \sigma^{11.48} t^{-0.72} \quad \text{(Eq. I-24)}$$

$$\dot{\varepsilon} = 2.87 \cdot 10^{-21} \sigma^{8.81} t^{-0.72} \quad \text{(Eq. I-25)}$$

Similarly, creep rates for Ti-24 at 150ºC are calculated from Equations (I-21) and (I-22) to be

$$\dot{\varepsilon} = 8.06 \cdot 10^{-37} \sigma^{12.15} t^{-0.75} \quad \text{(Eq. I-26)}$$

and

$$\dot{\varepsilon} = 8.51 \cdot 10^{-36} \sigma^{12.15} t^{-0.75} \quad \text{(Eq. I-27)}$$

respectively. The creep strain rates in Equations (I-23) through (I-27) are given in units of 1/h, stress is in MPa and time is in h.

All of these equations represent transient creep since the laboratory data show that true steady creep is never achieved. Although some of the authors report a steady, secondary creep rate, such

observation is an approximation of the asymptotic value of the creep rate made on the time scale of the duration of the test. The majority of the test results (e.g., Drefahl et al. 1985, Figures 3 and 10 [DIRS 174820]) indicate that the creep strain rate changes continuously with time. Consequently, the "steady" creep rates should be interpreted as minimum creep rates achieved for the duration of the creep test. The creep rates of Ti-7 and Ti-24 (or analogous materials) at RT after 1,000 h, obtained from experiments by Kiessel and Sinnott (1953), Figure 7 [DIRS 174853] and Odegard and Thompson (1974), Figure 3 [174818], are compared to the predictions of the equations discussed here. The fits to the experimentally determined rates are shown as solid lines in Figures I-12 and I-13 as functions of stress and stress scaled to the yield strength, respectively. The creep rates after 1,000 h are calculated from Equations (I-8), (I-9), (I-10), (I-19) and (I-20) and plotted in the same figures. Equations (I-8) through (I-10) approximate the creep strain of Ti-7 at RT and should be compared to the solid red lines in the figures. Equations (I-19) and (I-20) approximate the creep strain of Ti-24 at RT and should be compared to the solid blue lines in the figures. Creep equations for Ti-24 clearly predict larger creep rates than the fit to the experimental data for the range of stresses of any practical relevance. Similarly, for Ti-7, Equation (I-10) overpredicts the creep rate for stress levels greater than approximately 30 percent of the yield strength. The creep rates at stresses equal to or less than 30 percent of the yield strength are relatively small and unimportant from the standpoint of drip shield stability. Equations (I-8) and (I-9) underestimate the creep rate at RT after 1,000 h, for stresses less than approximately 80 percent of the yield strength leading to underestimates of the relaxation of residual tensile stresses resulting from an impact dent to the drip shield plates (see Section 5.5).

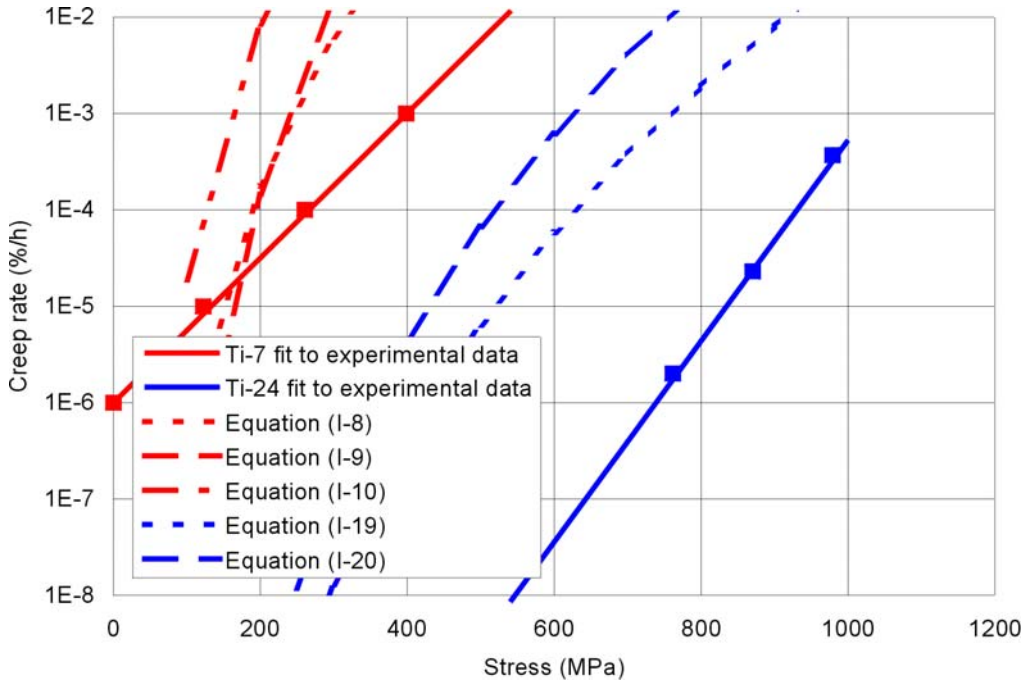

NOTE: The red points are data by Kiessel and Sinnott, Figure 7 (1953) [DIRS 174853]. The blue points are data by Odegard and Thompson (1974), Figure 3 [DIRS 174818].

Figure I-12. Comparison of Creep Rate after 1,000 h at RT as a Function of Stress Based on Fit to Experimental Data and Different Creep Equations

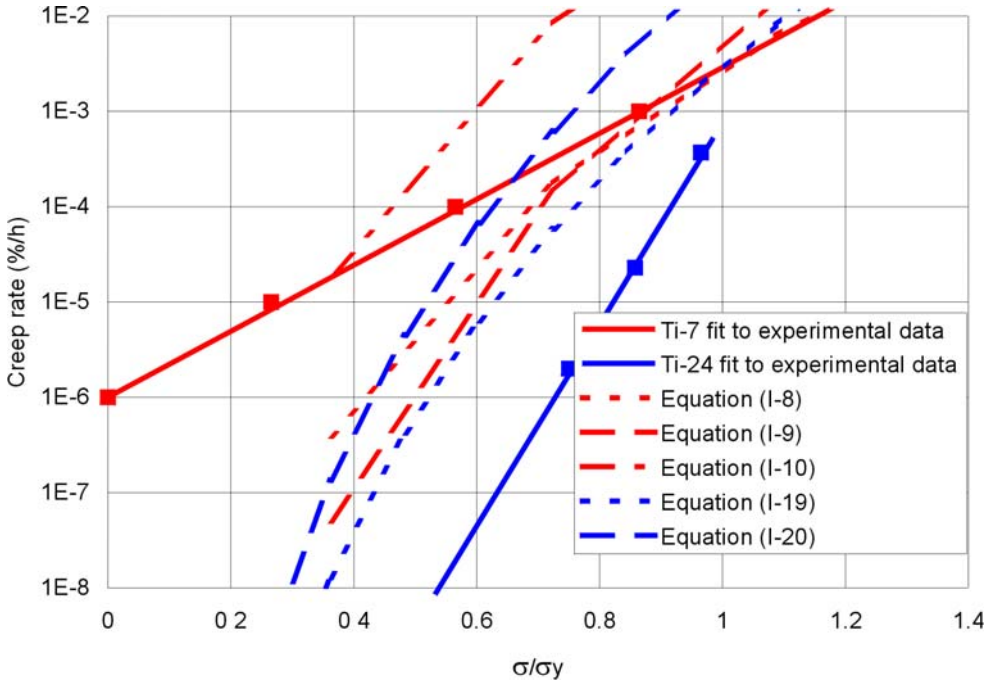

NOTE: The red points are data by Kiessel and Sinnott (1953), Figure 7 [DIRS 174853]. The blue points are data by Odegard and Thompson (1974), Figure 3 [DIRS 174818].

Figure I-13. Comparison of Creep Rate after 1,000 h at RT as a Function of Stress Normalized by the Yield Strength Based on Fit to Experimental Data and Different Creep Equations

I-6 CONCLUSIONS

Equations that provide estimates of creep deformation are derived for Ti-7 and Ti-24, titanium alloys to be used for drip shield structure. Different equations are derived to estimate drip shield stability due to creep, and residual stress relaxation. All available relevant data are used, but the largest weight is given to the laboratory results obtained from the longest lasting tests. The creep rates are provided as functions of time as the evolution parameter.

The creep strains (or equivalently corresponding creep strain rates) given by equations (I-8) and (I-9) are used as two bounding equations for Ti-7 at RT in the stress relaxation analysis. In the same analysis, Equations (I-13) and (I-14) were used as two bounding equations for Ti-7 at 150ºC. Equations (I-19) and (I-21) were used for Ti-24 at RT and 150ºC, respectively, in the stress relaxation analysis.

In the analysis of drip shield creep deformation (carried out for 150ºC), creep of Ti-7 is represented by Equation (I-15); creep of Ti-24 is represented by Equation (I-22).

ATTACHMENT II

ONE-DIMENSIONAL CREEP TEST SIMULATION

II-1. INTRODUCTION

A simple creep test of a titanium bar of uniform cross Section loaded by a constant uniaxial stress results in creep strains characterized by Equations II-1 and II-2 for Ti-7 and Ti-24, respectively (see Attachment I for details of the derivation of these equations from laboratory data). These creep strain rates are estimates of the creep strain of Ti-7 and Ti-24 at 150ºC, respectively. In this attachment, the FLAC3D numerical code is used to simulate this uniaxial creep test, and the results used for comparison to Equations II-1 and II-2.

$$\dot{\varepsilon} = 2.87 \cdot 10^{-21} \sigma^{8.81} t^{-0.72} \quad \text{(Eq. II-1)}$$

$$\dot{\varepsilon} = 8.51 \cdot 10^{-36} \sigma^{12.15} t^{-0.75} \quad \text{(Eq. II-2)}$$

In the equations above, the creep rate, $\dot{\varepsilon}$, is in 1/h, uniaxial stress; σ, is in MPa; and time, t, is in h.

II-2 RESULTS

Figure II-1 illustrates the geometry of the laboratory test and the equivalent FLAC3D model used to simulate the test. FLAC3D employs an adaptive time stepping scheme for use in creep simulations. The creep time step changes during the calculation as a function of the unbalanced force at any point in the simulation. If the unbalanced force is outside a range of predefined limits, the time step is either automatically increased or decreased to optimize the efficiency of the problem solution. This scheme allows efficient solution of creep problems for long simulated times, during which the load does not change and the creep rate significantly decreases as time progresses. Simple creep tests were analyzed using the same FLAC3D program solution settings as those used in the simulations of drip shield creep (Section 5.4).

Comparison of the laboratory creep data for Ti-7 and Ti-24 from Equations II-1 and II-2 are compared to simulations using the FLAC3D code in Figures II-2 and II-3. The test simulating Ti-7 creep was carried out for a constant tensile stress of 100 MPa, resulting in creep strain as a function of time as shown in Figure II-2. The total creep strain after 10,000 years is approximately 0.7. Because the creep equations for Ti-7 and Ti-24 [e.g., Equations II-1 and II-2] do not account for geometrical nonlinearities, which are important at such large strains, the problems were simulated in FLAC3D using small-strain approximation which does not make corrections for geometric change in the sample. (The actual drip shield creep deformation, as described in Section 5.4, was conducted accounting for large-strain deformation.) The results for Ti-24 and an applied 400 MPa tensile stress are shown in Figure II-3. The results of both simple tests show excellent agreement between the numerical and analytical results, thus verifying the correct implementation of the creep laws within the FLAC3D calculation.

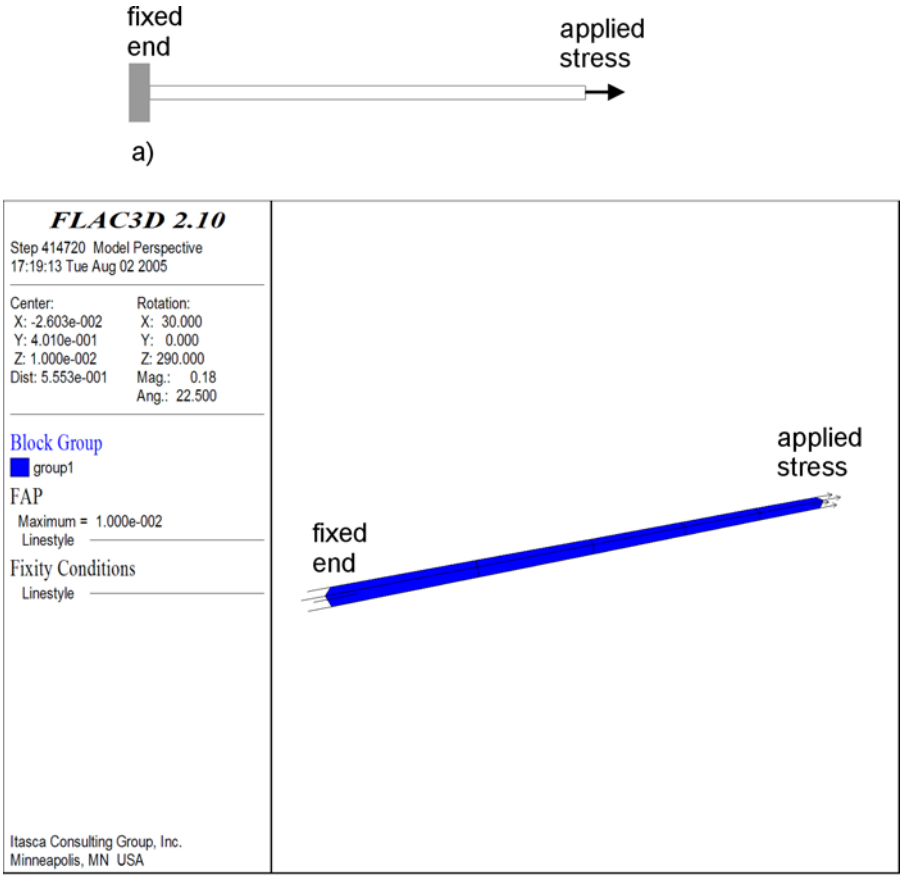

Figure II-1. (a) Schematic Illustration of a Uniaxial Creep Test on a Titanium Bar of Uniform Cross Section, and (b) the Equivalent FLAC3D Numerical Geometry used for Simulation of the Creep Test

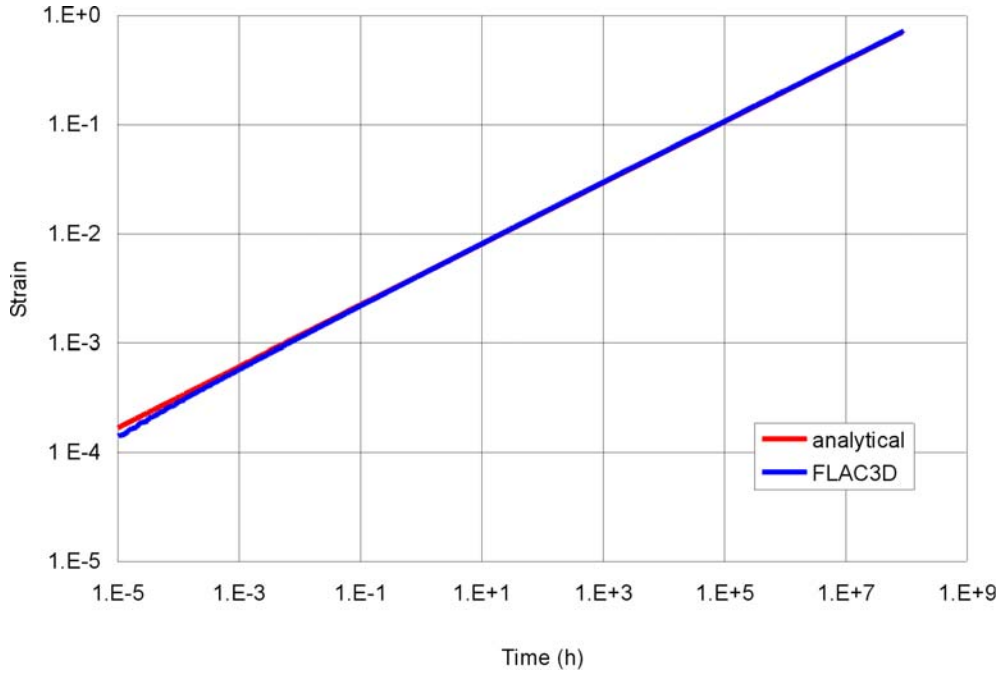

Figure II-2. Creep Deformation of a Straight Beam Loaded by a Constant Stress of 100 MPa Assuming Creep Equation II-1 (Representative of Ti-7)

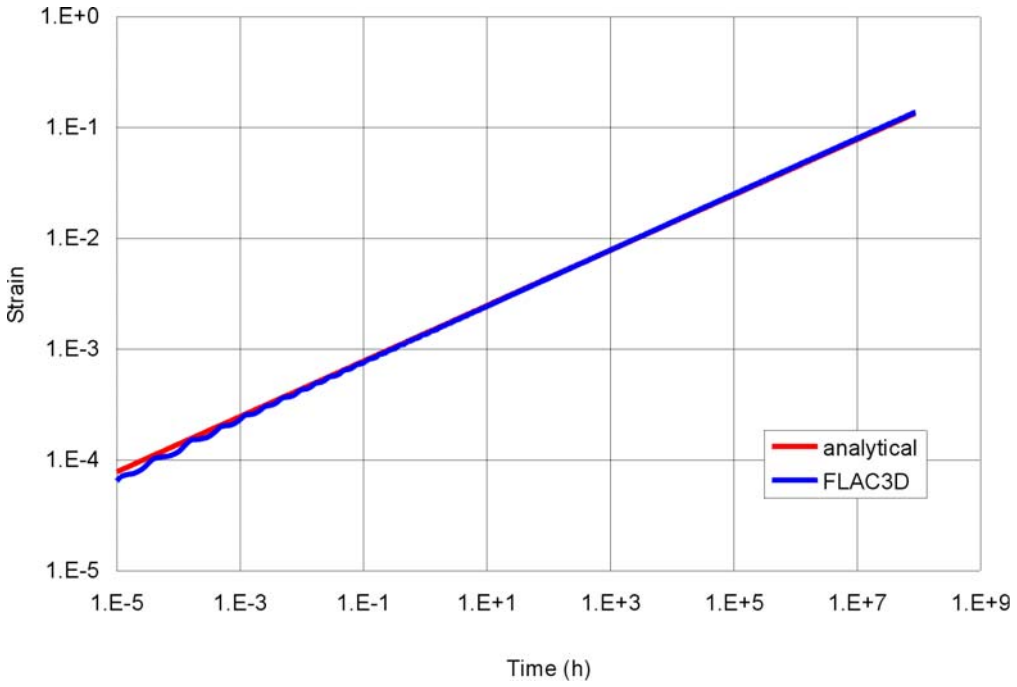

Figure II-3. Creep Deformation of a Straight Beam Loaded by a Constant Stress of 400 MPa Assuming Creep Equation II-2 (Representative of Ti-24)

INTENTIONALLY LEFT BLANK

ATTACHMENT III

EFFECT OF ELEMENT DISCRETIZATION ON DRIP SHIELD CREEP RESULTS FROM THE FLAC3D CODE

III-1 INTRODUCTION

The results of creep deformation presented in this report (Section 5.4) are derived from calculations in which the drip shield plates are discretized with two layers of elements across the thickness of the plate. Such discretization is too coarse to accurately represent the variation of the stresses in the cross-Section due to bending of the plate. The insufficient number of elements per thickness of the cross-Section will make numerical response of the plates overly-stiff, preventing accurate prediction of possible creep-induced sagging of the plates between the bulkheads when subjected to rubble loads. To investigate the effect of plate discretization on the creep deformation results, stability of the drip shield was analyzed for rubble load realization 3 with a refined numerical mesh; the plates were discretized with five layers of elements per thickness. (Mesh details are shown in Figure III-1. For reference, the coarse mesh with two layers of elements per plate thickness is shown in Figure III-2.) Interaction between the drip shield and the rubble was neglected in this calculation.

III-2 RESULTS

The new results of drip shield deformation calculated with the refined numerical mesh shown in Figure III-3 should be compared with the results shown in Figure III-4, obtained for the same loading conditions with a coarse mesh. The refined mesh predicts greater deformation; the maximum creep displacement obtained with the coarse mesh is approximately 27 percent less than that obtained with the refined mesh. The relative difference between the two results is large, but it does not affect the overall mechanical stability of the drip shield as described below. Also, the overall mode of deformation of the drip shield is unaffected by discretization. The configurations of the drip shield after initial deformation and 10,000 years of creep deformation are compared for the two mesh discretizations in Figure III-5. The following conclusions are made regarding the comparison of the results of these two mesh configurations:

- Both overall geometric configurations of the meshes after the initial, quasi-static short-term (e.g., no creep) deformation are almost identical; although there is a significant disagreement between the maximum creep displacements, the overall geometric configurations of the drip shield after 10,000 years of creep predicted by the coarse and the refined meshes are very similar.

- No localization of creep strain in the plates between the bulkheads and the support beams that could lead to a mode of structural instability is predicted for either the coarse or refined meshes.

- The increase in predicted displacements after refinement of the mesh is more than offset by the choice of the creep parameters, which overestimate creep deformation of titanium, used in the calculations. (The creep equations used for prediction of creep deformation of the drip shield exceed creep strains measured in the laboratory by more than an order of magnitude for some stress levels.)

- The difference between the results obtained with different numerical grids is amplified in the particular case presented here since the coupling of the drip shield deformations to reinforcement from the rubble itself is not included. As shown in Section 5.4, these

uncoupled numerical analyses are for unrealistic and unfavorable loading conditions, and result in significantly larger deformations than for the more realistic coupled analyses in which the rubble surrounding the drip shield limits the deformations.

Considering (a) the significant increase in simulation time for the refined mesh compared to that for the coarse mesh, (b) the same overall mode of deformation of the drip shield for different discretizations, (c) the extent by which the creep equations overpredict creep deformations observed in the laboratory tests used, and (d) the large factor of safety (e.g., the creep strain at the onset of tertiary creep compared to the maximum predicted peak creep strains) of the results obtained with the coarse mesh, it was deemed unnecessary to repeat all simulations with the refined mesh.

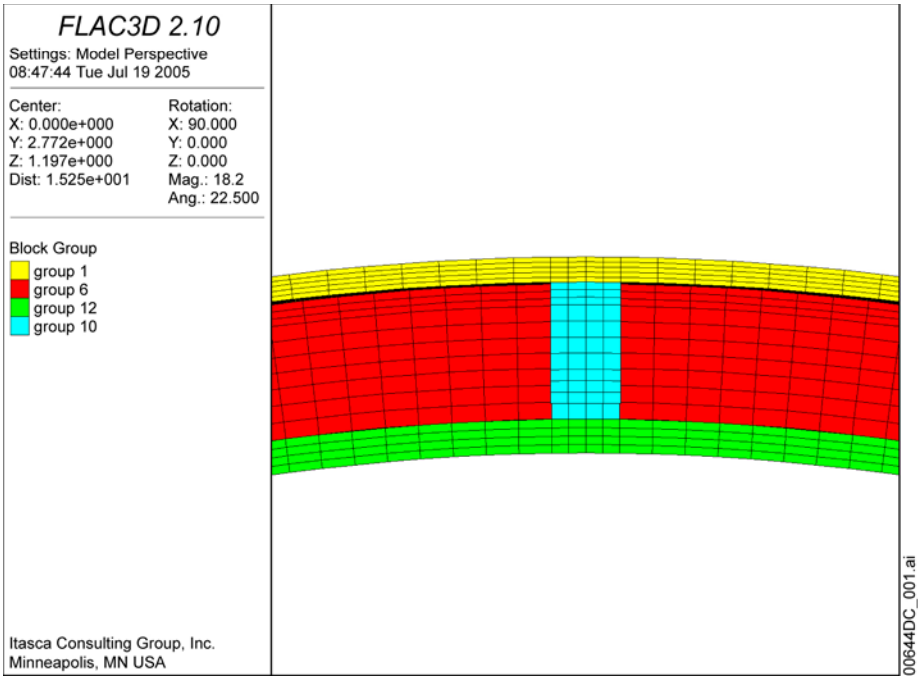

Figure III-1. Geometry of the Numerical Representation of the Drip Shield with Five Layers of Elements in the Plates Showing Groups of Elements Representing Different Parts of the Structure: Crown Detail

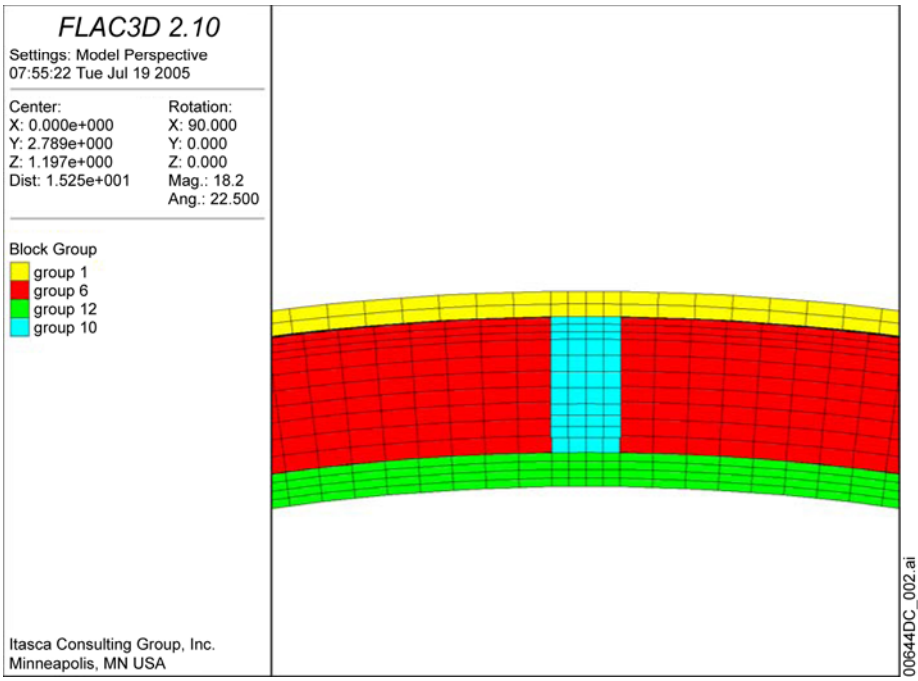

Figure III-2. Geometry of the Numerical Representation of the Drip Shield with Two Layers of Elements in the Plates Showing Groups of Elements Representing Different Parts of the Structure: Crown Detail

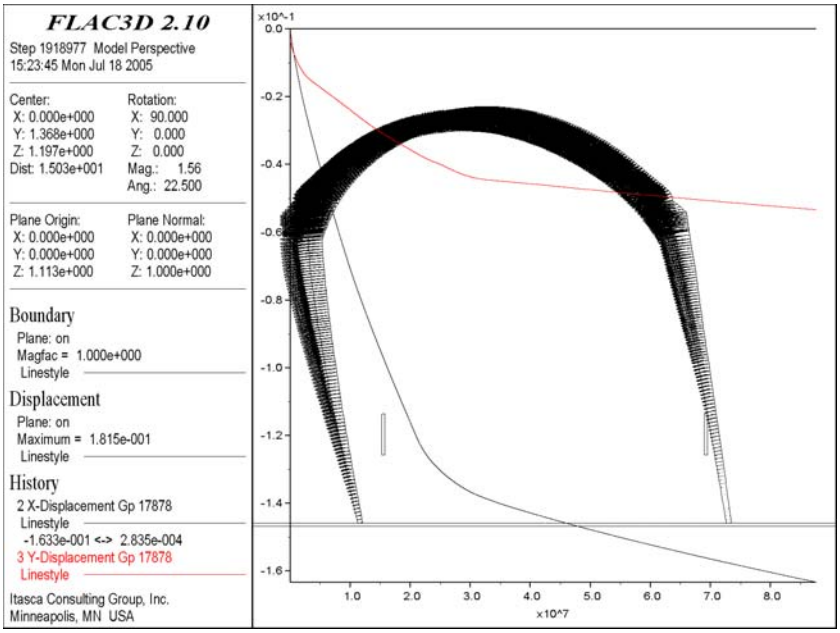

NOTE: The plot of displacement vector field overlies the plot of the displacement histories. Two thin vertically oriented rectangles inside the drip shield represent the emplacement pallet. Displacements are on the vertical axis; time is on the horizontal axis.

Figure III-3. Realization 3 with Five Layers of Elements in the Plates: Creep Displacement Vector Field (m) after 10,000 Years and Horizontal (Black) and Vertical (Red) Displacement (m) Histories of the Middle of the Crown versus Time (h)

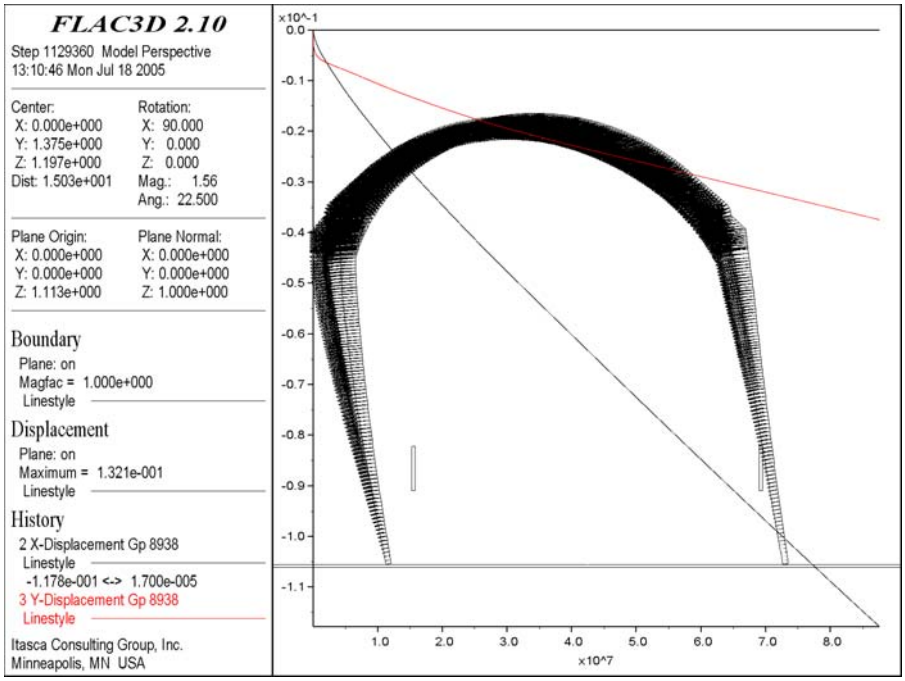

Figure III-4. Realization 3 with Two Layers of Elements in the Plates: Creep Displacement Vector Field (m) after 10,000 Years and Horizontal (Black) and Vertical (Red) Displacement (m) Histories of the Middle of the Crown versus Time (h)

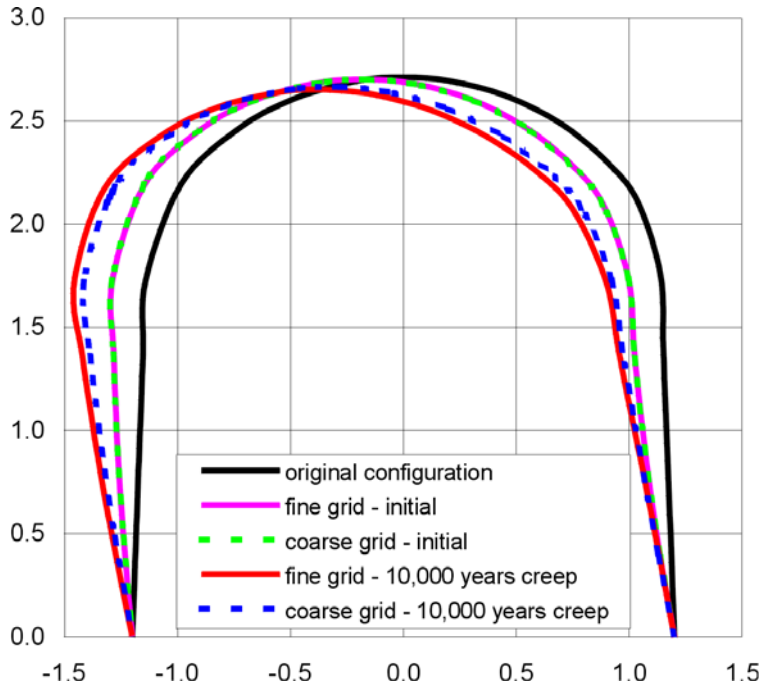

Figure III-5. Comparison of Drip Shield Configurations after Initial Deformation and 10,000 Years of Creep Obtained using Coarse and Refined Meshes

INTENTIONALLY LEFT BLANK

ATTACHMENT IV

COMPARISON OF FLAC3D TO ANALYTIC SOLUTION FOR CREEP-INDUCED STRESS RELAXATION IN A ONE-DIMENSIONAL BAR

IV-1 INTRODUCTION

A simple calculation of creep-induced stress relaxation in a bar clamped on both sides has been carried out by analytical integration of the creep equations for Ti-7 and by simulation using FLAC3D. (The stresses were initialized inside the bar, which is equivalent to stretching.) The comparison of these two results is used to provide verification of the stress relaxation calculation in FLAC3D and to provide a simple estimate of the time scale of stress relaxation, depending on the different creep equations used.

IV-2 RESULTS

Formula (IV-1) was used to calculate stress relaxation under isothermal conditions. Because the bar is clamped on both sides, the total strain is zero. That implies that the elastic strain, which causes stress change, is equal to but has opposite sign than the creep strain. Therefore, the stress change during a time interval Δt can be calculated from the creep strain, ε^{cr}, applying linearly elastic stress-strain relation:

$$\sigma^{t+\Delta t} = \sigma^{t} - E \int_{t}^{t+\Delta t} \dot{\varepsilon}^{cr}\, dt \qquad \text{(Eq. IV-1)}$$

where E is the Young's modulus, $\dot{\varepsilon}^{cr}$ is the creep strain rate. If the time increment Δt is sufficiently small and the temperature constant, it can be assumed that $\dot{\varepsilon}^{cr}$ is constant during the time interval and Equation (IV-1) can be approximated as:

$$\sigma^{t+\Delta t} = \sigma^{t} - E\dot{\varepsilon}^{cr}(\sigma^{t})\,\Delta t \qquad \text{(Eq. IV-2)}$$

Both numerical (FLAC3D) and semi-analytical approaches should yield the same results for comparison of the stress as a function of time. The calculations were conducted for four different creep equations for Ti-7 (the coefficients are listed in Table 5.3-2): two at RT; and two at 150ºC. The FLAC3D realization consists of a clamped-end bar in which a stress (representing a residual stress) of 170 MPa was initialized in the bar. (The maximum residual stresses in the plates after denting by rock block are approximately 170 MPa as shown in Figure 5.5-12.) The results of the calculations are shown in Figure IV-1 in terms of the stress in the bar as a function of time. As is seen, the stress relaxes over time as a result of creep. Clearly, there is excellent agreement between the semi-analytical calculation, based on Equation IV-2 above, and the FLAC3D simulation results. The plot also indicates 50 percent of the yield strengthes at RT and 150ºC. The calculations show that the 170 MPa initial stress would relax below 50 percent of the yield strength in less than one year at RT and in less than 100 years at 150ºC.

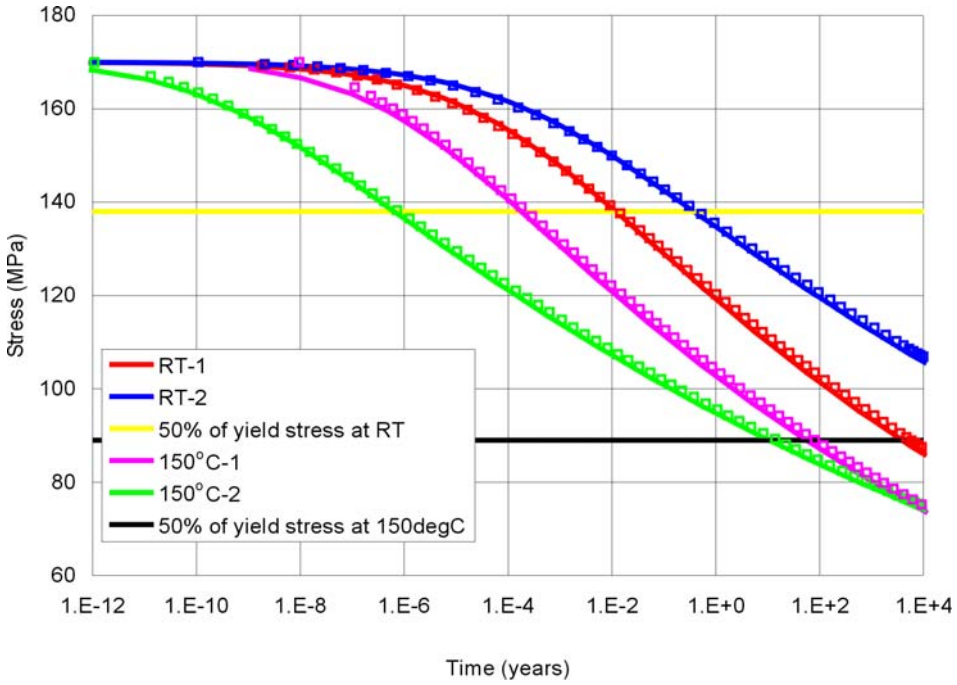

NOTE: Solid lines are directly integrated results. The dots are FLAC3D results.

Figure IV-1. Stress Relaxation Inside a Clamped Bar for Different Creep Equations for Ti-7—Initial Stress in Bar is Taken to be 170 MPa

ATTACHMENT V

DERIVATION OF SCALAR STRAIN MEASURE

V-1 INTRODUCTION

Strain is generally a tensor variable. However, when strain is used in a criterion for stability of a structure (e.g., Section 5.4), it is necessary to develop a scalar measure of strain. This scalar measure should coincide with measurable strain for simple uniaxial loading conditions.

V-2 DERIVATION

The following relation gives a form of the Norton power law implemented in FLAC3D (Equation 2.20 of Optional Features volume of FLAC3D manual, Itasca Consulting Group 2002 [DIRS 160331]):

$$\dot{\varepsilon}^{cr} = A\sigma^n \qquad \text{(Eq. V-1)}$$

where

$$\sigma = \sqrt{\frac{3}{2}\sigma_{ij}^d \sigma_{ij}^d} \qquad \text{(Eq. V-2)}$$

and σ_{ij}^d is deviatoric part of σ_{ij}, and $\dot{\varepsilon}^{cr}$ is the uniaxial measure of creep strain rate (measured in laboratory tests of creep on uniaxially loaded straight bars). The creep strain rate, $\dot{\varepsilon}_{ij}^c$, which for a uniaxial stress state is equal to the total strain rate, $\dot{\varepsilon}_{ij}$, can be written as (Equation 2.22 of Optional Features volume of FLAC3D manual, Itasca Consulting Group 2002 [DIRS 160331])

$$\dot{\varepsilon}_{ij} = \dot{\varepsilon}_{ij}^c = \frac{3}{2}\dot{\varepsilon}^{cr}\left(\frac{\sigma_{ij}^d}{\sigma}\right) \qquad \text{(Eq. V-3)}$$

If a bar is loaded uniaxially with stress σ_o, the total stress tensor can be devolved into spherical and deviatoric parts as follows:

$$\begin{bmatrix} \sigma_o & 0 & 0 \\ 0 & 0 & 0 \\ 0 & 0 & 0 \end{bmatrix} = \begin{bmatrix} \sigma_o/3 & 0 & 0 \\ 0 & \sigma_o/3 & 0 \\ 0 & 0 & \sigma_o/3 \end{bmatrix} + \begin{bmatrix} 2\sigma_o/3 & 0 & 0 \\ 0 & -\sigma_o/3 & 0 \\ 0 & 0 & -\sigma_o/3 \end{bmatrix} \qquad \text{(Eq. V-4)}$$

Consequently, from equation (V-2), it follows that

$$\sigma = \sigma_o \qquad \text{(Eq. V-5)}$$

The total strain rate (Equation V-3) can be written as

$$\dot{\varepsilon}_{ij} = \begin{bmatrix} 1 & 0 & 0 \\ 0 & -1/2 & 0 \\ 0 & 0 & -1/2 \end{bmatrix} \dot{\varepsilon}^{cr} \qquad \text{(Eq. V-6)}$$

If the strain measure, ε, is

$$\varepsilon = \sqrt{\frac{4}{3} J_2(\varepsilon_{ij}^d)} = \sqrt{\frac{2}{3} \varepsilon_{ij}^d \varepsilon_{ij}^d} \qquad \text{(Eq. V-7)}$$

it can be shown, using Equation (V-6), that

$$\varepsilon = \varepsilon^{cr} \qquad \text{(Eq. V-7)}$$

The strain measure (V-7) based on the second invariant of the deviatoric strain, $J_2(\varepsilon_{ij}^d)$, coincides with strains measured in the uniaxial creep experiments.